Universidade de Aveiro Departamento de Química
Ano 2011

Sónia Oliveira Pereira

Nanoestruturas híbridas de ouro/polieletrólito para bio-sensores óticos

Hybrid nanostructures of gold/polyelectrolyte for optical biosensors

Universidade de Aveiro Departamento de Química
Ano 2011

Sónia Oliveira Pereira

Nanoestruturas híbridas de ouro/polieletrólito para bio-sensores óticos

Hybrid nanostructures of gold/polyelectrolyte for optical biosensor

Dissertação apresentada à Universidade de Aveiro para cumprimento dos requisitos necessários à obtenção do grau de Mestre em Biotecnologia, ramo molecular, realizada sob a orientação científica da Doutora Ana Margarida Madeira Viegas de Barros-Timmons, Professora auxiliar do Departamento de Química da Universidade de Aveiro e do Doutor Tito da Silva Trindade, Professor Associado com Agregação do Departamento de Química da Universidade de Aveiro

Dedico este trabalho à minha família e ao meu namorado.

o júri

presidente

Prof. Doutor Jorge Manuel Alexandre Saraiva
investigador auxiliar do Departamento de Química da Universidade de Aveiro

Prof. Doutor Eduardo Jorge Figueira Marques
professor auxiliar da Faculdade de Ciências da Universidade do Porto

Prof. Doutor Tito da Silva Trindade
professor associado com agregação do Departamento de Química da Universidade de Aveiro

Prof. Doutora Ana Margarida Madeira Viegas de Barros-Timmons
professora auxiliar do Departamento de Química da Universidade de Aveiro

agradecimentos

Em primeiro lugar gostaria de agradecer à minha orientadora, Professora Doutora Ana Barros-Timmons, por me ter proporcionado a oportunidade de desenvolver este trabalho, pela valiosa orientação científica, pelo incentivo e disponibilidade permanente para o esclarecimento de dúvidas, pelos valiosos conselhos e sugestões, pela forma incansável e generosa como disponibilizou o seu tempo na elaboração desta dissertação e pelo seu excelente apoio.

Gostaria de agradecer ao Professor Doutor Tito Trindade, co-orientador desta dissertação, pela disponibilidade, incentivos, ensinamentos e proveitosas contribuições no decurso deste trabalho.

À Doutora Ana Violeta Girão pelas imagens de microscopia electrónica e por toda a ajuda e ensinamentos que me transmitiu sobre esta técnica.

À Mestre Celeste Azevedo pelo apoio nas técnicas espectroscópicas de UV-Vis e FTIR.

Agradeço à Professora Doutora Amparo Faustino pela disponibilização do fluorímetro para as medidas de fluorescência.

Agradeço aos meus colegas e laboratório – NanoLab, pela ajuda, companheirismo e amizade. Um agradecimento especial à Paula por toda a amizade e pela sua boa disposição.

Agradeço, de uma forma especial, aos meus amigos de curso por todos os momentos que me proporcionaram ao longo destes anos em Aveiro

Por fim, expresso a minha profunda gratidão, à minha mãe, às minhas irmãs e ao meu namorado, por toda força, apoio, confiança e amor que me deram ao longo desta etapa da minha vida.

palavras-chave

Bio-sensor, nanopartículas de ouro, propriedades óticas, nanoestruturas híbridas, polieletrólitos.

resumo

As nanopartículas de ouro (NPs de Au) têm recebido uma grande atenção devido às suas propriedades óticas serem sensíveis ao tamanho, forma, estado de agregação e ao meio envolvente, o que pode potenciar a sua aplicação em bio-sensores.

Neste trabalho, NPs de Au foram preparadas por dois métodos distintos: (i) o método de redução por citrato, que permite obter NPs de Au com 14.9 ± 2.7 nm de diâmetro e um máximo de absorvância (λmax) a 522 nm; e (ii) o método *in situ* utilizando como agente redutor o hidrocloreto de polialilamina (PAH). Estas NPs de Au têm um diâmetro de 22.0 ± 3.3 nm e um máximo de absorvância (λmax) a 538 nm. O efeito das diferentes reações nas propriedades dos nanomateriais foi avaliado por espetroscopia ótica, dispersão dinâmica de luz (DLS, do inglês *dynamic light scattering*), medidas de potencial zeta e microscopia electrónica de transmissão (TEM). Para avaliar a robustez das nanoestruturas, as amostras preparadas pelo método do citrato foram submetidas a uma série de ciclos de lavagens para verificar a remoção do PAH. Após cada ciclo, foram caracterizados por espectroscopia no visível e por medidas de potencial zeta. Estes estudos indicam que após o terceiro ciclo de lavagem a quantidade de PAH é residual.

Para utilizar as suspensões coloidais de Au como bio-sensor, foram exploradas diferentes estratégias de funcionalização do PAH. Primeiro o PAH foi funcionalizado com o isotiocianato de fluoresceína (FITC) e com biotina. O polieletrólito quimicamente modificado resultante foi usado para revestir as NPs de Au preparadas pelo método do citrato. A funcionalização destas nanoestruturas com biotina *a posterior* deu origem a um sistema mais sensível. Quanto às NPs preparadas *in situ* foram testadas quatro estratégias de modificação e purificação tendo-se concluído que a única estratégia viável envolve a seguinte sequência: síntese das NPs de Au *in situ* seguida de modificação do PAH com FITC garantido que o pH da solução se mantém à volta de 9; purificação através de centrifugação/dispersão até pH ligeiramente ácido e finalmente funcionalização com a biotina. As nanoestruturas híbridas resultantes foram caracterizadas por espectroscopia no visível, fluorescência e medidas de potencial zeta.

Finalmente, a resposta ótica e a especificidade das nanoestruturas funcionalizadas na presença de avidina foi avaliada por espectroscopia no visível e fluorescência. Para este fim foram utilizadas as nanoestruturas originais bem como nanoestruturas em que o PAH foi apenas funcionalizado com biotina, sem FITC e vice-versa. Os resultados indicam que estas nanoestruturas híbridas podem ser utilizadas como bio-sensor uma vez que foi observada uma resposta específica, nomeadamente quando as NPs de Au foram preparadas pelo método do citrato.

keywords

Biosensor, gold nanoparticles, optical properties, hybrid nanostructures, polyelectrolytes.

abstract

Gold nanoparticles (Au NPs) have been receiving significant attention due to the fact that their optical properties are very sensitive to characteristics such as size, shape, state of aggregation and surrounding environment which can find potential applications in biosensors.

In the present work Au NPs were prepared by two distinct methods: (i) the standard citrate method which yielded Au NPs with 14.9 ± 2.7 nm diameter and an absorption maximum (λmax) at around 522 nm, and (ii) an *in situ* procedure using poly(allylamine hydrochloride) (PAH) as reducing agent. The ensuing Au NPs had a diameter of 22.0 ± 3.3 nm and an absorption maximum (λmax) at around 538 nm. The effect of the reaction conditions on the materials properties was assessed by optical spectroscopy, dynamic light scattering (DLS), zeta potential measurements and transmission electron microscopy. To investigate the robustness of the ensuing citrate nanostructures, the samples were submitted to a series of washing cycles in order to assess PAH removal. Upon each cycle the materials were analyzed by visible spectroscopy and zeta potential measurements. These studies indicated that from the third cycle the amount of PAH was residual.

In order to use the Au colloidal suspensions as biosensors, different strategies to modify PAH were used. The PAH chains were first functionalized with fluorescein isothiocyanate (FITC) and biotin. The chemically modified polyelectrolyte was used to coat the Au NPs prepared via the citrate method. The functionalization of the nanostructures with biotin *a posteriori* yielded a more sensitive system. For the Au NPs prepared *in situ* four different functionalization and purification routes have been explored. Only the following sequence proved successful: *in situ* synthesis of Au NPs, followed by reaction with FITC to ensure the pH is kept around 9; the ensuing nanostructures were then purified by centrifugation and re-dispersion to slightly acid pH and finally modification with biotin was preformed. The resulting hybrid nanostructures were characterized by visible spectroscopy, fluorescence and measurements of zeta potential.

Finally, the optical response and specificity of the functionalized nanostructures towards avidin was evaluated using visible and fluorescence spectroscopies. For comparison purposes, the original Au NPs coated with PAH were used as blanks as well as nanostructures prepared specifically for this purpose which were functionalized either with FITC or with biotin. The results show that these hybrid nanostructures have potential to be used as biosensor, since a specific response was observed namely when the gold NPs were prepared via the citrate method.

CONTENTS

ABBREVIATIONS AND SYMBOLS

DLS	Dynamic Light Scattering
DNA	Deoxyribonucleic acid
DMSO	Dimethyl sulfoxide
EDC	N-(3-dimethylaminopropyl)-N'-ethyl-carboiimide
FITC	Flourescein Isothiocyanate
FRET	Fluorescence Resonance Energy Transfer
FTIR	Fourier transform infrared
LbL	Layer-by-Layer
NPs	Nanoparticles
PAH	Poly(allylamine hydrochloride)
PBS	Phosphate Buffer Saline
PCs	Polyelectrolyte chains
PEI	Polyethyleneimine
PPV	Poly(phenylene vinylene))
PL	Photoluminescence
PSS	Poly(sodium styrene sulfonate)
SEM	Scanning Electron Microscope
SPR	Surface Plasmon Resonance
TEM	Transmission Electron Microscope
UV-Vis	Ultraviolet - Visible
λ	Wavelength
ζ	Zeta potential

LIST OF FIGURES

LIST OF TABLES

PART I

INTRODUCTION

PART I – INTRODUCTION

Nanotechnology and Nanoscience are areas that have attracted a great interest in the scientific community due to the fact that nanomaterials have distinct properties/characteristics of their bulk analogues and their dimensions (typically from 1 to 100 nm) make these materials very interesting. The great diversity of nanoparticles (e.g. semiconductors quantum dots, iron oxides, Au and Ag nanoparticles) and the possibility to modify their surface allows a wide range of applications, such as in transistors, drug delivery and biosensors, for example. In particular gold nanoparticles (Au NPs) have been exhaustively studied due to the Surface Plasmon Resonance (SPR) that is very sensitive to the size, shape and the surrounding environment (such as the interparticle interaction and surface modification), which make these NPs of high interest in biosensing. [1-2]

1. Gold nanoparticles in biosensors

Gold nanoparticles have been widely studied for applications in biomedicine, biosensing, imaging and therapy due to their biocompability, dimensions, easy characterization and easy surface modification[1]. For the application of Au NPs in biological systems their stability in aqueous medium is important and surface modification is a way to achieve colloidal stability[2-3]. Furthermore, surface modification of NPs allows their functionalization enabeling several applications as mention above.

This work will focus on the surface modification/functionalization of Au NPs towards applications in biosensors. Hence, in the next section a brief definition of biosensors will be presented and the application of Au NPs as biosensors and the synthesis and functionalization of Au NPs briefly reviewed.

1.1 Biosensors

A biosensor can be generally defined as a measuring device that contains a biological agent (e.g. enzyme, antibody, biological tissue) [4-5], comprising three fundamental components

which are interconnected: 1) the biological agent that recognizes the analyte; 2) a transducer that works as interface in signal communication; 3) a detector that measures and quantifies the signal [4-7]. This is illustrated in Figure 1.

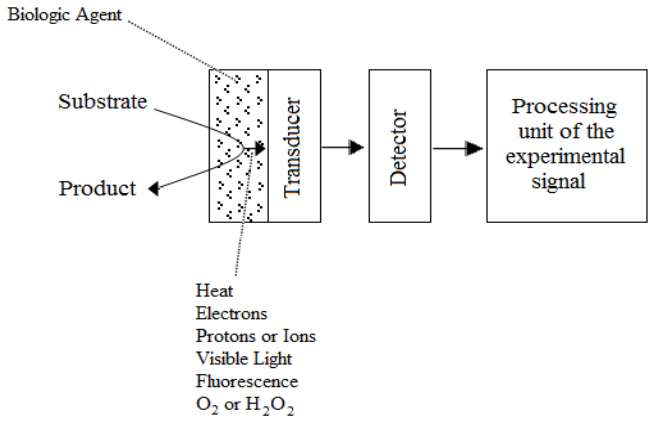

Figure 1 – Scheme of a typical biosensor [5].

The biological component, the main part of the device, interacts with the analyte and converts the analyte into another chemical species through a biochemical reaction; produces or releases another chemical product in response to the analyte stimulus; changes its optical, electrical or mechanical properties; or other type of response that can be quantified. The output signal from a biosensor depends on the type of transducer it uses [4-5]. There are electrochemical biosensors, sensors based on impedance spectroscopy, sensors exploring field-effect transistors and optical biosensors [6]. Optical biosensors include UV-Vis absorption and fluorescence spectroscopy which depending on the device are of higher sensitivity [6]. Several types of biosensors can be constructed by conjugating the materials components, in order to achieve the best molecular recognition for the characteristics of each analyte and the detection mechanism appropriate for the signal transduction [7-8].

An ideal biosensor should have high selectivity and sensitivity. The selectivity is fundamental because the biosensor should only respond to the target analyte, and can not be influenced by the presence of other (bio)chemical species. The sensitivity is directly related with the amount of analyte that can be detected. Hence, the ideal biosensor should be easily calibrated, should exhibit a linearity that allows measurements over the concentration range from zero to the maximum substrate concentration that can be physically dissolved in the measurement medium; the background signal should be

subtracted to prevent its effect on sensitivity and should not be affected by its past history of measurements. Ideally, the sensitivity of a biosensor should remain constant during its lifetime and should be sufficiently high to allow convenient measurement of the transducer output signal. Other properties required are long lifetime and high stability, since the biosensor should remain sensitive under normal operational conditions over time with the biological agent being the component less stable in the whole system. Dynamic response is also important because a slow response can affect the range of applications, so the physical properties and relative size of a biosensor probe determines how fast it will respond to a change in concentration of the target analyte. A biosensor should be reutilized to minimize the manufacturing costs and for biosensors for medical applications involving implantation in the human body, biocompatibility is also required[4-5]

In the case of aqueous colloidal systems there is not a solid device. Hence, the three components of a biosensor discussed above are not present. Instead, so the biosensor in this case is defined only by two components: a biological receptor and a transducer. In the biological receptor occurs the biological recognition. Thus, it should have high selectivity and sensitivity. Usually these are antibody/antigen, enzymes, nucleic acids (RNA and DNA), cellular structures or cells. The transducer will depend of the biological receptor and of the type of signal that results of the interaction between the analyte and the biological receptor which is converted into some kind of detectable/measurable signal. So biosensors can be classified according to the transduction, which include: optical detection, electrochemical detection, mass-based detection and voltaic and magnetic detection[1-2], as can be seen in the scheme shown in Figure 2.

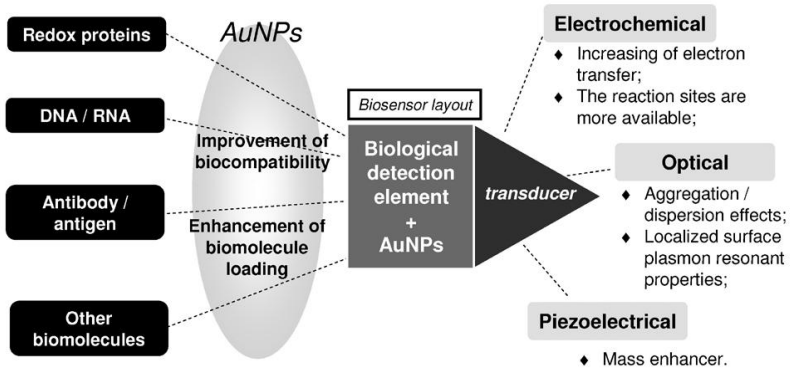

Figure 2 – Examples of the use of Au NPs in biosensors[2].

This work focuses on the optical transduction due to the unique optical properties of Au NPs, and in the next sections only this type of response will be considered.

1.2. Gold nanoparticles in biosensing

Au NPs have emerged as favorite nanoparticles for bio-applications due to their low toxicity, biocompability, dimensions, easy surface modification and due to their optical properties associated to the Surface Plasmon Resonance (SPR)[2].

The SPR of Au is influenced by the size and shape of particles and also by the refractive index of the surrounding medium and the distance between neighboring nanoparticles. The SPR results from the interaction between the electromagnetic radiation and the Au nanoparticle, that results in an oscillation frequency of the conduction electrons forming a dipole, as shown in Figure 3, which result in an absorption band in the visible spectrum[9].

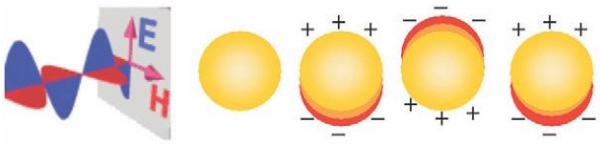

Figure 3 – Scheme illustrating the interaction of electromagnetic radiation with a metal nanosphere[9].

The SPR in Au NPs allows their use to identify the interaction between the analyte and the receptor. This is because aggregation of Au NPs result in changes of the SPR band[1]. Indeed, this phenomena can be easily observed by naked eye: when Au NPs dispersed in water present a red color, but when aggregation is induced the color changes to purple or blue depending on the aggregation state. Examples of the use of this property include the recognition of a specific DNA strand, as well as the system Avidin-Biotin, which will be discussed in the next sections.

1.2.1. Specific recognition of nucleic acids using Au NPs

Au NPs can be functionalized with a single strand of DNA that in the presence of the complementary strand leads to hybridization. For example, Sato *et al*[10] reported that Au

NPs functionalized with DNA hybridize with the complementary sequence, reducing the repulsive interaction in the Au NPs and causing aggregation, as illustrated in Figure 4.

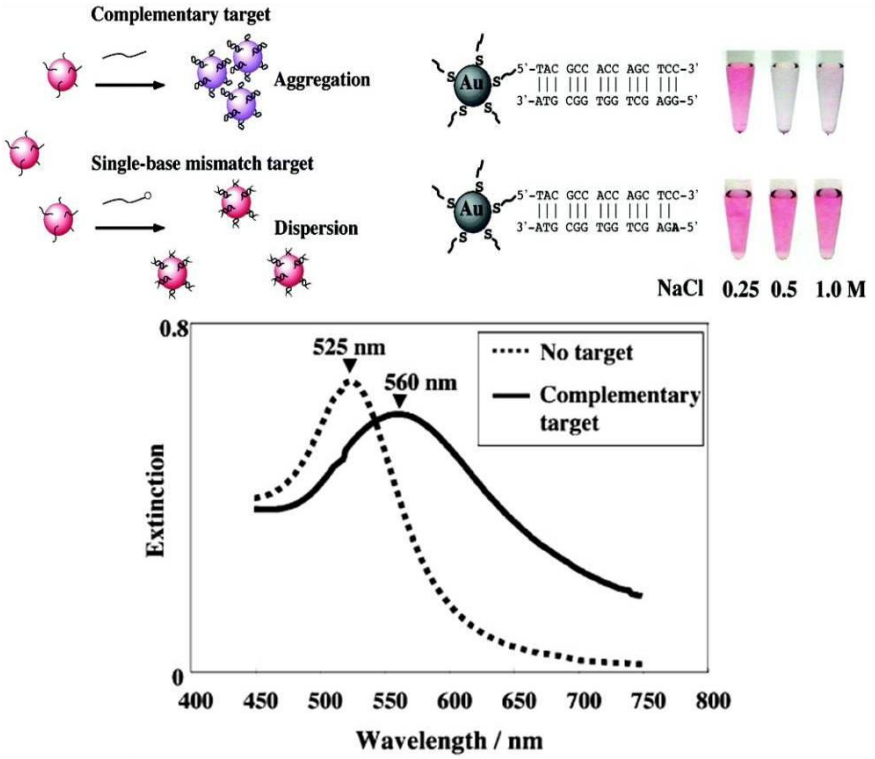

Figure 4 – Illustration of the results obtained by Sato *et al*[10]. (top) Aggregation behaviours of the DNA-gold nanoparticles at various NaCl concentrations at room temperature; and (bottom) the corresponding visible spectra (0.5 M NaCl).

A method that allows measurement of the length of DNA strand was reported by Storhoff *et al*[11]. They have modified two sets of Au NPs (A and B) with DNA and the complementary sequence had at each end the complementary sequence of A and B (see Figure 5). They observed different aggregation profiles depending on the DNA complementary length. For the small strand aggregation occurred faster and a red shift (from 524 nm to 581 nm) occurred; for the bigger strand the aggregation takes more time and the shift to red is not so big (from 524 nm to 540 nm).

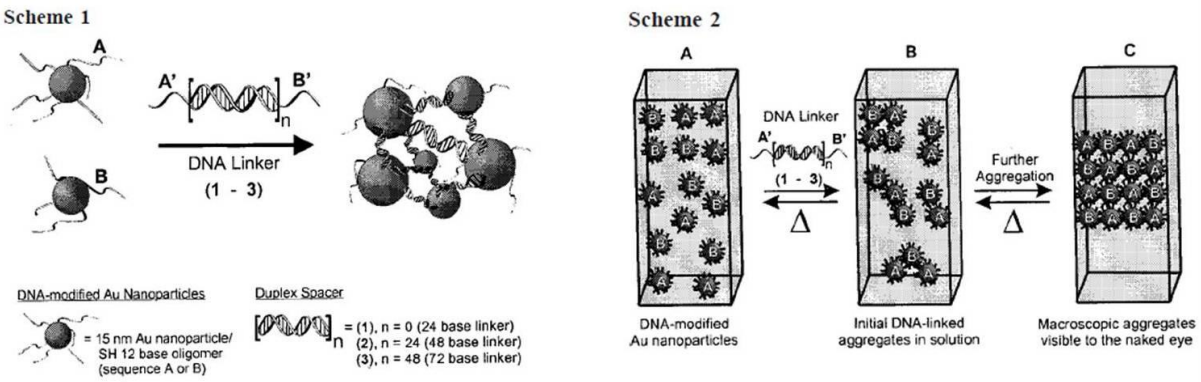

Figure 5 – Illustration of scheme used in the work of Storhoff *et al*[11]. Scheme 1 - DNA-Linked Au nanoparticles assemblies from 24, 48 and 72 base pair linkers; Scheme 2 – behaviour of the DNA-Linked Au nanoparticles assemblies in the presence of DNA linker.

1.2.2. Avidin-Biotin system for application in biosensing with Au NPs

Avidin is a glycoprotein (~67 kDa) that is positively charged (isoelectric point ~10) and is found as a minor component in the egg-white of birds, reptiles and amphibia. It is normally extracted from chicken egg-white as a highly stable homo-tetrameric protein (have four identical subunits, each one with 128 amino acids residues, whose sequence is known). Avidin can contain mannose and N-acetylglucosamine however deglycosylated avidins are expected to have lower nonspecific binding. Avidin binds up to four molecules of biotin, in a non-covalent interaction which is extremely tight, having a affinity constant of 10^{15} L/mol. This is among the highest affinity constant reported, three to six orders of magnitude higher than that of typical antigen-antibody complexes. The high affinity ensures that once the complex formed, it is not disturbed by changes in a wide pH range or by the presence of chaotropics agents or manipulations such as multiple washings. Moreover, when the complex is immobilized it ensures that the binding is directed to the target of interest[12-13].

Biotin is a small molecule with 244.31 Da that is known as vitamin H (Figure 6). Several biotinylation reagents (active biotin derivatives) have been developed to facilitate the labelling of proteins and carbohydrates. Hence, theses biomolecules can be introduced as a component in the system biotin-avidin[13]. Biotin can be

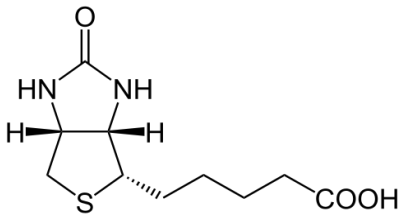

Figure 6 – Structure of biotin.

easily anchored to compounds that contain amine groups using a carbodiimide which mediates the formation of an amide linkage between a carboxylate group and an amine[14]. The reaction scheme can be seen in Figure 7.

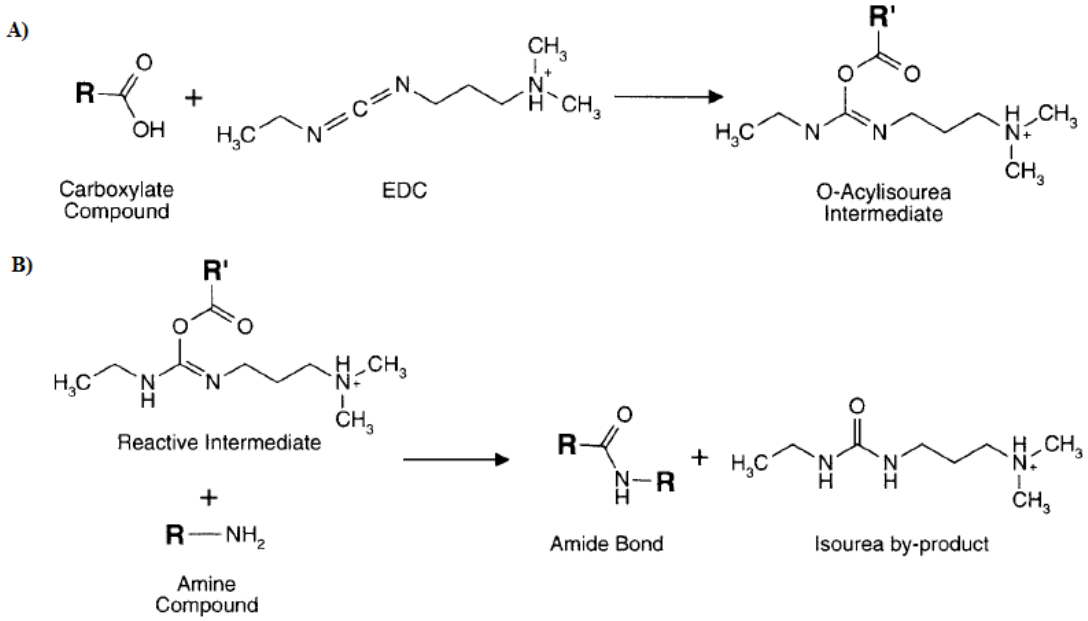

Figure 7 – Representation of the reaction between a carboxylate group and an amine group, using *N*-(3-dimethylaminopropyl)-*N'*-ethylcarbodiimide hydrochloride (EDC) as a mediator agent[14].

These molecules are also interesting because they are cheap and are commercially available with a high purity. Also there is a large collection of derivatized avidin (e. g. with fluorophores, enzymes, metals, proteins) that contribute to the use of this system in many applications[13]. The interaction between avidin and biotin shows characteristics that make them an ideal system in diverse applications, such as protein purification, enzymology, immunoassays, nucleic acid hybridization techniques, cytochemistry, diagnostics and biosensors[12-13]. So their specific interaction, like in the case of DNA, is very interesting in the studies of Au NPs as biosensors because it allows induce and control the aggregation state of biotinylated Au NPs in the presence of avidin, therefore the response can be followed by colorimetric tools.

Kohut *et al.*[15] showed the possibility of controlling the aggregation rate and the size of aggregation by controlling the experimental time, degree of biotinylation and avidin concentration. Figure 8 shows the Au NPs functionalization with biotin and subsequent interactions with avidin.

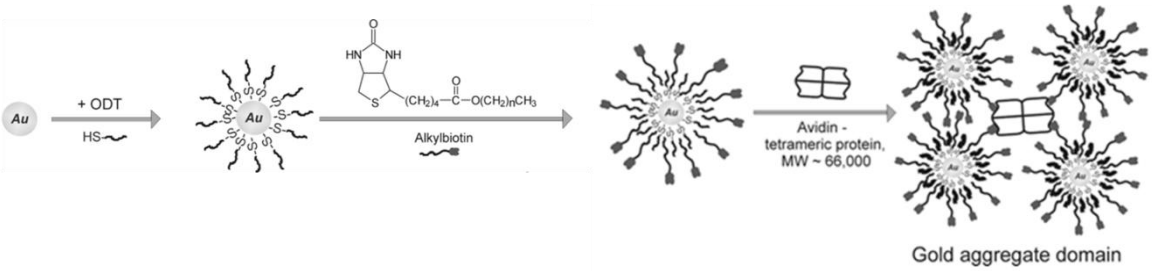

Figure 8 – Illustration of gold nanoparticles functionalization with biotin and the interaction with tetrameric avidin by Kohut *et al*[15].

An important contribution to be mentioned though not involving avidin but streptavidin (which is a protein similar to avidin) is the work of Aslan *et al* 2004 [16] studied the aggregation of biotinylated gold nanoparticles with streptavin, as illustrated in Figure 9. The authors functionalized gold nanoparticle with biotin which formed aggregates in the presence of streptavidin, as a consequence of biomolecular recognition. The aggregation was found to be dependent on the concentration of streptavidin, biotinylated gold nanoparticles and the quantity of biotin per nanoparticle. With 24 nM streptavidin and 0.80 nM biotinylated gold nanoparticles the maximum aggregation was verified. They also observed reversible aggregation upon addition of free biotin. The free biotin competes with the AuNP-biotin-streptavidin and disaggregation occurs, along with the shift of the SPR band back to the initial peak (peak of biotinylated gold).

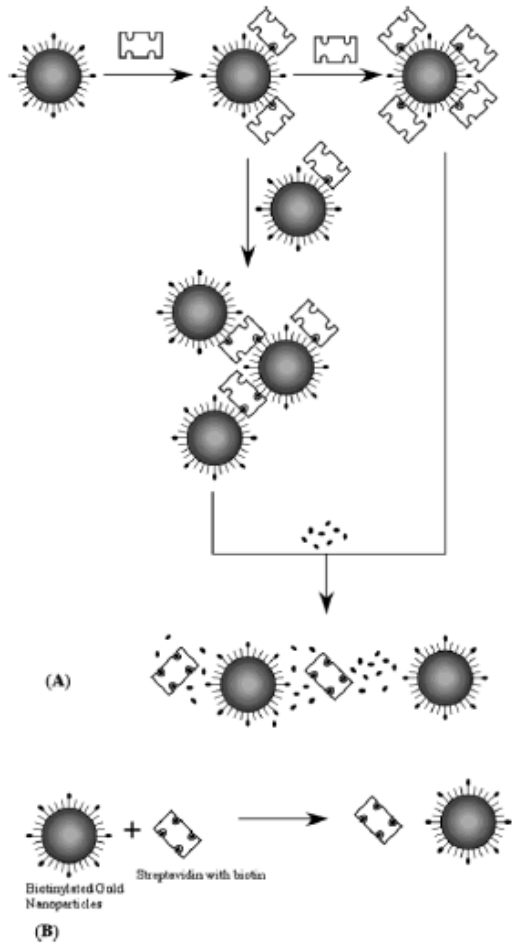

Figure 9 - Schematic representation of possible interactions of streptavidin with biotinylated gold nanoparticles. Addition of streptavidin to biotinylated gold nanoparticles can result in monolayer coverage of streptavidin on the surface of the nanoparticles, or it can induce nanoparticles aggregation. (A) Addition of soluble biotin leads to dissociation of streptavidin with subsequent disaggregation. (B) If streptavidin is saturated with soluble biotin it does not interact with the biotinylated gold nanoparticles [15].

2. Gold nanoparticles synthesis and surface modification

There are several methods to synthesize Au NPs which can result in different sizes and shapes of NPs. The most popular is the citrate method invented by Turkevich *et al.*[17] which involves the formation of Au NPs by the reduction of $HAuCl_4$ in boiling sodium citrate aqueous solution. This method yields NPs with diameters between ~10 and 100 nm. New methods to synthesize NPs, namely *in situ* methods, have also been published. One of these methods uses a polycation with amine groups, poly(allylamine) hydrochloride (PAH) as reducing agent which also stabilizes the Au NPs. This method yields NPs with diameters in the range from 5 to 50 nm[18]. The surface modification of Au NPs is very important, as was said before, because Au NPs are stabilized and can be subsequently functionalized. In this latter method, the synthesis and the stabilization of Au NPs occurs in one single step.

2.1. Citrate method

The citrate method allows the control of the average particle diameter in a wide range (~10–100 nm) by varying the concentration ratio between the gold salt and the sodium citrate [9]. For the preparation of gold nanoparticles by the citrate method, tetrachloroauric acid ($HAuCl_4$) is reduced by trisodium citrate ($Na_3[(COO)_3C_3H_5O]$). The citrate works as reducing agent and colloidal stabilizer. The proportion of the two reagents is very important because influences the size and shape of nanoparticles. The next equations summarizes the possible mechanism of the reduction of Au(III)[19].

First, the citrate is oxidized (equation 1) and the auric salt (Au^{3+}) is reduced to the aurous ion Au^{1+} (equation 2).

$$(^{-}OOCCH_2)_2C(OH)COO^{-} \rightarrow (^{-}OOCCH_2)_2CO + CO_2 + H^{+} + 2e^{-} \qquad \textit{(Equation 1)}$$

$$AuCl_3 + 2e^{-} \rightarrow AuCl + 2Cl^{-} \qquad \textit{(Equation 2)}$$

Kumar *et al.*[19] suggested the reduction from $AuCl_3$ species and not the $AuCl_4^-$ ion in solution. However, it is possible that $AuCl_4^-$, in spite of their stability, in solution can be in equilibrium with the $AuCl_3$ (equation 3).

$$AuCl_4^- \rightleftharpoons AuCl_3 + Cl^- \qquad \textit{(Equation 3)}$$

Next, Au^{1+} suffers disproportionation resulting in metal gold (Au^0) (equation 4). This step is facilitated by the formation of the complex between Au^{1+} and dicarboxy acetone (Figure 10) resultant of the citrate oxidation.

$$3AuCl \rightarrow 2Au^0 + AuCl_3 \qquad \textit{(Equation 4)}$$

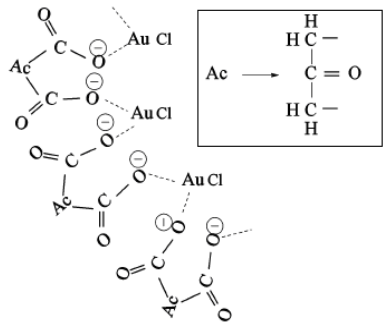

Figure 10 – Complex formation between Au^{1+} and the dicarboxy acetone[19].

The disproportionation reaction of Au^{1+} can occur at the surface of formed Au NPs and nanoparticles can grow further. It is important to note that with the citrate method the gold nanoparticles have a negatively charged surface due to the citrate anion adsorbed at the surface of nanoparticles.

2.1.1. Layer-by-Layer (LbL) method applied in nanoparticles

Nanoparticles science has become a central topic in colloid and materials science. Many requisites, such as composition, stability, storage, scale-up and also functional nanoparticles, have been studied. Typically, nanoparticles are synthesized in a medium containing a stabilizing agent, however surface modification is necessary to ensure adequate stabilization and functionalization of nanoparticles. Au NPs can be modified with diverse chemical groups, e.g. thiols[20-21] and PLGA-SS (disulfide bond-attached poly(L-

glutamic acid)[22] that confer negative charge, and DMAP (4-(dimethylamino)pyridine) that confer positive charges[23]. Another way to obtain stable Au NPs is coating NPs by the method Layer-by-Layer (LbL), introduced by Möhwald and Caruso[24] and applied for the first time to gold nanoparticles by Gittins and Caruso[21]. This kind of coating stabilizes the nanoparticles and also allows surface modifications that allow their functionalization[25]. The functionalization of NPs is a recent area of major interest due to the possibility of controlling the shell composition, charge, thickness and the possibility of labelling with molecules, such as antibodies and fluorophores. This allows the application of Au NPs in areas like pharmaceutical, biomedical diagnosis, drug deliver and gene deliver[26]**.** In the LbL method a charged particle is coated by alternating polycations and polyanions with intermediate washing and centrifugation steps to remove excess polyions[21, 24, 27] (see Figure 11).

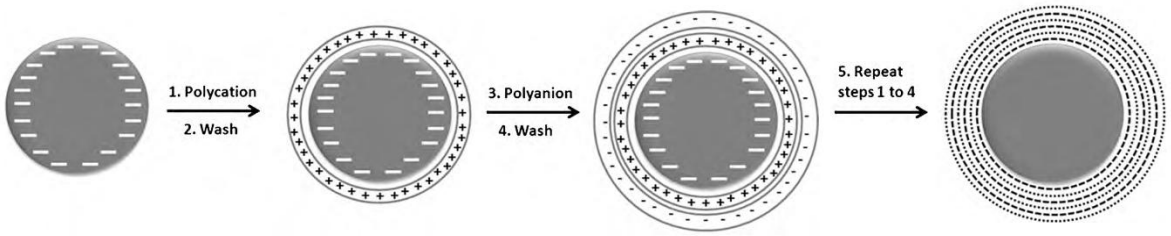

Figure 11 – Outline of the LbL method for the modification of nanoparticles, adapted from[26].

However, it is necessary to understand the experimental conditions to yield stable coated nanoparticles and avoid nanoparticles aggregation, i.e. ensure an efficient separation of nanoparticles after the coating**.** [26, 28].

Schneider *et al.*[28], coated Au NPs with 20 layers of PAH and PSS. They observed by visible spectroscopy that a red-shift of 0.5 to 10 nm which is related to the surface modification with the polyelectrolyte and a red-shift of 80 – 150 nm which is related to interparticle bridging and aggregation. They obtained a very stable dispersion of Au NPs with a diameter of 13.5 nm and noted the stabilization increased with increasing number of layers. Other studies to successfully modify nanoparticles were developed by Mayya *et al.*[29] and Dorris *et al.*[30].

In 2008, Schneider *et al.*[31] studied several parameters that control the formation of multilayers onto nanoparticles. This research included: 1) the adsorption of the first layer – PAH; 2) Determination of the surface charge of NPs and the minimum amount of required

citrate to have stabilized nanoparticles; 3) Determination of optimum excess of polyelectrolyte chains (PCs) during the adsorption of the first layer; 4) Effect of the degree polymerization and of the NPs concentration; 5) Consequences of stoichiometry of the polyelectrolyte and the NP; and the length of the adsorption chain of polymer during the build of multilayer; 6) Tunable layer thickness with Added Salt; and 7) Influence of the ionic strength on the dispersion stability. The authors monitored the colour of the colloidal dispersion, the position and intensity of SPR band as well as the diameter of the NPs by DLS measurements and TEM studies. For this study, Schneider *et al.* had to assume a parameter PCs/NP that is the ratio of polyelectrolyte chains per nanoparticles, and admit three possible situations: Regime I - excess of colloids (< 10 PCs/NP); Regime II - Equal charge proportion of NPs and polyelectrolytes (= 10 PCs/NP is equivalent to a stoichiometric to 1:1); Regime III - Excess of polyelectrolytes (> 10 PCs/NP).

In the first study (1) regarding the adsorption of the first layer – PAH, they concluded that for regime I (0.1 to 10 PCs/NP) the intensity of the Plasmon band decreased with a contribution of a band that appears at 600-650 nm, the red solution (0 PCs/NP) change to purple (2-4 PCs/NP), then change to blue (5 PCs/NP), and after some hours precipitation occurs as the result of strong aggregation (10 PCs/NP) and the solution turn black. They also observed an increase of NPs per aggregate when the amount of was PAH increased. For the transition of regime II (10 PCs/NP) to regime III (excess of PAH), they observed a shift of 1.5 – 2 nm of 4000 – 200 PCs/NP comparing with native NPs, and the intensity of the band at 600-650 nm increased when the excess of PAH decreased. For smaller excess, they observed the color, 100 PCs/NP was purple-red and changed to purple when the ratio decreased (40 PCs/NP), and changed again to bluish-purple (30 PCs/NP). With an excess in a ratio of 4000 – 200 PCs/NP the aggregation is negligence comparing with 9<PCs/NP<100. Figure 12 shows a scheme that helps to understand the influence of the proportion of polyelectrolyte chains per nanoparticle.

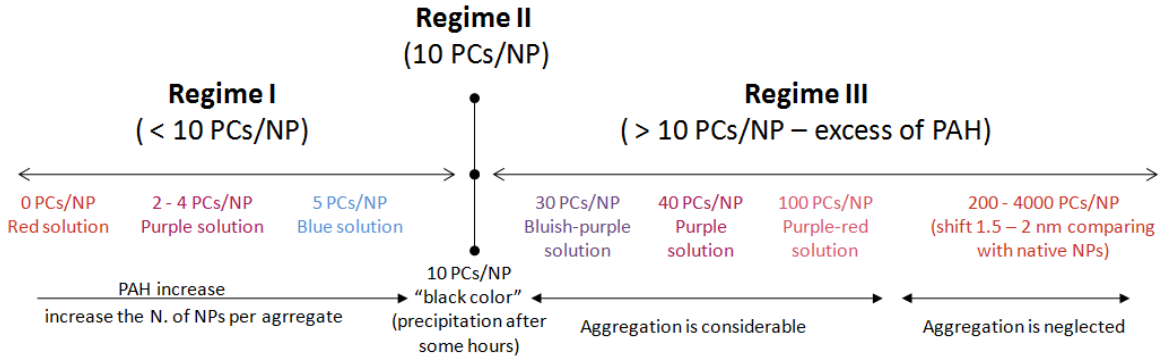

Figure 12 – Scheme of the influence of the proportion of polyelectrolyte chains per nanoparticle.

In a second study (2), they determined the surface charge of NPs and the minimum amount of citrate required to have stabilized nanoparticles. For the calculation they consider a 1:1 charge stoichiometry which is achieved with 10 PCs/NP. The determination of the optimum excess of polyelectrolyte chains during the adsorption of the first layer was the third study that they did. They verified that the optimum excess is 60 000 PCs/NP (λ =519 nm, 80 % recovery, 97% single nanoparticles, 2% aggregates with two NPs, 1% aggregates with more than three NPs). After that, Schneider *et al.* studied the effect of the degree of polymerization and of the NPs concentration. They utilized as long chains PAH and PSS 70 000 g/mol, and as short chains PAH 15 000 g/mol and PSS 13 500 g/mol. They observed that short chains cause minor deviations and less aggregates than long chains. Long chains generate bridges and aggregates are easily formed, while short chains limit the bridging flocculation, as we can see in Figure 13.

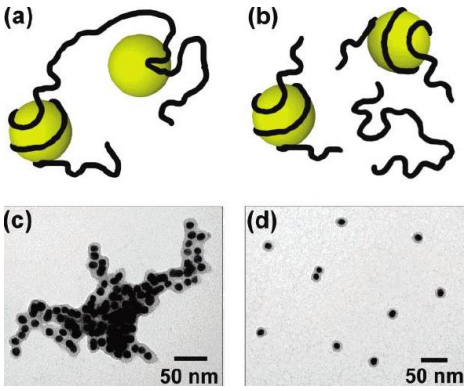

Figure 13 – Oversimplified representations of particles being aggregated by bridging flocculation (a) and being individually wrapped by polymer chains (b); Lower part shows electron micrographs of aggregated particles (c) and of particles predominantly ensheathed individually (d) [31].

For higher concentration of NPs (44nM), easily flocculation occurred via bridge formation, so more aggregates were formed causing a higher deviation of the SPR band. On the other hand, for lower concentration of NPs (6 nM) the shift was smaller and less flocculation via bridge formation were formed.

In brief, the optimized conditions for obtaining coated nanoparticles stabilized via the LbL (for the first adsorbed layer) are: PAH (15 000 g/mol) – 60 000 PCs/NP; and 3 nmol/L of Au NPs. Their conclusions were summarized in the diagram shown in Figure 14.

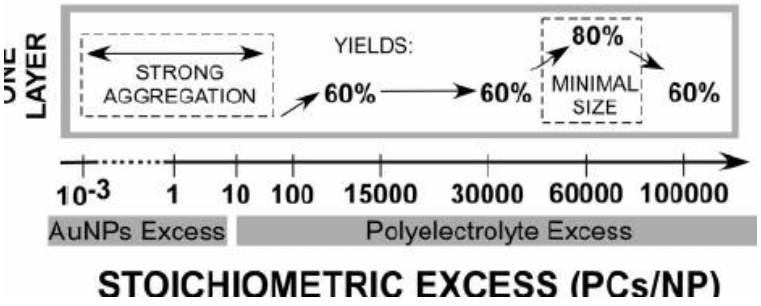

Figure 14 – General trends resulting from the studies of the effect of the proportion of the polyelectrolyte chains per nanoparticles[31].

As a general conclusion of Schneider *et al.* work, the excess of chains of polyelectrolyte per nanoparticle (PCs/NP) should be kept as low as possible, because a higher excess increases the wasted polyelectrolyte per adsorption step. Regime I results in an incomplete coating of the surface and a few polyions on the surface; Regime II should be avoided due to the proximity to stoichiometric conditions, unless the solution is diluted; Regime III results in a excellent coating and good stability of the suspension and avoids dilution; the drawback of this regime, is that in each step of adsorption there is an excess of polyelectrolyte that should be removed before the next adsorption step. This could be important for the functionalization of polyelectrolytes. A parameter of utmost relevance is the length of the polyelectrolyte chain (if the chain is too long the bridging flocculation is favoured; if the chain is too short the recovery yield of NPs is much reduced). As regards the concentration of NPs care must be taken. Whilst there is a need to have a high concentration of NPs in suspension, the lower distance between NPs favoures the bridging flocculation and should be avoided.

2.2. *In situ* method

Several reducing/capping agents for the synthesis of Au NPs have been reported, as reviewed by Dumur *et al.*[32] which include the use of microorganisms, plants extracts and physiological molecules, inorganic reagents and metal complexes, organic molecules, organic acids and salts, liposomes and polymers. Some of the reducing/capping agents in these studies contain the amine groups because they are present in several biological and environmental systems, such as amino acids and polymers[33-37].

Newman *et al.*[18] reported the synthesis of Au NPs using as reducing agent the amine group of PAH. Depending on the reaction conditions they controlled the generation of gold NPs in a size range between 5 -50 nm. In a previous work of these authors[34] it was proved that for the reduction of Au^{3+} three amine groups are necessary (equation 5). They showed the importance of the reduction potential of each amine group: amines have the reduction potential between that of the oxidation of Au^0 to Au^{+1}, and the reduction of $HAuCl_4$ to Au^0 and thus are candidates to be used as reducing agent.

$$HAuCl_4 + 3\ NR_3 \rightarrow Au^0 + 3NR_3^{+\bullet} + H^+ + 4Cl^- \qquad \textit{(Equation 5)}$$

Newman *et al.*[18] have also studied the kinetics of formation of Au NPs and showed the influence of the ratio between the PAH and the $HAuCl_4$ on the size of Au NPs, as can be seen in Figure 15. A PAH:$HAuCl_4$ ratio around 2 – 3 yields Au NPs with diameters around 15 nm.

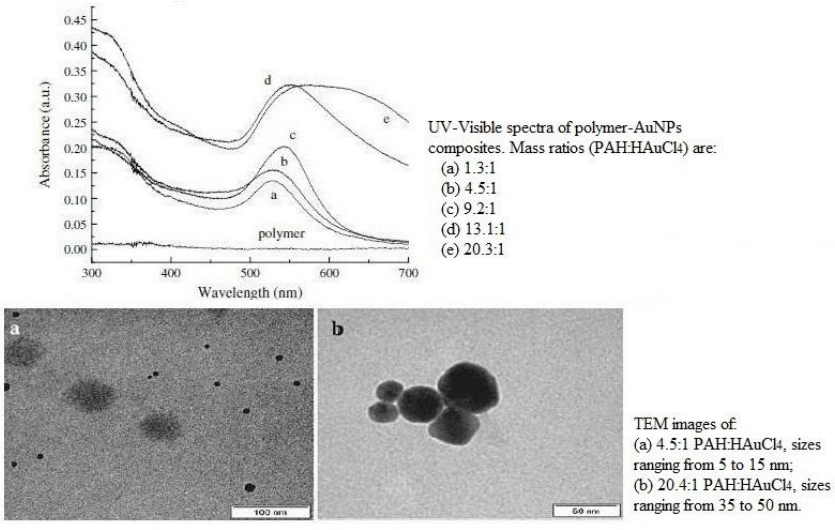

Figure 15 – Effect of the PAH:$HAuCl_4$ ratio on the diameter of Au NPs[18].

3. Luminescence as a tool in biosensing

Luminescence is an emission of ultraviolet, visible or infrared photons from electronically excited species[38]. The various types of luminescence can be classified according to the mode of excitation, as summarized in Table 1.

Table 1 - Types of luminescence [38].

Phenomenon	*Mode of excitation*
Photoluminescence (fluorescence, phosphorescence, delayed fluorescence)	Absorption of light (photons)
Radioluminescence	Ionizing radiation (X-rays, α, β, γ)
Cathodoluminescence	Cathode rays (electron beams)
Electroluminescence	Electric field
Thermoluminescence	Heating after prior storage of energy (e.g. radioactive irradiation)
Chemiluminescence	Chemical process (e.g. oxidation)
Bioluminescence	Biochemical process
Triboluminescence	Frictional and electrostatic forces
Sonoluminescence	Ultrasounds

3.1. Fluorescence

Fluorescence is a mode of luminescence where the excitation involves the absorption of photons, which brings the absorbing species to an electronic excited state. The fluorescence occurs when the species suffer relaxation with the emission of photons (see Figure 16), which is one of the possible physical effects resulting from the interaction of light with matter [38].

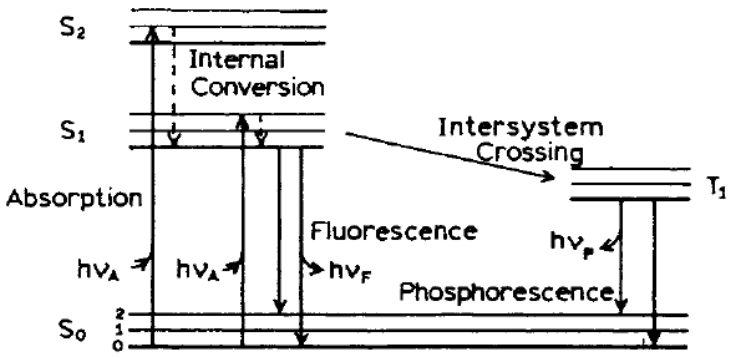

Figure 16 – Jablonski diagram [39].

When a molecule is excited by the absorption of a photon, it can return to the ground state with emission of fluorescence, but many other pathways for de-excitation are also possible, such as energy transfer [38], as illustrated in Figure 17.

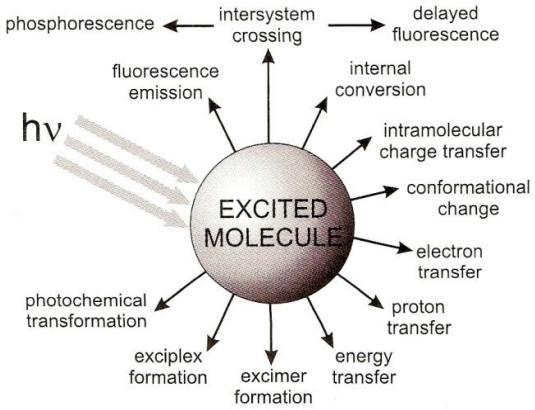

Figure 17 – Possible de-excitation pathways of excited molecules [38].

The fluorescence characteristics (decay time and/or fluorescence quantum yield) of excited species (M*) can be affected by the presence of quenchers (Q) as a result of competition between the intrinsic de-excitation and the intermolecular process, which include energy transfer [38]:

i) After excitation by a light pulse, the excited-state M* population, and consequently the fluorescence intensity, decrease more rapidly than in the absence of an excited-state interaction with quencher species.

ii) The fluorescence quantum yield is decreased. The loss of fluorescence intensity is called fluorescence quenching whatever the nature of the competing intermolecular process and even if this process leads to a fluorescent species (the word quenching applies only to the initially excited molecule).

The term *resonance energy transfer* (RET) also known as FRET (*fluorescence resonance energy transfer*) is one of the quenching effects. In this case, non-radiative transfer of excitation energy requires interaction between a donor and an acceptor. Therefore the emission spectrum of the donor overlaps with the absorption spectrum of the acceptor. As a result, several vibronic transitions in the donor have practically the same energy as the

corresponding transitions in the acceptor, as illustrated the diagram in Figure 18. The interactions may be long-range dipole-dipole interactions (Förster's mechanism) or short-range multi-polar interactions. For the Förster interaction the critical distance, Förster radius, is generally 15-60 Å [38].

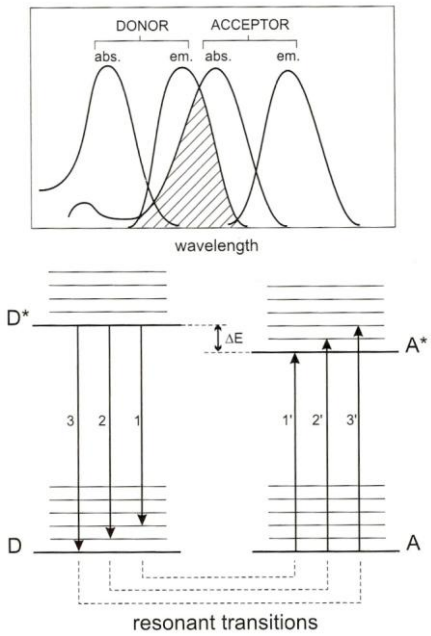

Figure 18 – Energy level scheme of donor (D) and acceptor (A) molecules showing the coupled transitions in the case where vibrational relaxation is faster than energy transfer (very weak coupling) and illustration of the integral overlap between the emission spectrum of the donor and the adsorption of the acceptor [38].

One example of application of the FRET effect is the work developed by Richter *et al.* [40], who studied the steady state Förster energy transfer in multilayer structures of films prepared by LbL. They used a single layer of PPV (poly(phenylene vinylene)) as donor, PAH/PSS layers as transparent spacer, and a single layer of dye labeled PAH as an acceptor. Rhodamine B and fluorescein were used as dyes. With the PAH/PSS layers they controlled the distance between the donor and the acceptor. Films without PPV when excited at 405 nm (λ_{ex} PPV = 405 nm) did not have fluorescence. They also found that when rhodamine was at a distance of 20 Å from the PPV layer the intensity decreased and the peak of PPV and the peak of rhodamine (580 nm) appeared. For the fluorescein the same was observed. At a distance of 141 Å the intensity decreased and the peaks of PPV and of fluorescein (530 nm) appeared. But if the fluorescein was at a shorter distance (*d*)

more close (d=13 Å) only the peak of fluorescein appeared. So, they observed the energy transfer between fluorophores at differents distances using the LbL method.

Another group, Peralta *et al*. [41], also studied this energy transfer process but using three fluorophores. They constructed a film well compartmented from a set of polyelectrolytes which allowed them to have 3 layers with different fluorescent markers, as shown in Figure 19, and studied the energy transfer between these fluorophores, i.e. the FRET effect. From the first compartment, pyranine, transfers to the second, FITC, this in turn transfers to the third, Blue Nile.

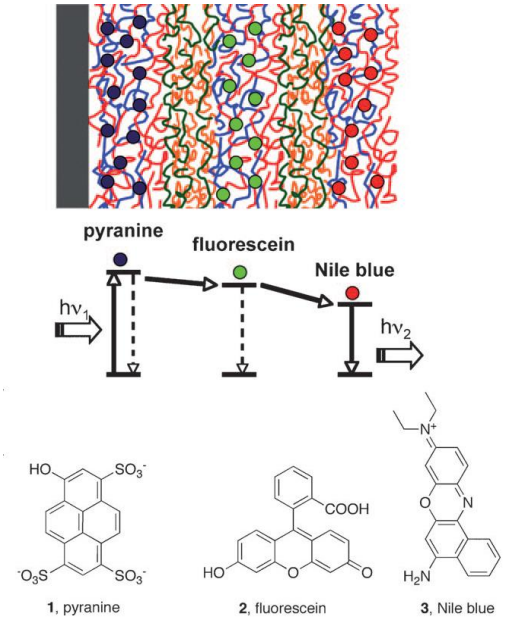

Figure 19 – Structure of nanocompartmentalized multilayers doped with complementary dyes allowing a cascade of FRET and chemical structures of the dyes[41].

Fluorescence spectroscopy has had a great success as an investigative tool in studying the structure and dynamics of matter of living systems because the fluorometric techniques have high sensitivity. Furthermore the specific characteristics of fluorescence due to the micro-enviroment of the emitting molecules, and the ability of some emitting molecules to provide spatial and temporal information (e.g. polarity, hydrogen bonds, pH, pressure, viscosity, temperature, quenchers, electric potential and ions) [38] make this a prime analytical tool in the field of biosensors.

As a consequence of the strong influence of the surrounding medium on fluorescence emission, fluorescent molecules are currently used as probes for the investigation of

physicochemical, biochemical and biological systems. Probes can be applied for example in polymers, solid surfaces, surfactant solutions, biological membranes, vesicles, proteins, antibodys, nucleic acids and living cells[38]. There are three classes of fluorescent probes: intrinsic probes, extrinsic covalently bound probes and extrinsic associating probes. The extrinsic covalently bound probes usually have functional groups, such as isothiocyanates, chlorotriazinyl derivates, hydroxysuccinimido active esters, which allow labelling very easily. Derivatives of probes, such as fluorescein, rhodamine and erythrosine, with the functional groups referred above are the mostly used[38].

3.2. Fluorescein Isothiocyanate (FITC)

Fluorescein isothiocyanate (Figure 20) is the most widely used extrinsic fluorescence probe in bioscience. Fluorescein has a high extinction coefficient, large fluorescent quantum yield, and methods for its conjugation to biomolecules are well established[42-43].

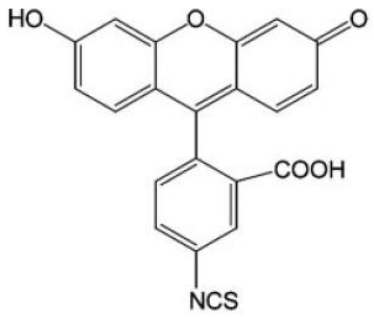

Figure 20 – Chemical structure of FITC, NCS –isothiocyanate group[43].

The isothiocyanate group allows an easy linkage to amine groups yielding a thiourea group. The reaction occurs at alkaline pH values where the amine group is unprotonated[14], as can be seen in Figure 21.

Figure 21 - Representation of the reaction between the amine group and the isothiocyanate group[14].

The fluorescein chromophore in aqueous solutions is well known to take several forms (cationic, neutral, anionic and dianionic – see Figure 22) which make the spectra of solutions dependent of the pH (Figure 23). In fact FITC is also known as a pH probe [43] hence it is very important to control the pH of medium.

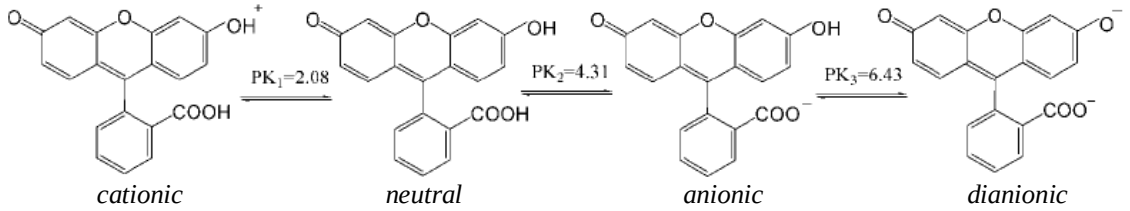

Figure 22 – Representation of fluorescein structures at different pH values [44].

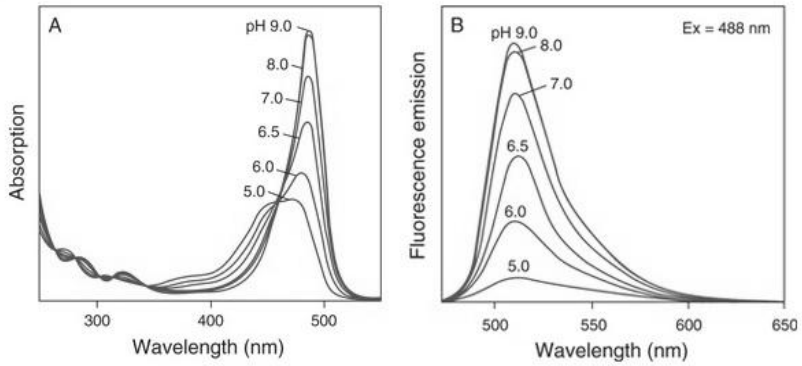

Figure 23 - The pH-dependent spectra of fluorescein. A) absorption spectra and B) emission spectra[45].

3.3. Quenching fluorescence and gold nanoparticles

As already mentioned, the fluorescence is affected by the presence of quenchers. When a fluorophore is close to a metal surface energy transfer from the fluorophore to the metal occurs, resulting in fluorescence quenching. For example, gold nanoparticles have been applied as quenchers. Surface Plasmon (SP) modes have been utilized to promote resonant energy transfer or excitation enhancement, resulting in a higher degree of quenching or emission, reflecting binding and unbinding states of analytes to sensors. This allows monitoring of receptor/ligand binding and release events through changes in fluorescence intensity or lifetime of the fluorophore [46].

In 2005, Kato *et al.* [46], extended the study of Richter *et al.*[40] to evaluate the quenching effect of gold nanoparticles on FITC and the biotin/avidin and biotin/anti-biotin systems. First, they studied the quenching dependence on the amount of Au NPs with a fixed distance between the Au NPs and the FITC-PAH layer. Between Au NPs and FITC-PAH a bi-layer of polyethyleneimine (PEI) and poly(sodium styrene sulfonate) (PSS) was deposited. It was found that increasing the deposition time, the adsorption of Au NPs increases (SP band around 540 nm) and the intensity of FITC peak at 528 nm decreases. Upon 9 minutes of deposition the quenching is considerable and after 20 minutes they achieved 90% of quenching. However, for 20 minutes, a red-shift of the SPR band was observed due to the packing. The second study was the quenching dependence on the distance between the Au NPs and FITC-PAH layers with a fixed Au NPs adsorption (20 minutes). Between the Au NPs and the FITC-PAH they deposited various multilayers of (PSS/PAH)*n*, varying the *n* ($n = 0 – 5$). They found that each PSS/PAH bilayer has 2.7 nm, and with the increase of *n*, the fluorescence intensity increased too. They calculated the energy transfer dependence on the distance (*d*) between acceptor and donor and verified that the obtained value ($d = 14.9$ nm) was much larger than the typical value involved in the Förster-type energy transfer (2 – 6 nm). This can be due to the interpenetration of adjacent layers in the multilayer film. For a biosensor, it is expected that this large critical distance would contribute to the quenching of fluorophores that are conjugated to large proteins, e.g. immunoglobulin G, with a size about 10 nm, making the system attractive for such studies.

In 2006 Schneider *et al.*[47] showed the dependence of the distance between the nanoparticles of gold and two fluorophores (FITC and LISS) on the quenching effect, as illustrated in Figure 24. This distance was achieved by coating the nanoparticles with polyelectrolytes - PAH (Mw 15 000 g/mol) and PSS (Mw 13 400 g/mol), by LbL. They found that at a distance of five bilayers (PAH / PSS), which corresponds to a distance of about 4 nm, the quenching is notable. Next, when the Au NP core was dissolved with KCN, the band intensity of FITC increased until the total dissolution of AuNPs was verified by the absence of the absorption peak. They also found, that increasing the distance between the fluorophore and the core the fluorescence signal increased and the quenching is still significant at n = 10 (8 nm of distance).

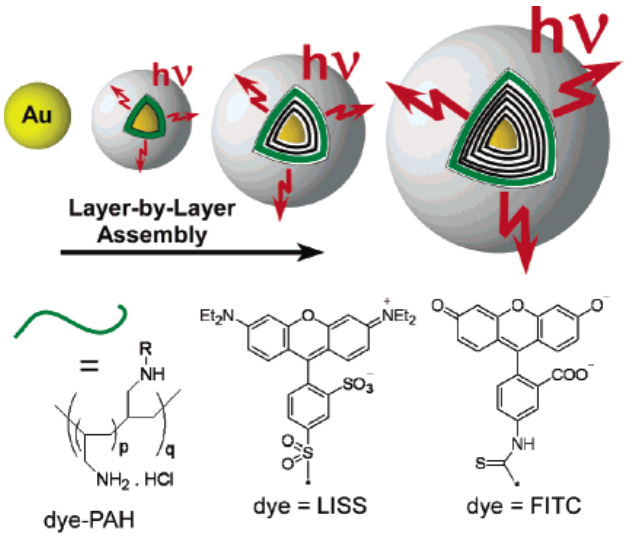

Figure 24 – Layer-by-Layer assembly for the construction of core-shell nanoparticles containing fluorescent layer [47] .

Parallel to the studies mentioned above, Aslan *et al.* 2004[48] and 2006[49], studied the fluorescence quenching effect using biotinylated gold nanoparticles, but instead of using avidin they used anti-biotin labeled with a fluorophore (Alexa™ 488). They observed that, immediately, after addition of biotinylated gold nanoparticles to a solution with anti-biotin a strong decrease of the emission intensity is observed. According to Aslan [48] this decrease of emission can be due to three combined effects: 1) a dilution effect after adding an aliquot of biotinylated gold nanoparticles; 2) strong absorption/scattering caused by the presence of biotinylated gold nanoparticles; and 3) actual quenching of the emission intensity by the gold surfaces as the antibody binds to biotin groups on the surface of the nanoparticles. However, they have also observed that after this quenching effect, if they added to the solution free biotin the fluorescence emission increased, see the illustration in Figure 25.

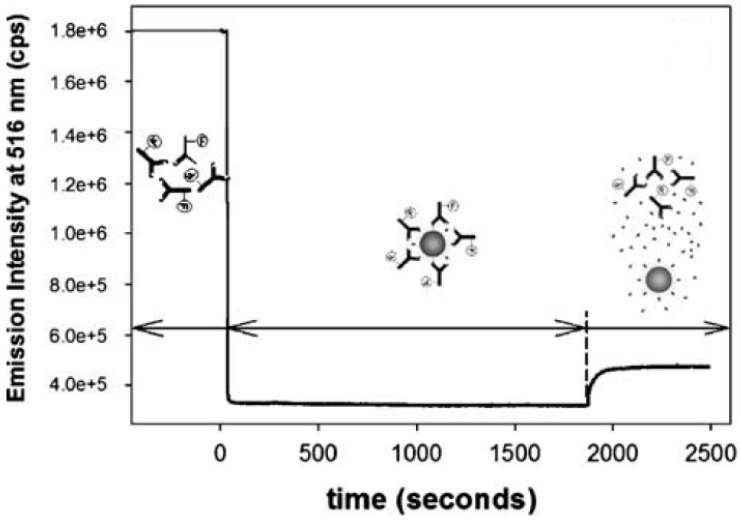

Figure 25 – Time progression of the emission intensity from Alexa™ 488-labeled antibiotin and its interaction with biotinylated gold nanoparticles [49].

In addition, Aslan *et al.* [49] observed a non-radiative energy transfer from the Alexa™ 488-labelled antibiotion molecules to the biotinylated gold nanoparticles and the energy transfer is terminated when soluble biotin interacts with Alexa™ 488-labelled antibiotin. So, this technique offers a rapid, sensitive, and selective detection of small molecules through measurements of the emission intensity and/or lifetimes of the excited states of fluorescent molecules.

4. Context of the work

Nanotechnology has gained a major importance in biosensing because it allows building bionanostrutured systems with high selectivity and sensitivity. So much effort in research is dedicated towards the synthesis of novel nanostructures for application in biosensors. Gold nanoparticles are the most studied type of NPs due to their unique optical properties and their easy surface functionalization.

In this research two methods of Au NPs synthesis have been studied: the standard citrate method and an *in situ* method. Several strategies to functionalize these Au NPs with a fluorophore (FITC) and biotin (Vitamin H) were performed and the optical response of the hybrid nanostructures towards a specific analyte (Avidin) was evaluated.

PART II

EXPERIMENTAL

PART II – EXPERIMENTAL

1. Reagents

Hydrogen tetrachloroaurate (III) trihydrate, 99.9+% ($HAuCl_4.3H_2O$), sodium citrate tribasic dehydrate, ≥ 99% ($Na_3C_6H_5O_7.2H_2O$), biotin, ≥ 99%, avidin from egg white ≥ 98%, fluorescein isothiocyanate isomer I (FITC), N-(3-dimethylaminopropyl)-N'-ethyl-carboiimide (EDC) and poly(allylamine hydrochloride) MW 15 000 (PAH) were purchased from Sigma-Aldrich. The water used throughout the work was ultrapure water purified using a Station 8000/Station 9000 purification unit.

2. Instrumentation

- The visible spectra of the colloids as prepared collected using quartz cells and a Jasco V-560 UV/VIS spectrometer. Water was used as reference.
- The fluorescence spectra of the colloids as prepared were recorded using quartz cells were obtained with a FluoroMax-3 Horiba Jobin Yvon spectrometer.
- 1 or 2 mL of the colloid was dried in an oven at 70 ºC. To the resulting solid residue KBr was added and pellets were prepared. The FTIR spectra were recorded using a FT Mattson 7000 Spectrometer, the resolution was 4 cm^{-1} after 256 scans.
- Transmission Electron Microscopy (TEM) and Scanning Electron Microscopy (SEM) micrographs were obtained using a Hitachi H-9000 microscope operated at 300 kV and a Field Emission Gun (FEG)-SEM Hitachi SU70 microscope, operating at 15 kV, either in the secondary electron and/or scanning transmission image modes, respectively. The samples were prepared by placing a suspension drop, containing the colloidal solutions dispersed in water, on a copper grid coated with an amorphous carbon film, and left to evaporate.
- The Zeta Potential and Dynamic Light Scattering (DLS) measurements were carried out on a ZetaSizer nano ZS Model Zen 3500 from Malvern using appropriate cells. For DLS measurements one drop of the colloidal solution was diluted in circa 1 mL of water. For zeta potential the colloids were analysed as prepared.

3. Synthesis of gold nanoparticles via the citrate method

10 mL of sodium citrate solution (38.8 mM) were added to 100 mL of $HAuCl_{4.3}H_2O$ solution (1mM) previously brought to a rolling boil with vigorous stirring. After 1h the heating was switched off and the agitation was kept overnight (see Figure 26). The concentration of the gold nanoparticle stock solution obtained was estimated according to the method published by Schneider *et al.*[47] to be around 12 nmol/L in particles. Before using, this solution was centrifuged in 1.5 mL eppendorfs for 1.5 h at 14 000 rpm. The supernatant was removed from each tube and replaced by 2-fold the initial volume of ultrapure water. The diameter of Au NPs determined by TEM images and DLS was 14.9 nm.

Figure 26 – Experimental set up for the Au/Citrate NPs synthesis.

4. Effect of the modification time of Au NPs with PAH

25 mL of the colloidal solution prepared in **3** was added dropwise, under vigorous stirring, to 25 mL of a PAH solution (5mg/mL) and the mixture was stirred for 14h. Aliquots (10 mL) were removed after 30 min, 1h, 1h30 min, 2h and after 14h (2h+12h). Each aliquot was centrifuged during 60 minutes at 14 000 rpm. The supernatant was removed and the precipitate re-dispersed in Milli-Q water. This centrifugation process was repeated one more time and the re-dispersed volume after this second centrifugation was adjusted in order to obtain a final volume of 5 mL for each aliquot.

5. Modification of PAH with FITC

PAH (208.6 mg) was dissolved in 20 mL of water and a (3M) aqueous KOH solution was added dropwise to the stirred solution to adjust the pH to 9.4. Next, fluorescein isothiocyante (8.4 mg) was added, and the solution was stirred overnight under exclusion of light. The mixture was dialysed (Spectra/Por® Dialysis Membrane MWCO 6-8 kDa from SpectrumLabs.com) against water to remove unreacted fluorophore (see Figure 27), in absence of light, the dialysate was monitored by optical spectroscopy. As this proved to be a very slow procedure, various attempts were made to remove unreacted FITC. These include precipitation in non-solvent, adjustment of ionic strength and use of co-solvents. Finally, addition of DMSO (~0.1 %V/V) the aqueous mixture proved very efficient upon one week.

Figure 27 - Dialysis of PAH-FITC to remove the excess of FITC.

6. Modification of PAH (PAHF) with Biotin

2 mL of biotin solution (1mg/mL) and 2 mL of EDC solution (2mg/mL) were added to 20 mL of a PAH solution (5 mg/mL, pH=5.5) or to 10 mL of PAHF (~5 mg/mL, pH=5.5). The solutions were mixed and stirred for 1h at room temperature. These solutions were not dialyzed and were used to modify Au NPs.

7. Surface modification of Au/Citrate NPs with PAH, PAHF, PAHB and PAHFB

10 mL of the colloidal solution prepared in **3** was added dropwise, under vigorous stirring, to 10 mL of a solution of PAH, PAHF, PAHB or PAHFB (~5mg/mL). The mixtures were

stirred for 2h at room temperature. Those with FITC were protected from the light. Each mixture was centrifuged during 60 minutes at 14 000 rpm. The supernatant was removed and the precipitate re-dispersed in Milli-Q water. This centrifugation process was repeated one more time and the re-dispersed volume after this second centrifugation was adjusted in order to obtain a final volume of 10 mL for each colloidal solution.

8. Synthesis of Au NPs *in situ* with PAH

The procedure **8.1.** was the first attempted to synthesize Au NPs *in situ* with PAH. These NPs had a diameter around 13 nm and the first colour (pink) started appearing after 2h. After 5h the colour remained deep pink. However, when the procedure was scale up from 10 to 50 mL it was not reproducible. Either the reduction did not occur or much longer reaction times (~12h) were required. So, were tried to have a tighter control of the conditions of synthesis using a jacket reactor (Figure 28) equipped with a mechanical stirred and a thermostatic bath. In this case (procedure **8.2**.) the reaction took 6h.

8.1.

In a round bottom flask (25 mL), 10 mL of a PAH solution (5 mg/mL) whose pH had been adjusted to 9 was boiled under vigorous stirring using an oil bath and magnetic stirrer. 0.4 mL $HAuCl_4$ (3.36 mM) was added to the previous solution (ratio PAH:$HAuCl_4$ ~2.5:1). After 5h the heating was switched off and the agitation was kept for 2 hours more. Then, the NPs *in situ* were centrifuged (60 min, 14 000 rpm) to removed excess of PAH, the supernatant was removed and replaced by water (final volume - 10mL).

8.2.

50 mL of a PAH solution (5 mg/mL) whose pH had been adjusted to 9 was transferred to a jacket reactor equipped with a thermostatic bath set at 90ºC and a mechanical stirrer set at 100 rpm. When the temperature stabilized at 90ºC $HAuCl_4$ (1.75 mL, 3.36 mM) was added (ratio of PAH:$HAuCl_4$ ~2.5:1) and the mixture was stirred for 6h at 90ºC followed by 2 more hours whilst cooling at room temperature. NPs *in situ* were centrifuged (60 min, 14

000 rpm) to removed excess of PAH. The supernatant was removed and replaced by water (final volume - 50mL).

Figure 28 - (left) Experimental set up for the synthesis of Au/PAH *in situ*; (right) detail of the reactor.

9. Synthesis/functionalization of Au NPs *in situ* with FITC

Several strategies were attempted to synthesize Au NPs with PAH and FITC in order to combine the need to have the amine groups deprotonated (i.e. pH around 9) in order to react with FITC and to prevent colloidal aggregation. Indeed, in a first attempt the pH of PAH-Au *in situ* (pH ≈ 6) raised to 9 using a KOH solution which led to immediate aggregation of the Au/PAH NPs and the solution turned blue. Therefore, various efforts to modify Au/PAH with FITC were performed and are described below (**9.1.**, **9.2.**, **9.3.**, **9.4.**).

9.1.

In a round bottom flask (25 mL), the pH of the PAHF solution (5 mL, ~5mg/mL) previously prepared in **5** was adjusted to 9 and was boiled under vigorous stirring using an oil bath and a magnetic stirrer, away from light. 0.2 mL of $HAuCl_4$ (3.36 mM) was added to the previous solution (ratio PAH:$HAuCl_4$ ~2.5:1) and the mixture was heated for 5h after switched off the heating agitation was kept for 2 hours more. Then, the NPs *in situ* were centrifuged (60 min, 14 000 rpm) to remove excess of PAHF. The supernatant was removed and replaced by ultrapure water (final volume - 5mL).

9.2.

PAH (208.6 mg) was dissolved in 20 mL water and a (3M) KOH solution was added dropwise to adjust the pH to 9.4. Next, fluorescein isothiocyante (8.4 mg) was added, and the solution was stirred overnight under exclusion of light. Next, this solution was boiled under vigorous stirring using an oil bath and magnetic stirrer, under a exclusion of light, and a 0.8 mL $HAuCl_4$ (3.36 mM) was added to the previous solution (ratio PAH:$HAuCl_4$ ~2.5:1). After 5h the heating was switched off and the agitation was kept for 2 hours more. The ensuing NPs *in situ* were centrifuged (60 min, 14 000 rpm) to remove excess of PAHF and FITC. The supernatant was removed and replaced by ultrapure water (final volume - 20mL).

9.3.

5 mL of a PAH solution (5mg/mL) whose pH had been adjusted to 9 was added to 1 mL of aqueous FITC solution (1mg/mL) and the mixture was stirred overnight, under exclusion of light. Next, 0.2 mL $HAuCl_4$ (3.36 mM) was added to the previous solution and the reaction mixture was heated for 6h. Upon switching off the heating the agitation was kept for 2 hours more.

9.4.

As prepared Au/PAH NPs as described in **8.1.** or **8.2.**, i.e. without being submitted to any centrifugation/re-dispersion, were placed in a beaker and 1 mL of aqueous FITC solution (1mg/mL) was added. The mixture was stirred overnight under exclusion of light. Then, the NPs *in situ* were centrifuged (60 min, 14 000 rpm) to remove excess of PAH+F and FITC. The supernatant was removed and replaced by ultrapure water.

10. Modification of Au/PAH and Au/PAH+F *in situ* with Biotin

0.5 mL of biotin (1mg/mL) and 0.5 mL of EDC (2 mg/mL) were added to a previously prepared solutions of Au/PAH or of Au/PAH+F (12 mL). The mixtures was stirred for 1 hour and then centrifuged (60 min, 14 000 rpm) to remove the unreacted biotin. The supernatant was removed and replaced by water (final volume = 12mL).

Note that for an easy comparison of the results, Au/Citrate/PAH NPs were also functionalized by the procedure followed for the Au/PAH NPs. Hence two more sets of nanostructures where synthesized. They are Au/Citrate/PAH+B and Au/Citrate/PAHF+B. The "+" means that the functionalization of PAH is after the surface modification of the Au NPs. The schemes in Figure 29 and Figure 30 summarize the various strategies followed for the preparation of the hybrid nanostructures prepared.

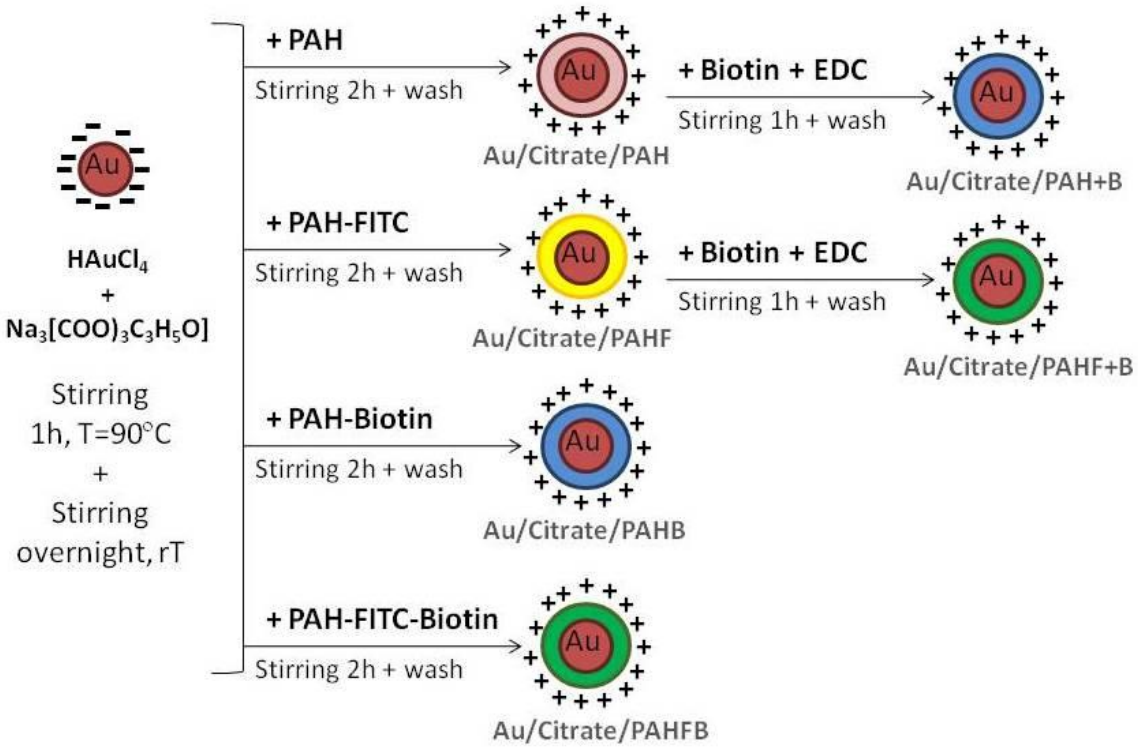

Figure 29 – Scheme of the functionalization of Au/Citrate/PAH NPs.

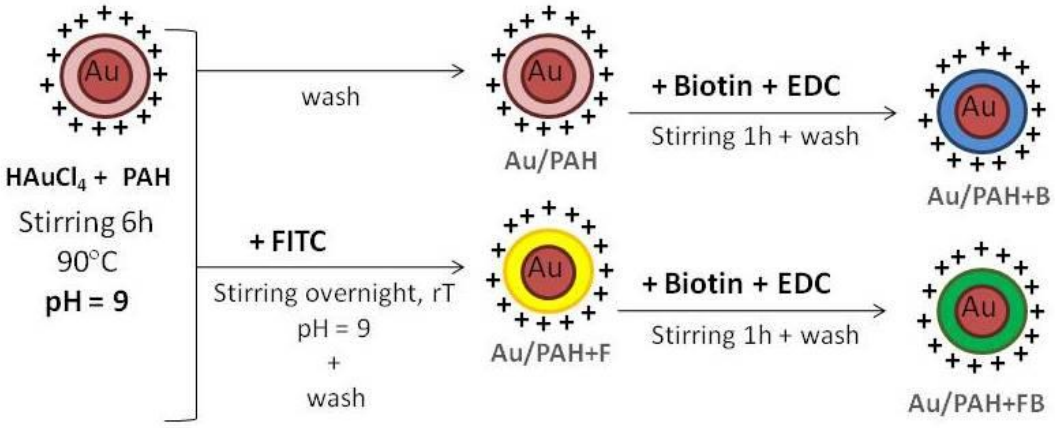

Figure 30 - Scheme of the functionalization of Au/PAH NPs.

(Note: Au/PAH+F results from the **9.4.** procedure)

PART III

RESULTS AND DISCUSSION

PART III - RESULTS AND DISCUSSION

1 – Synthesis and characterization of Au and PAH assemblies

The importance of using Au NPs in biosensors has been increasing due to their optical characteristics that are very sensitive to changes of the surrounding medium. The common method to synthesize gold nanoparticles is the citrate method introduced by Turkevich *et al.*[17]. This method allows the synthesis of Au NPs with diameters around 15 nm using the right ratio between the gold salt and the reducing agent (citrate). The resulting NPs can be functionalized if they have been previously modified with different chemical groups[20-23]. One way of achieving this modification is via the electrostatic interactions between Au/citrate, that have negative charge, and polycations, using the LbL method, introduced by Caruso *et al.*[24], which results in a core-shell structure.

In previous work developed in the group Au NPs with 15.4 nm were modified by the LbL method using polyelectrolytes with high molecular weights, i.e. Mw PAH = 56 000 and Mw PSS =70 000. However, in the literature it was found that using polyelectrolytes with smaller Mw reduces the number of aggregates of Au NPs as the bridging flocculation during polyelectrolyte adsorption is prevented. So we can obtain individually modified Au NPs using PAH with Mw = 13 000 and this allows enhancing the stability of the colloid. Another aspect very important in the aggregation state is the proportion between the amount of polyelectrolyte chains and the amount of NPs, i.e. the stoichiometry which was studied in depth by Schneider *et al.*[31].

A different way to obtain this core-shell structure is to synthesize *in situ* the Au NPs using the polyelectrolyte as a reducing and stabilizing agent. *In situ* synthesis using PAH is possible because the amine groups of the polication work as reducing agent and the Au NPs stay confined inside of PAH. Just as noted above it is very important the ratio between the gold salt and the reducing agent (amine groups), as described by Kumar *et al.*[19], but more details will be discuss in **1.2.**.

The synthesis of Au NPs via the citrate and the *in situ* methods were explored in this work. The first Au NPs were obtained via citrate method and modified with PAH by electrostatic interactions (Au/citrate/PAH) and will be discuss in **1.1.**. In **1.2**., the second method to

synthesize Au/PAH *in situ* will be discussed. Finally the two methods will be compared in section **1.3.**.

1.1. Assemblies of PAH-Au from Au/citrate colloids (Au/Citrate/PAH)

Au NPs were synthesized by the citrate method which confers a negative charge to the Au NPs surface. This colloid was then modified with a cationic polyelectrolyte (PAH). The PAH can then be easily functionalized via reactions of the amine groups with fluorophores as well as other functional molecules, such as biotin (vitamin H).

1.1.1. Synthesis and characterization of Au/Citrate/PAH

The first step was to find the optimum contact time for PAH adsorption onto Au NPs. According to the method available in the literature[28, 31] 2h under vigorous stirring followed by 12h under reduced agitation were required to modify Au NPs with PAH. As this procedure was found too long a simple preliminary test was carried out to verify the needed of the extra 12h. Figure 31 presents the visible spectra of Au/Citrate NPs and Au/Citrate/PAH upon different modification times. Differences in the intensity of the maximum absorbance between each sample are related to Au/Citrate/PAH collected after centrifugation. Thus 30 min and 1h of stirring led to less NPs as compared to 1h30, 2h and 2h+12h. From these spectra and the data summarized in Table 2 it can be concluded that the time of modification does not influence the surface Plasmon resonance (SPR). The SPR of Au/Citrate NPs is at 521.5 nm and when they are modified with PAH a small shift around 1 nm occurs due to the presence of PAH which causes a slight change in the environment surrounding the Au NPs. However, the zeta potential measurements showed that longer contact time of PAH with Au NPs led to a slight increase of the charge density. However, since the difference of zeta potential values is not significant between 2h and 2h + 12h, in the following studies the contact time was always 2 hours.

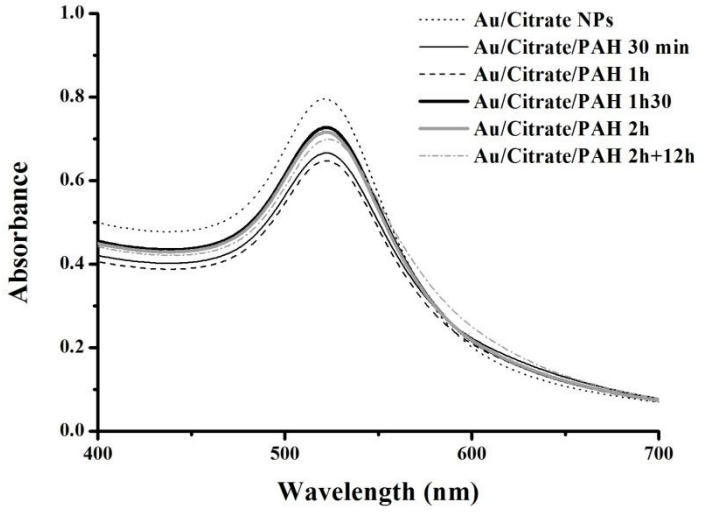

Figure 31 – Visible spectra of Au NPs synthesized by the citrate method and of Au NPs modified with PAH with different times of agitation.

Table 2 – Wavelength values of the maximum of SPR, zeta potential values and its standard deviation (std) of Au/Citrate NPs and modified with PAH for different contact times.

	λmax (nm)	ζ potencial (mV)	std (mV)
Au/Citrate NPs	521.5	- 38.40	11.53
Au/Citrate/PAH 30min	522.0	+ 41.75	15.40
Au/Citrate/PAH 1h	522.5	+ 40.35	12.05
Au/Citrate/PAH 1h30	523.0	+ 46.00	21.65
Au/Citrate/PAH 2h	522.5	+ 45.25	15.55
Au/Citrate/PAH 2h + 12h	523.0	+ 50.85	11.55

The diameter of the Au/Citrate/PAH nanocomposite was analysed by absorption spectroscopy and TEM which also provided information regarding the morphology.

From the visible spectrum of Au/Citrate/PAH NPs shown in Figure 31 the maximum peak at 522 nm indicates the presence of nanoparticles with diameter around 15 nm. This value was confirmed by TEM (d=14.9 ± 2.8 nm), see Figure 32. DLS measurements were also performed but it was difficult to conclude about the size of a single NP due to the aggregation of NPs and/or agglomerates of PAH. For the Au/Citrate NPs an average diameter of 16.2 nm was obtained considering the size as function of the number of

particles. Yet for Au/Citrate/PAH NPs the size is inconclusive (Annexe A). Regarding the modification of Au/Citrate with PAH, this was proved by the zeta potential measurements. The value of zeta potential for Au/Citrate was -34.03 mV, as expected, and when modified with PAH the surface charge changed to + 59.77 mV. This indicates that surface modification was achieved. Furthermore, in the TEM images the presence of a layer of ca 1.5 nm around the Au NPs can be seen confirming the presence of PAH. A layer around Au NPs was also observed by Schneider *et al.*[47] though they measured a bi-layer (PAH/PSS) with a thickness of 1.5 nm. Even so notice should be made to the fact that there are some NPs with this layer but for some NPs it can not to be seen.

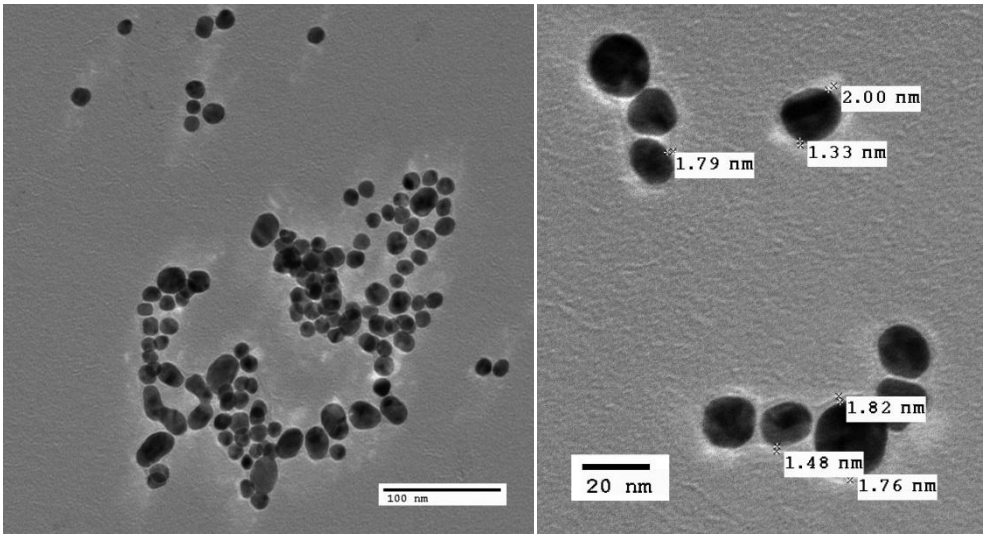

Figure 32 - TEM images of Au/Citrate/PAH.

1.1.2. Functionalization and characterization of PAH with FITC and biotin

To functionalize Au/Citrate/PAH with FITC and biotin, first the PAH was functionalized and then Au/Citrate NPs were modified with the functionalized PAH. However, there were some problems regarding the separation of PAH labelled with FITC (PAHF) and free FITC. Following Schneider's[47] procedure the separation was made by dialysis however this took over one month. To overcome this time constraint other ways for this separation were tried. First, by centrifugation using a high speed (20 000 rpm), low temperature (4ºC) and long centrifugation times (3 x 20 min). Unfortunately, the amount of precipitate was very small and it was very difficult to remove the supernatant without removing the precipitated. Then the separation by the precipitation with a non solvent and also varying

ionic strength was attempted. Ethanol, methanol and toluene which do not dissolve the PAH and dissolve FITC were tested. Yet, the precipitation of the PAHF (see Figure 33) did not occur. The precipitation with KCl was also unsuccessful (not shown).

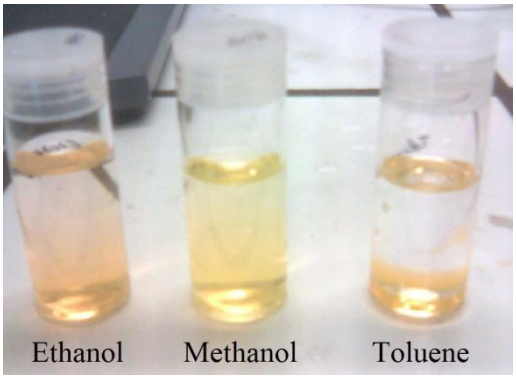

Figure 33 – Mixture of PAHF and excess of FITC dissolved in three different solvents (ethanol, methanol and toluene).

Yet in parallel, the dialysis against water was running but very slowly. As the other purification attempts failed a new set of tests was carried out this time regarding the dialysis conditions. A FITC solution at pH=9.4 (the pH of the reaction between the isothiocyanate group of FITC and the amine group of PAH) was introduced in dialysis membranes which were dialysed against (1) water, (2) 1:1 water/ethanol, and (3) Phosphate Buffer Saline (PBS) pH=7.4. From these three tests a difference in the FITC diffusion from the inside of the membrane (retentate) to the outside of the membrane (dyalisate) was observed, which can be explained by the difference in the solubility of FITC in each solvent. It was verified that after 150 minutes, in the case of PBS, the dialysate and the retentate had almost the same color, which means that the dialysate and the retentate were in balance. In the case of water and water:ethanol this color/balance was not observed, as can be seen in Figure 34. The separation was monitored over 150 minutes by analyses of the retentate by fluorescence spectroscopy. So it can be concluded that the FITC diffusion is greater using PBS, so the dialysis can be faster.

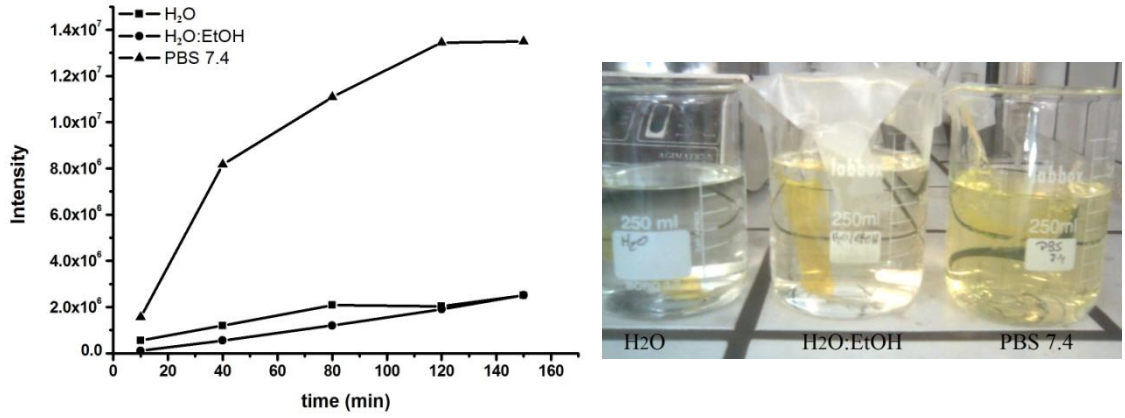

Figure 34 – (left) Monitoring of the dialysis by the emission band (λexc=488) of the dialysate, corresponding to the FITC during the dialisys against: water (H_2O), water/ethanol (H_2O:EtOH), and PBS pH=7.4.; (right) Photograph of the set up.

However, the use of salts would not to be viable because Au NPs tend to aggregate when the ionic strength of the medium is increased. In the meantime, another way to increase the FITC solubility and decrease the dialysis time which was reported by Kato *et al.*[46] was found. This involves the use of an aqueous solution of DMSO as the solubility of FITC increases in the retentate, diffusion of FITC is faster. So the PAHF prepared in this work was purified by dialysis against water with DMSO (~0.1% V/V) over a maximum of one week (changing the water 12 in 12 hours). It can be observed in Figure 35 the result of the dialysis using DMSO after the first 12h.

Figure 35 - Photograph of the dialysis with water/DMSO after 12h.

Regarding the functionalization of PAH with biotin, contrary to what was observed for FITC, it was not possible to assure that free biotin was completely dialyzed. However, in the case of biotin there is no problem if there is free biotin because being the last to be

added to the polyelectrolyte it will be removed by centrifugation step after the modification of Au/Citrate NPs with this functionalized polyelectrolyte.

Infra-red spectroscopy (FTIR) was used to confirm that covalent bonds between the FITC and biotin with PAH were formed, the bond between FITC and PAH is a thiourea and biotin forms an amide linkage with PAH. The spectra are shown in Figure 36.

The FTIR bands of PAH were identified using the works of Rivas *et al.*[50], Zucolotto *et al.*[51], Tristán *et al.*[52] and an infrared spectroscopy book[53]. The presence of the band at 1569 cm^{-1} in the spectrum of PAHF attributed to the thiourea group confirms the linkage of FITC to PAH. However, it should be noted that Lex *et al.*[54] referred the appearance of a band at 1550 cm^{-1} with the formation of thiourea group. The band at 1324 cm^{-1} is characteristic of the xanthene ring[42] of the FITC. The band at 1550 cm^{-1} in the spectrum of the PAHB is related to the amide bond confirming the covalent linkage to PAH. The weak bands at 1078 cm^{-1} (PAHF) do not have an assignment but they appear in the FTIR spectra in Figure 49, which it will be discussed later.

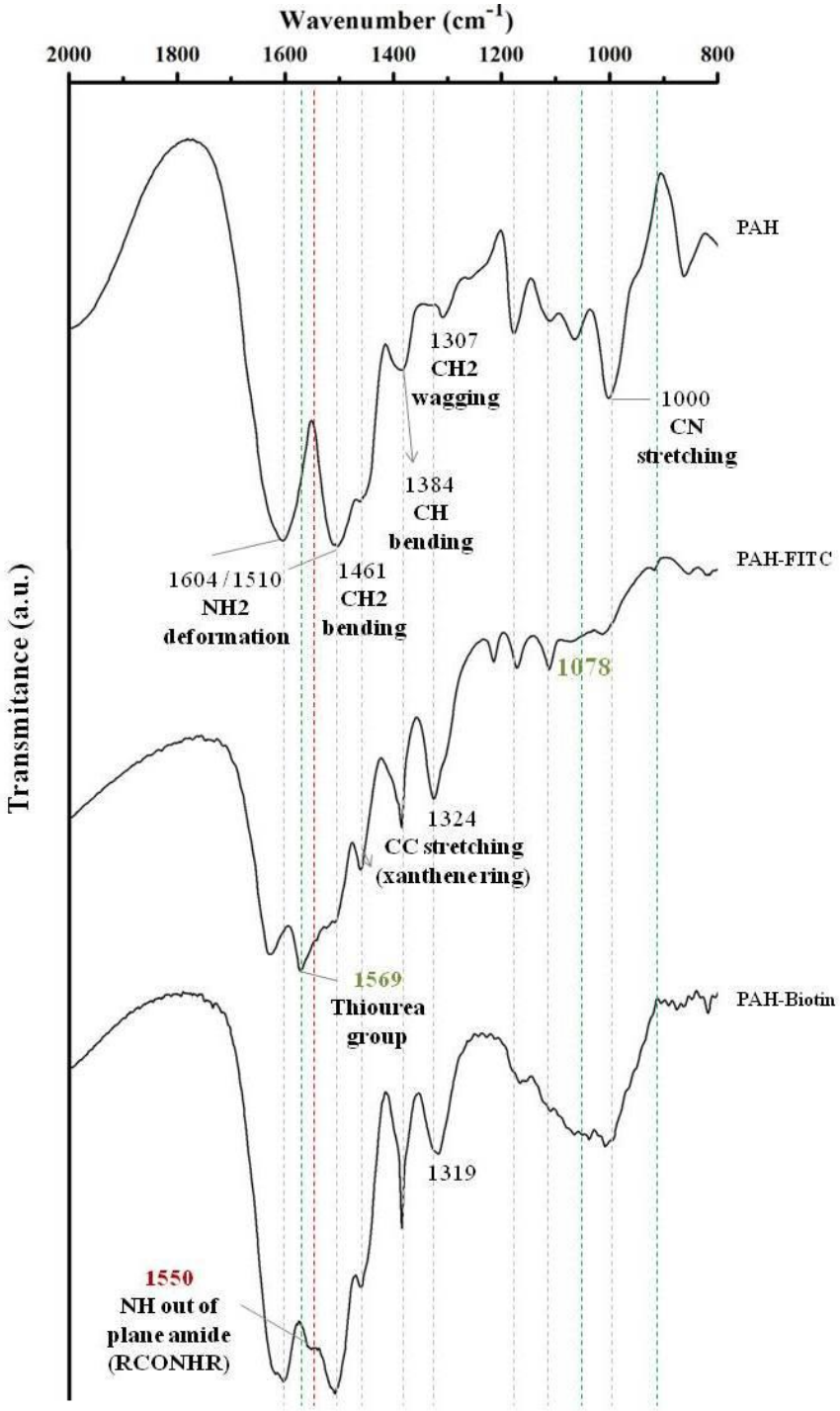

Figure 36 - FT-IR spectra of PAH, PAHF and PAHB.

The PAHF and PAHFB were characterized by fluorescence spectroscopy and the spectra are shown in Figure 37. For comparison the spectrum of FITC is also plotted (not shown). A shift of the emission maximum for the modified PAH is observed when comparing with the FITC in solution, this can be due to the linkage of the FITC to the PAH.

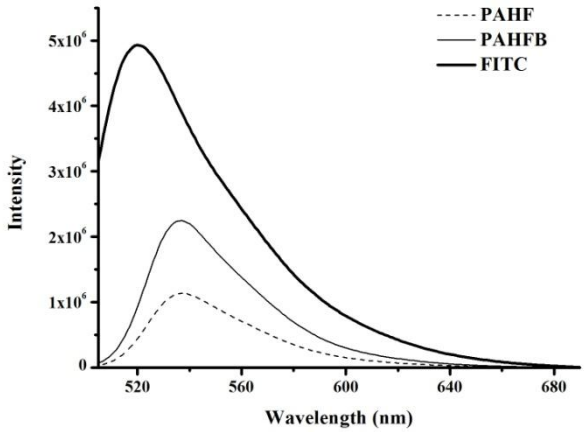

Figure 37 - Fluorescence spectra of PAHF, PAHFB and FITC (λexc = 494 nm).

As a conclusion, the PAH was functionalized by a covalent linkage with the FITC and biotin yielding PAH functionalized with FITC (PAHF), with biotin (PAHB) and with both (PAHFB).

1.1.3. Characterization of functionalized Au/Citrate/PAH NPs

The functionalized Au/Citrate/PAH NPs were characterized by visible and fluoresence spectroscopies to monitor the effect of the functionalization strategy on the optical properties and stability of the colloids. Zeta potential measurements and the pH were also recorded to assess the effect of such strategies on the particles charge density. For comparison purposes the unmodified Au/Citrate/PAH NPs were also analyzed. As regards the optical properties from the visible spectra of the different composite particles shown in Figure 38 (left) it is clear that the Au/Citrate/PAHF and Au/Citrate/PAHFB solutions contain an excess of FITC as the corresponding spectra are dominated by the strong peak at 497 nm which is the wavelength at which the absorption of FITC is maximum. In fact, this result was expected in view of the colour exhibited by the colloid during the modification with FITC (see Figure 39). In the visible spectra of the remaining functionalized NPs, the characteristic SPR peak of Au NPs is clearly detected at 523 nm. Yet, notice should be made that the intensity of the SPR peak of the Au/Citrate/PAHF+B is reduced, which can be due to the recovery of NPs in the centrifugation/re-dispersion cycle. Furthermore, the peak at 497 nm due to the FITC is not detectable. This result may be

justified by the fact that when Au/Citrate/PAHF is modified with biotin one washing step is involved during which some free FITC or PAHF may be removed. This hypothesis was confirmed by the fluorescence spectra shown in Figure 38 (right) which on the one hand confirms the presence of FITC on the Au/Citrate/PAHF+B NPs, and on the other hand shows more intense peaks for the Au/Citrate/PAHF and Au/Citrate/PAHFB NPs.

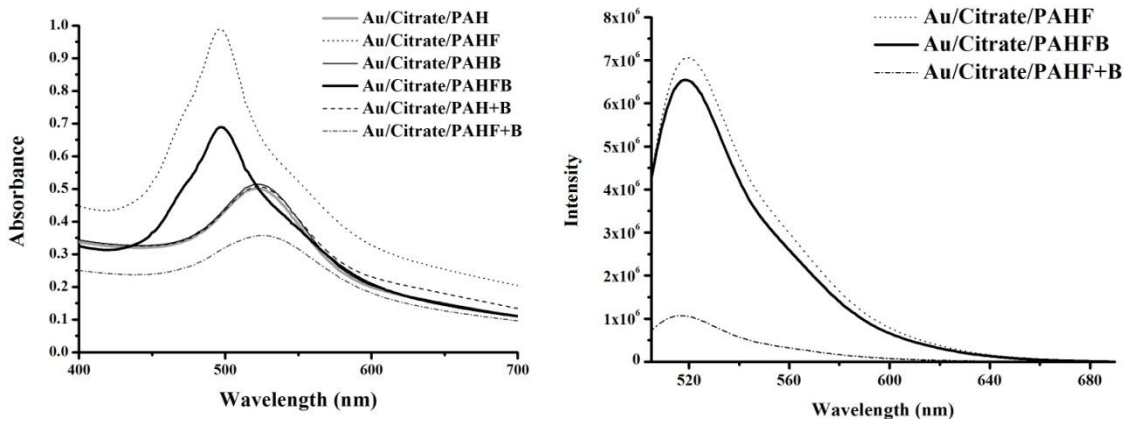

Figure 38 – Visible (left) and fluorescence – λexc= 494 nm (right) spectra of Au/Citrate/PAH nanostructures.

Figure 39 – Photograph of Au/Citrate/PAHF during the modification of Au/Citrate with PAHF.

The effect of the functionalization strategy on the surface charge density and pH of the colloidal solutions was also checked and the results are summarized in Table 3 together with those obtained from the visible and fluorescence spectra.

As regards the zeta potential values, notice must be taken that these are average values as more than one peak were detected. Although some oscillations are detected in the pH of the colloidal solutions and on the zeta potential values, they are not remarkable confirming

the presence of a positively charge polyelectrolyte around the Au/Citrate NPs. The small variations detected can be explained by substitution of the protonated amine groups by FITC and biotin, the presence of residual salts involved in the PAH modification procedures and even conformational differences resulting from the polyelectrolyte functionalization. Furthermore, despite of the presence of multiple peaks and the resulting high deviation registered for each average, the data collected indicate that the charge density of the modified NPs is essentially kept regardless of the modification process.

Table 3 –Absorption and emission maxima, zeta potential and pH of the functionalized nanocomposites Au/Citrate/PAH.

	λ_{max}Abs (nm)	$\lambda_{Em(494\ nm)}$ (nm)	ζ potencial (mV)	pH
Au/Citrate/PAH	522	---	+ 55.9	4.18
Au/Citrate/PAHF	497	519	+ 67.9	4.95
Au/Citrate/PAHB	523	---	+ 49.4	4.47
Au/Citrate/PAHFB	497	519	+ 50.8	5.46
Au/Citrate/PAH+B	523	---	+ 57.9	4.65
Au/Citrate/PAHF+B	525	516	+ 57.0	5.26

The multiple peaks in the zeta potential plots mentioned above may result from the presence of modified and unmodified NPs and eventually of polymer aggregates. In Schneider *et al.*[31] work the samples (Au/Citrate/PAH NPs) were submitted to two washing steps prior to characterization yet they do not comment or refer the presence of aggregates. In the present study, three peaks were detected after two washings at 24.4 mV; + 48.7 mV; + 78.6 mV (i.e. average = + 55.9 ± 24.7 mV). Hence, a third washing was carried out and the corresponding zeta potential plot showed only two peaks at + 30.5 mV; + 58.8 mV (average = + 33.2 ± 10.3 mV) – see plots in Annexe B.

These results suggest that an excess of PAH is present in the original colloid and/or that adsorption of the polyelectrolyte to the Au/Citrate NPs is very strong. Hence a systematic study was carried out to assess the effect of washings on the stability of the colloids

Au/Citrate/PAH NPs were submitted to five cycles of centrifugation/re-dispersion cycles using water. Between each cycle photographs of the solutions, visible spectra and zeta potential measurements as well as pH were taken. The results are summarized in Figure 40 and Table 4.

As can be seen clearly in the photograph shown in Figure 40(right) the appearance of the blue colour indicates aggregation of NPs, and is in agreement with the visible spectrum where a peak at around 650 nm is observed and the peak at 523 nm decreased as the number of washings increased. Although the pH of the colloid was not significantly affected by the number of washing, the charge density and the number of aggregates were. Whilst in the original colloidal three types of particles could be detected, after the first washing only two were detected. Moreover, their relative proportion was significantly altered suggesting that aggregates of PAH and eventually some of the PAH adsorbed on the NPs were removed.

Upon the second washing only one peak was detected corresponding to a much lower charge density indicating significant removal of the polyelectrolyte. From the second to the third washing the change is not relevant. However, the fourth washing brought a major decrease in charge density and the appearance of negative charges suggesting depletion of the PAH and exposure of the negative charges of the citrate. This was further aggravated by the fifth washing cycle.

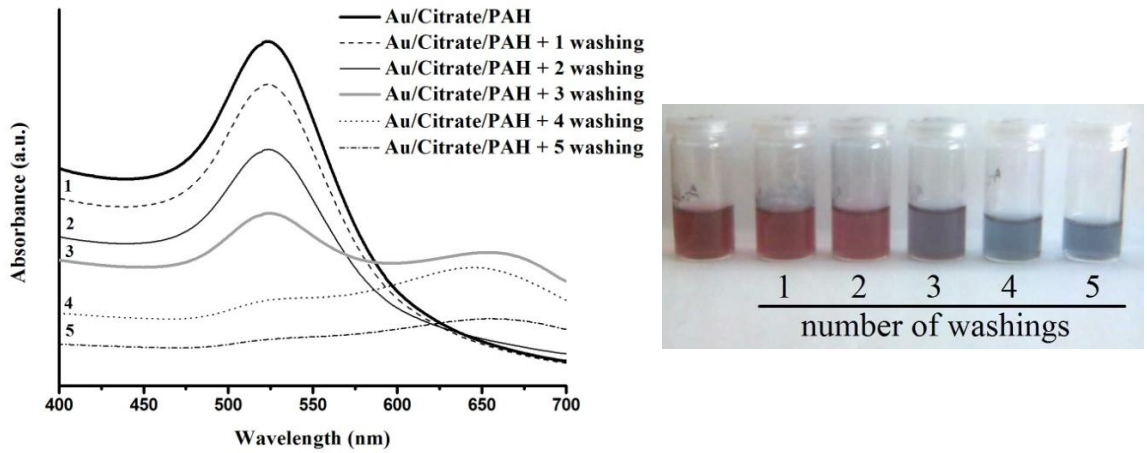

Figure 40 - Visible spectra of Au/Citrate/PAH (left) and photograph of colloids (right) with several cycles of washings.

Table 4 - pH and zeta potential of Au/Citrate/PAH with several cycles of washing.

	pH	Potential Zeta (mV) ζ_1	ζ_2	ζ_3	ζ_{mean}
Au/Citrate/PAH		4.25 (5.60%)	25.0 (26.3%)	54.0 (61.3%)	45.8
	5.74	39.7 (66.1%)	73.0 (24.2%)	104 (5.80%)	51.3
Au/Citrate/PAH			37.0 (94.9%)	73.3	38.3
1 washing	6.67		37.8 (95.8%)	77.3	39.1
Au/Citrate/PAH		29.0 (100%)			29.0
2 washing	6.8	28.7 (100 %)			28.7
Au/Citrate/PAH		24.5 (100%)			24.5
3 washing	6.88	25.4 (100 %)			25.4
Au/Citrate/PAH		4.80 (90 %)	-15.0		2.90
4 washing	6.88	- 0.65 (98 %)	-2.67		-1.01
Au/Citrate/PAH		-2.09 (100%)			-2.09
5 washing	6.24	-2.32 (100%)			-2.32

1.2. Assemblies of PAH-Au using *in situ* generated Au NPs (Au/PAH)

Another way to synthesize Au NPs modified with PAH is via *in situ* synthesis using PAH as reducing agent. This procedure reduces the synthesis time since in this procedure the synthesis of NPs and surface modification take place simultaneously. However, *in situ* synthesis has some limitations because the reaction conditions had to be optimized to obtain NPs with tight size distribution and spherical shape as will be discussed in the next sections.

1.2.1. *In situ* Synthesis

In situ synthesis of Au NPs has been achieved using reducing agents that act also as capping/stabilizing agent, such as amino acids and polymers (e.g. polycation –PAH). However, in this work there were some problems with the reproducibility and the shape of Au NPs. In the beginning the procedure of Newman *et al.* [18] was followed. Taking into account the amount of $HAuCl_4$ used in the citrate method the PAH:$HAuCl_4$ ratio used was approximated 2.5 in order to obtain Au NPs with a diameter around 15 nm and to allow an easy comparison later.

In a first attempt a volume of 25 mL was used but after 8h the solution remained colourless. Although Newman *et al.*[18] did not make any reference to the pH of the solution, considering that when PAH is dissolved in water the pH is around 4 and that the pKa of PAH is 8-9 it was thought that the pH had to be adjust to 9 to ensure deprotonation of the amine groups so that they could reduce the $HAuCl_4$. Hence, in the next attempt the pH was increase to 9 and the volume of the reaction used was 10 mL. After 2h a pink/red colour started to appear and after 6h reduction of $HAuCl_4$ was complete. Newman *et al.*[18] reported the synthesis of Au NPs with PAH at 95ºC for 45 minutes and at room temperature (ratio 100:1 PAH:$HAuCl_4$) which took much longer times with the first colour appearing only after 3h of mixing of reactants solutions.

These NPs synthesized *in situ* were called Au/PAH. This procedure was repeated but using a bigger volume (20 mL) which required changes of the experimental set up.

1.2.1.1. Characterization of Au/PAH NPs prepared at micro scale

The success of *in situ* synthesis of Au NPs with PAH (10 mL of reaction volume) was indicated by the appearance of the pink-red colour and was then proved by the visible spectrum of the ensuing colloid shown in Figure 41. The SPR at 542 nm is shifted from the characteristic SPR of Au NPs at 522 nm due to the presence of PAH. Measurements of zeta potential confirmed that these colloids have positive charge (+ 50.3 mV) as expected because PAH is a polycation. The size of the NPs (13.4 ± 2.4 nm) was calculated from the TEM images (Figure 42), but the DLS measurements were not conclusive due to the presence of aggregates (Annexe C1). Still from the TEM images it can be seen that these NPs are nearly spherical. Moreover, like in Au/Citrate/PAH a layer of about 3 nm can be seen around the Au/PAH.

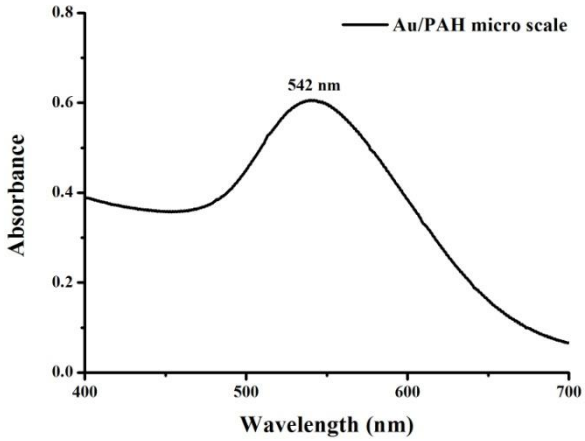

Figure 41 - Visible spectrum of Au/PAH.

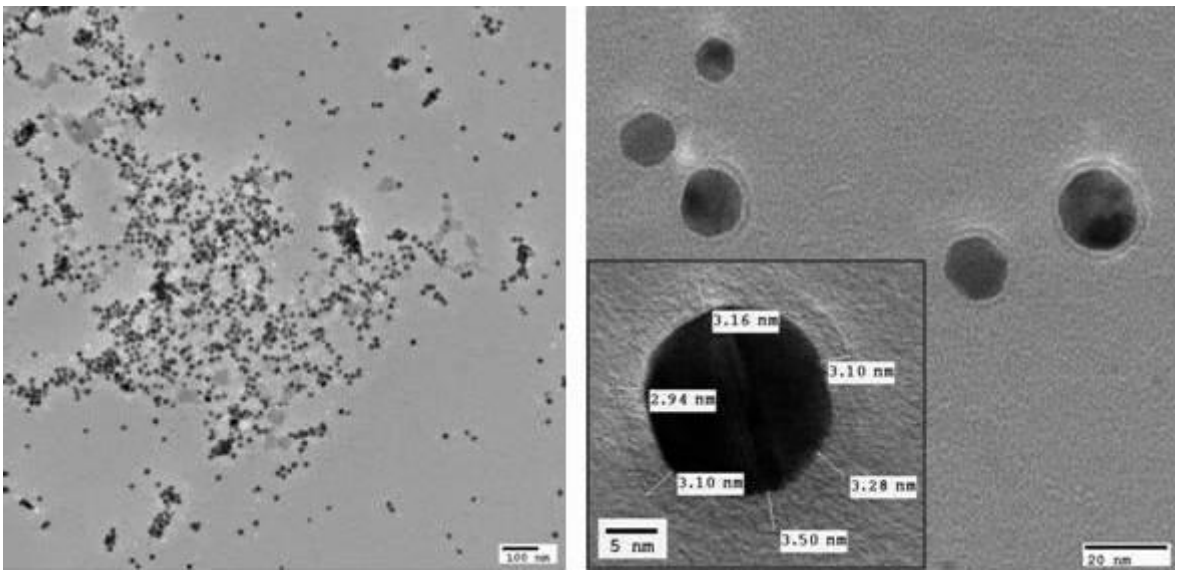

Figure 42 - TEM images of Au/PAH (micro scale).

1.2.1.2. Characterization of Au/PAH NPs prepared at laboratory scale up

As the reaction scale was indeed rather small attempts were made to double it. However, a variety of difficulties were encountered. Either the reaction did not take place or it was very slow considering that the proportion of the reagents was kept and the pH was adjust to 9 it was thought that heat transfer issues might be responsible for the lack of reproducibility observed. Hence, a jacket reactor equipped with a thermostatic bath and a mechanical stirred were used in order to have adequate control over the reaction temperature and stirring and thus of the heat transfer process. Using a 50 mL reactor, the

synthesis was completed in 6h and proved to be reproducible. However the NPs shape was not spherical (Figure 43).

Furthermore, from the TEM images the size of NPs was measured and was verified that the NPs have an average diameter about 22.0 ± 3.3 nm. These images help understanding the difficulty of determining the size of NPs by DLS due to the aggregates of NPs and also due to the PAH that is yet in solution despite of the fact that the NPs had been washed once. In spite of the presence of these aggregates, the diameter determined by DLS as a function of the number of particles was 27.12 nm for these NPs (Annexe C2). Upon a second washing the NPs were analyzed by STEM. From the images shown in Figure 44 it is interesting to see the PAH layer around the Au NPs which can not be detected in Figure 43 where only agglomerate of PAH or of Au/PAH can be seen.

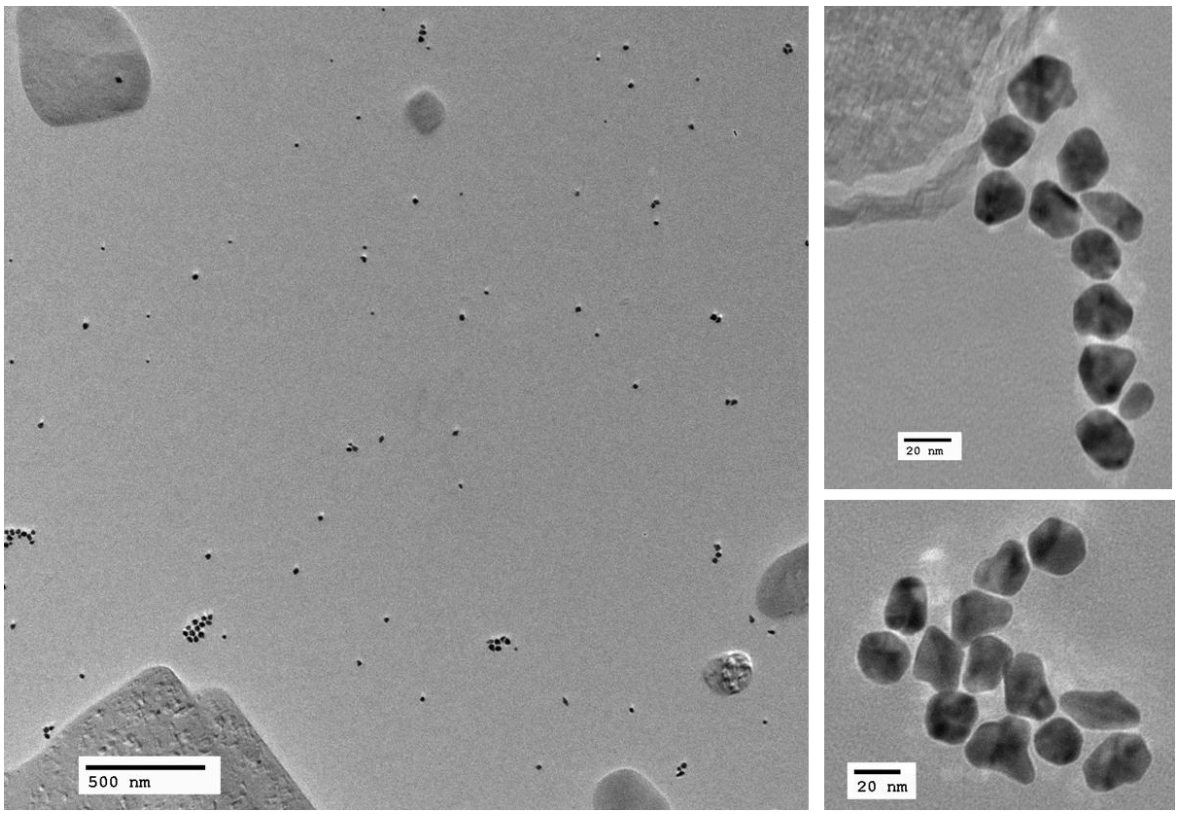

Figure 43 - TEM images of Au/PAH (laboratory scale).

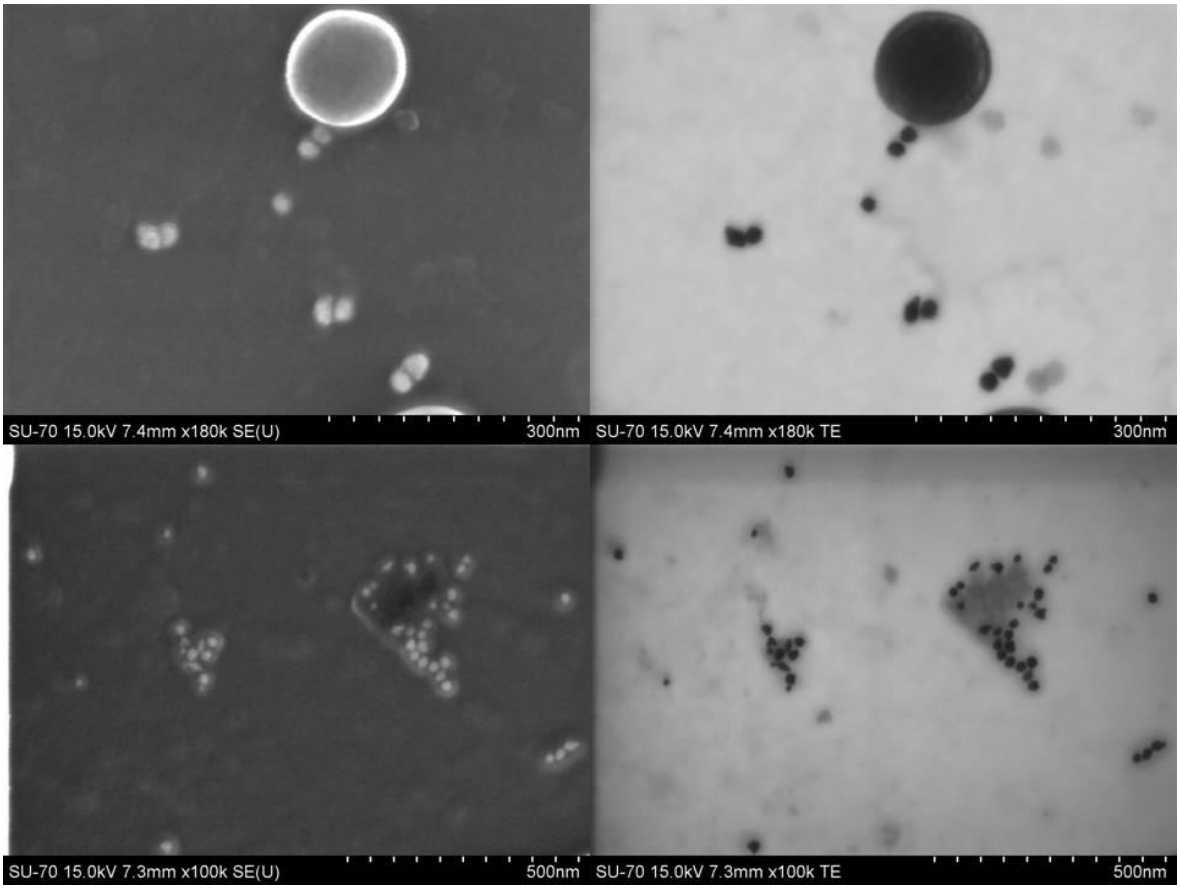

Figure 44 – STEM images of Au/PAH upon an extra washing.

The visible spectra of Au/PAH prepared using the two experimental set ups are shown in Figure 45, and prove that the SPR are similar. As regards the charge density the zeta potential plots show only one positive peak charge (+ 63.1 mV). However, upon one washing multiple peaks were present at + 71.5 mV; + 48.4 mV; + 23.9 mV (average = + 56.7 ± 21.8 mV) – see plots in Annexe D. These results suggest that some adsorbed PAH or some excess of PAH was removed by the centrifugation/re-dispersion cycle, as happened in the Au/Citrate/PAH. Notice that the presence of a single peak in the zeta potential plot and the result of DLS show that these samples without washing are more homogenous.

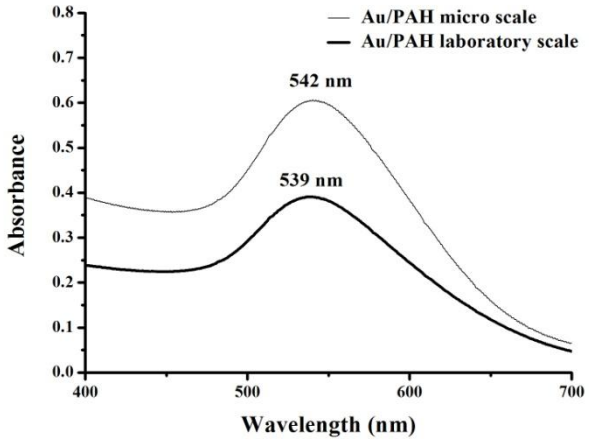

Figure 45 – Visible spectra of Au/PAH laboratory scale versus Au/PAH micro scale.

The PAH:$HAuCl_4$ ratio and the solutions concentration used were the same both in the micro and laboratory scale experiments. Yet, the morphology of NPs was not spherical for the second case. These morphological differences are related with the mass transfer due to the increase of volume. In spite of the better heat transfer achieved using the jacket reactor, this non-spherical morphology can be due to inadequate agitation.

Another parameter that can influence the mass transfer and consequently the shape of Au NPs, is the solutions concentration which does not apply to our study. Increasing the concentration, but maintaining the ratio PAH:$HAuCl_4$, the viscosity of solution increases and the NPs will be more confined in the PAH. In the work of Newman *et al.*[18], they kept the concentration of PAH constant in order to maintain constant the viscosity, and they vary the concentration of $HAuCl_4$ to achieve the different ratios studied. In fact their Au NPs were almost spherical, even though they have work with higher concentration. Yet they did not mention the reaction volume. Besides the concentration, stirring conditions and viscosity of the reaction mixture, the sequence of the addition of reagents may also influence the morphology of the *in situ* generated particle. Indeed this parameter was reported by Ojea-Jiménez *et al.*[55] in connection with the synthesis of Au NPs via the citrate method and might be worth evaluating for the *in situ* synthesis of these NPs.

1.2.2. Functionalization and characterization of Au/PAH NPs

For the functionalization of Au/PAH with FITC some preliminary tests were carried out using the Au/PAH micro scale NPs. Four different strategies were attempted to synthesize Au NPs with PAH and FITC in order to combine the need to have the amine groups deprotonated (i.e. pH around 9) and to prevent colloidal aggregation as described in Part II - Experimental **9**.

When PAH modified with FITC was used without being dialysed, or when free FITC was added to the reaction mixture, the synthesis of Au NPs did not occur. In the first case one could attribute the synthesis failure to the heat transfer problems as the reaction volume used was large (20 mL). Yet, in the second case the reaction volume used was only 5 mL. Hence, even though we can not fully explain the failure of these synthesis it seems reasonable to admit that the presence of free FITC seems to hinder the reduction of the gold precursor.

In view of these results it was decided to use previously modified PAH with FITC (PAHF) as reducing agent upon purification by dialysis. In this case the presence of Au NPs in this solution was only fully confirmed by TEM as the colour of colloidal solution was dominated by the colour of FITC as proved by the visible and fluorescence spectra, shown in Figure 46.

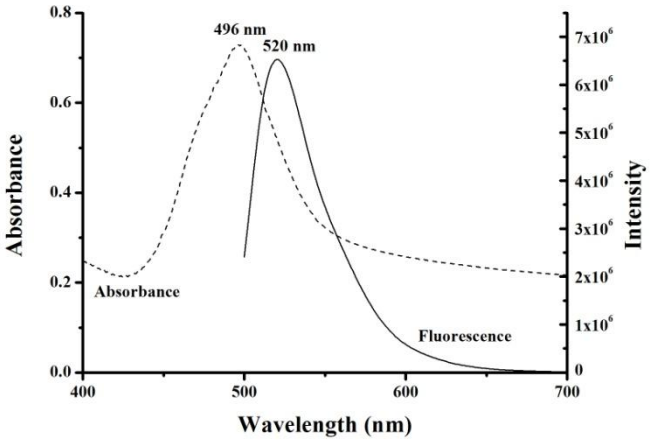

Figure 46 – Visible and fluorescence (λexc = 494 nm) spectra of Au/PAHF.

TEM images (Figure 47) show Au/PAH whose diameters range from 20 to 60 nm. These values are bigger than expected as the PAH:$HAuCl_4$ ratio used is the same as the ratio used

in the preparation of Au/PAH. However, the amount of free amine groups is smaller due to the FITC molecules linked to the amine groups of the PAH. Nevertheless, this result might seem to be inconsistent with Newman *et al.*[18] who referred that the higher the PAH:$HAuCl_4$ ratio, the higher the was the size of the NPs whilst for a lower PAH:$HAuCl_4$ ratio the NPs would be smaller. However, considering that the PAHF may adopt a distinct conformation from that of PAH and that this can influence the availability of the amine groups responsible for the reduction of the gold salt, the results obtained are not surprising. In fact, according to Newman *et al.* three amine groups are required to reduce one Au^{1+}. Furthermore, the FITC may also help the reduction of Au^{1+} and in view of this one could hardly expect a marrow distribution of sizes.

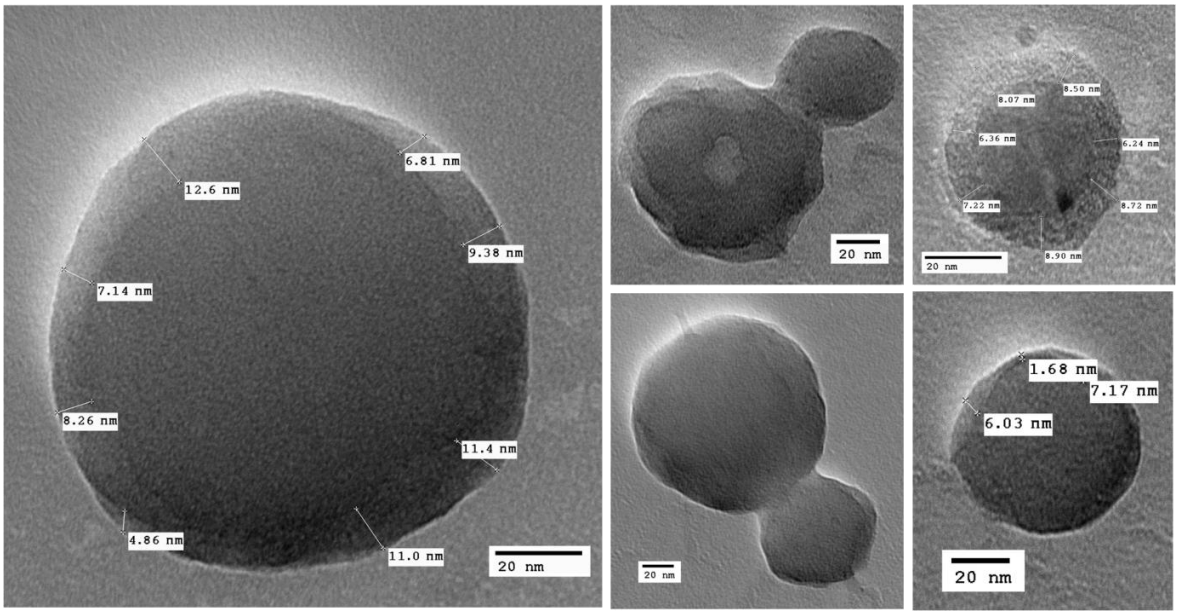

Figure 47 - TEM images of Au/PAHF.

To overcome this wide size distribution another approach was tested. In this case FITC was added to *in situ* generated Au/PAH NPs which were not submitted to any washing procedure. Despite of the excess of PAH in solution as the pH of the colloidal solution was near 9, the reaction between the isothiocyanate group of FITC and amine group of PAH could occur. As a preliminary test, this approach was performed in a round bottom flask (5 mL) and the linkage was confirmed by FTIR. Also, the functionalization of Au/PAH with biotin was firstly performed at micro scale and the linkage confirmed by FTIR. Since these functionalization procedures proved to be successful efforts were then direct towards the

preparation of hybrid nanostructure assemblies in bigger amounts and the ensuing materials characterized as will be discussed next.

Having optimized the functionalization procedure using the Au/PAH NPs prepared at micro scale, Au/PAH prepared under the so called laboratory scale up was functionalized with FITC (Au/PAH+F), biotin (Au/PAH+B) and both (Au/PAH+FB). The optical properties of the ensuing NPs were assessed by visible and fluorescence spectroscopies to monitor the effect of the functionalization strategy on the optical properties and stability of the colloids. Zeta potential measurements and the pH were also recorded to assess the effect of such strategies on the particles charge density. For comparison purposes the unmodified Au/PAH NPs were also analyzed. As regards the optical properties, the visible spectra of the different composite particles shown in Figure 48 (left), clearly show that Au/PAH+F contains an excess of FITC as the spectrum has a peak at 497 nm near the SPR of Au NPs, which is the wavelength at which the absorption of FITC is maximum. In the visible spectra of the remaining functionalized NPs, the characteristic SPR peak of Au NPs is clearly detected at 539 nm. Yet, notice should be made that the Au/PAH+FB does not show the peak of FITC at 497 nm. This can be justified by the fact that when Au/PAH+F is modified with biotin one washing step is involved during which some free FITC or PAHF may be removed. This hypothesis was confirmed by the fluorescence spectra shown in Figure 48 (right) which on the one hand confirms the presence of FITC on the Au/PAH+FB NPs, and on the other hand shows more intense peaks for the Au/Citrate/PAH+F.

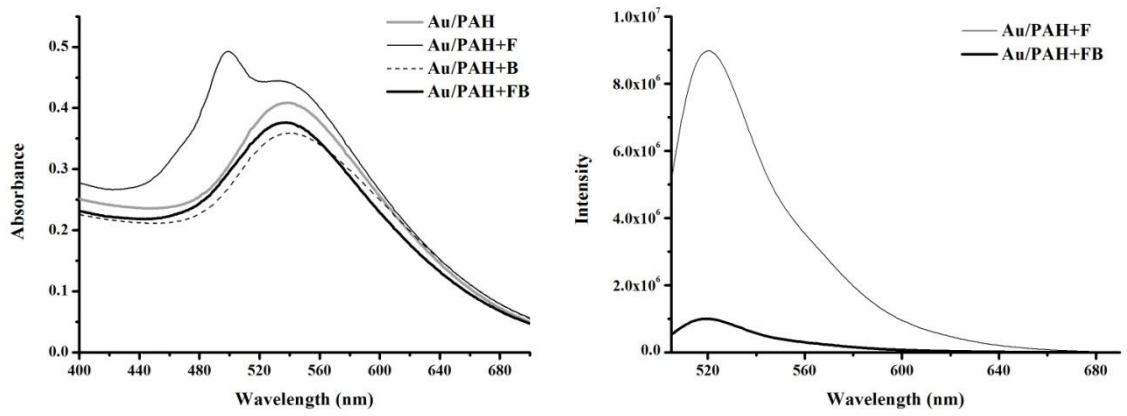

Figure 48 - Visible (left) and fluorescence - λexc =494 nm (right) spectra of functionalized Au/PAH NPs.

The effect of the functionalization strategy on the surface charge density and pH of the colloidal solutions was also checked and the results are summarized in Table 5 together with those obtained from the visible and fluorescence spectra.

As regards the zeta potential values, notice must be taken that these are average values and in the case where the nanocomposite was modified with biotin as more than one peak was detected. The small variations detected can be justified by the substitution of the protonated amine groups by FITC and biotin. Despite of, the presence of multiple peaks and the resulting high deviation registered for each average the results indicate that the charge density of the modified NPs is essentially kept regardless of the functionalization process.

Table 5– Values of the absorption and emission maximum peaks, zeta potential and pH of the functionalized nanocomposites Au/PAH.

	λ_{max}Abs (nm)	$\lambda_{Em(494\ nm)}$ (nm)	ζ potencial (mV)	pH
Au/PAH	539	---	+63.4	6.40
Au/PAH+F	497/539	519	+55.2	6.46
Au/PAH+B	539	---	+53.4	6.39
Au/PAH+FB	539	519	+49.6	6.37

Infra-red spectroscopy (FTIR) was used to confirm that covalent bonds between FITC and biotin with PAH were formed, as shown in Figure 49. However, to analyze the FTIR spectra is not easy because the amount of PAH around the NPs is rather small so it is difficult to obtain a good spectrum. Moreover, as the PAH is confined around the Au NPs some of the bands are shifted or with less intensity. The thiourea and amide bands associated with the linkage of FITC and biotin, respectively, do not appear in these spectra as opposed to what was observed in the spectra of the functionalized PAH (Figure 36). Instead, a band at 1631/1637 cm^{-1} is present in these spectra. The peak of the xanthenes ring was found at 1328 cm^{-1} but this only indicates the presence of FITC and not the linkage. The band at 1076 cm^{-1} (Au/PAH+F) which was not attributed, but as discussed in

1.1.2., it also appears in the spectrum of PAHF, and do not appears in the spectrum of PAH neither FITC, which may indicate the linkage. The band at 1184 cm^{-1} (Au/PAH+B) which was not attributed, but do not appears in the spectrum of PAH neither biotin, which may indicate the linkage.

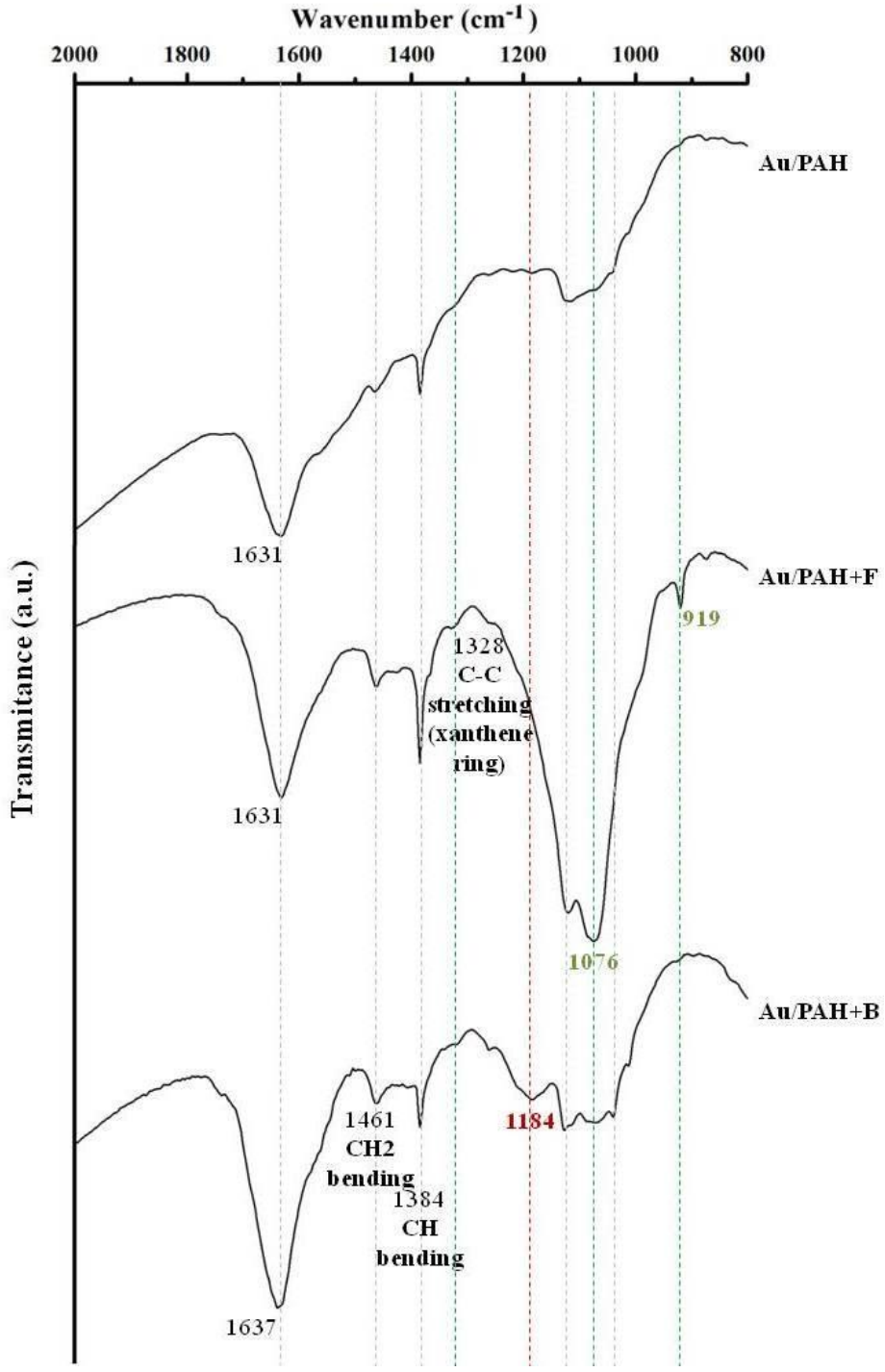

Figure 49 – FT-IR spectra of Au/PAH, Au/PAH+F and Au/PAH+B.

1.3. Comparative studies between Au/Citrate/PAH and Au/PAH assemblies

In this section the optical properties of the nanocomposites prepared via the different methods are summarized as well as the morphological ones, as shown in Figure 50, Figure 51 and Table 6. The nanocomposites were compared by visible spectroscopy and TEM to conclude about the SPR band and the morphology of Au NPs, respectively. In relation to the visible spectrum the same shift of the SPR band was founs for the micro and laboratory scale NPs prepared *in situ* when comparing with the SPR of the Au/Citrate/PAH NPs, as illustrated in Figure 50. There is a big difference between the morphology of Au NPs synthesized at micro scale and those prepared at laboratory scale. The shape of Au/PAH NPs prepared at micro scale is similar to that of the citrate Au NPs as can be seen in Figure 51, they are spherical. In this figure a layer of PAH around NPs can be observed, whose thickness for Au/PAH micro scale is around 3 nm and for Au/Citrate/PAH is around 1.5 nm. For the Au/PAH laboratory scale this PAH layer is not observed, even though if the zeta potential is positive as mentioned before.

The huge difference between these two methods is the procedure for the functionalization with FITC and biotin. For the Au/Citrate/PAH NPs, the PAH is functionalized with FITC and/or biotin and then Au/Citrate NPs were modified with this new PAH. For the Au/PAH NPs, the modification with FITC must be after the synthesis of the Au NPs without any washing to keep the pH of solution at 9. After the washing the pH of solution decreases to approximately 6 and it is possible modify Au/PAH or Au/PAH+F with biotin. To facilitate the comparison of these methods Au/Citrate/PAH and Au/Citrate/PAHF were modified with biotin using the same methodology as that followed for the NPs prepared *in situ*. However, the same procedure could not followed for the modification with FITC as this functionalization requires that the pH of the solution is around 9 and it is not possible to increase the pH of the colloidal solution (Au/Citrate/PAH or Au/PAH) because when the pH is increased aggregation occurs immediately. In fact this procedure was performed and upon addition of one drop of NaOH 0.01 M the colour of solution changed from red/pink to blue. Finally it should be remarked that the amount of FITC and biotin was not quantified in this work however for future work this will be necessary.

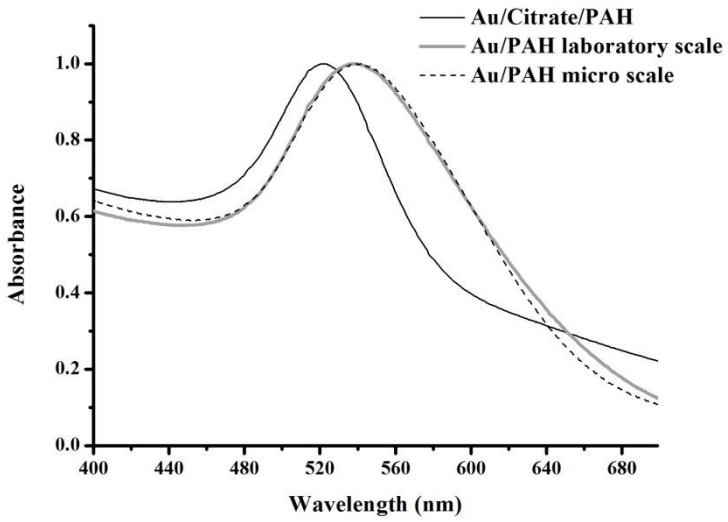

Figure 50 - Visible spectra of Au/Citrate/PAH and Au/PAH synthesized at a micro scale and laboratory scale.

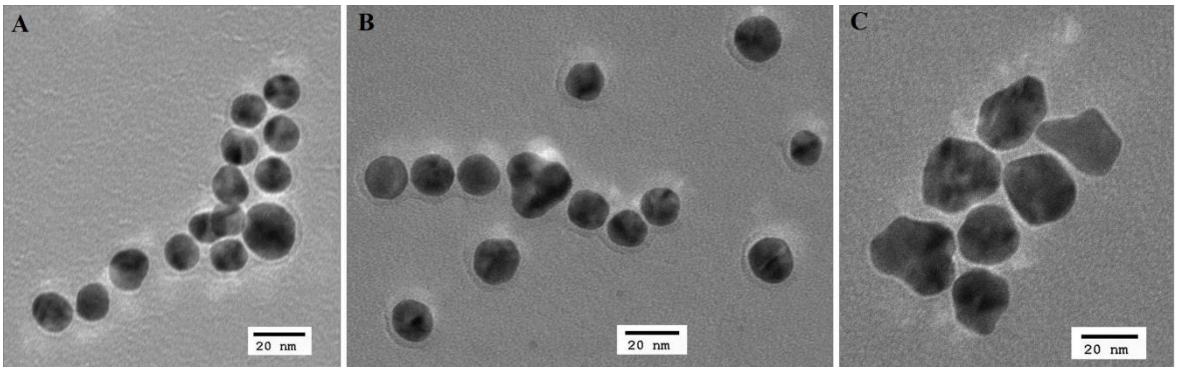

Figure 51 - TEM images of A) Au/Citrate/PAH, B) Au/PAH micro scale and C) Au/PAH laboratory scale.

Table 6 – Summary of the values of the absorption and emission maximum peaks, zeta potential and pH of the Au/Citrate/PAH and Au/PAH.

	λ_{max}Abs (nm)	Diameter (nm)	ζ potential (mV)	pH
Au/Citrate/PAH	522	14.9 ± 2.8	+ 55.9	4.18
Au/PAH micro scale	542	13.4 ± 2.4	+ 50.3	6.36
Au/PAH laboratory scale	539	22.0 ± 3.3	+ 63.4	6.40

2 – Optical evaluation of the response of Au assemblies towards Avidin

One preoccupation of the use of colloidal systems in bio-applications is their stability under physiological conditions, i.e. controlled conditions of pH, which implies the use of a buffer solution, because small changes in the pH of the environment can change the activity or even inactivate biomolecules presents in the system. This concern was taken in consideration but the tests made using phosphate buffer pH=5.5, phosphate buffer saline (PBS) pH=7.4, Tris buffer pH=7 and bicarbonate buffer pH=8.3 led to aggregation. To overcome this problem however, throughout this work only deionized water was used, the pH of each colloidal solution was always verified and the range was kept between 5 and 7. Notice that biotin and avidin can link in the pH range of 4 to 12[56]. However, future strategies will have to consider the integration of these colloidal systems in buffered solutions, to allow their use in biological systems.

The attempts to obtain the colloids in buffer solutions involved the centrifugation of Au/Citrate/PAH aqueous colloidal and re-dispersion in different fluids: PBS pH 7.4, phosphate pH 5.5, Tris buffer pH 7 and bicarbonate pH 8.3 and water. In all cases when a buffer was used the Au NPs aggregated, and as result the colour changed from pink to blue, as can be seen in Figure 52. However, when water was used the colloid remained stable.

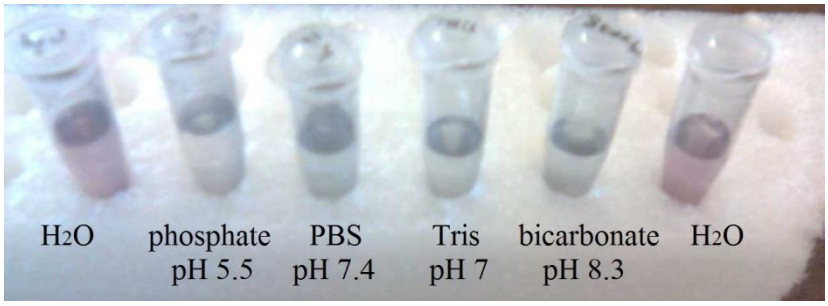

Figure 52 – Au/Citrate/PAH after re-suspension in phosphate buffer pH 5.5, PBS pH 7.4, Tris buffer pH 7, bicarbonate buffer pH 8.3 and water.

In another attempt, Au NPs were modified with PAH dissolved in the PBS buffer. During the modification of NPs with PAH the colour of the mixture was pink, but after the first centrifugation very little precipitate was collected when compared when water was used. Moreover, the resulting solution was only slightly pink and upon the second washing the pink colour disappeared. In all these experiments the zeta potential was measured and the

values for all situations were negative, which indicates that in the buffer the PAH does not adsorb onto the Au NPs. The procedure of centrifugation and re-dispersion of NPs in buffers was also performed for Au/PAH NPs which resulted in aggregation.

The potential use of the colloidal systems prepared as biosensor was studied using avidin as analyte to verify the response of each colloidal system to this analyte. Visible and fluorescence spectroscopies were used to monitor the optical response of the various hybrid nanostructures prepared in the presence of avidin.

A first attempt to observe if the colloidal systems responded to the presence of avidin was made by adding ~30 µL of avidin solution (0.2 mg/mL) to each colloid. Regarding the nanocomposites without FITC, Figure 53, the absorption band did not show any change indicating that aggregation due to the presence of avidin did not occurred. The differences in the absorption intensity seem to be related with the recovery of the nanocomposite because when comparing the nanocomposites washed, those that have avidin showed less absorption. Which may indicate some non-specific interactions between the avidin and the PAH.

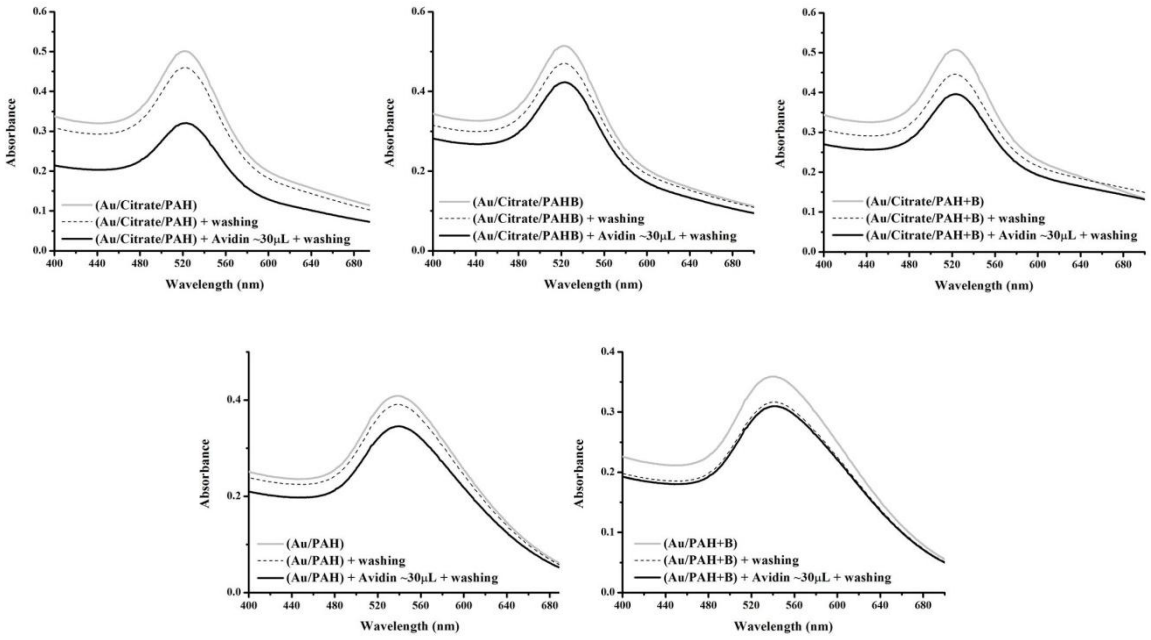

Figure 53 – Visible spectra of Au assemblies when in the presence of ~30 µL of avidin solution (0.2 mg/mL). Top – Au/Citrate/PAH nanocomposites, bottom – Au/PAH nanocomposites.

Concerning the nanocomposites with FITC, shown in Figure 54 and Figure 55, Au/Citrate/PAHF and Au/PAH+F were used as reference for the citrate and *in situ* nanocomposites, respectively. In both figures the visible spectra are similar to the blanks (nanocomposites without FITC). Yet, for the Au/Citrate/PAHF+B the appearance of the band around 650 nm and the change of the colour from red/pink to purple/blue indicates that some aggregation occurred. As regards the fluorescence spectra, the fluorescence intensity of Au/Citrate/PAHFB increased relative to the reference. However, an explanation for this result has not been found wlhilst for the Au/Citrate/PAHF+B, the fluorescence intensity slightly decreased. Yet, can not conclude if this result is significant. However, it should be noted that this sample presents aggregation in the visible spectrum. As regards the nanostructures prepared *in situ*, shown Figure 55, the fluorescence intensity of the Au/PAH+FB decreased in the presence of avidin, comparing to the reference. In this case, the fluorescence spectrum is similar to the Au/Citrate/PAHF+B. However, aggregation in the visible spectrum was not detected as the absorbance band did not changed. Thus, only the fluorescence spectroscopy showed that some aggregation may have occurred.

Although, for the nanocomposite Au/Citrate/PAHF+B the specific response is not fully proved this is the more responsive nanocomposite towards the presence of avidin. However, further evidence is required as one has to keep in mind that the nanostructures were prepared via distinct synthetic methods and functionalization strategies which can affect the interaction of the resulting nanostructured assemblies with avidin. Should this interaction not be specific towards avidin, a possible hypothesis is that the presence of avidin destabilizes the nanostructure and when it was washed aggregation occurred.

Before further conclusions, it was thought that the amount of avidin added could be small to trigger a specific response. Hence, to each colloid the theoretical quantity of avidin to interact with all the biotin in the system was add, i.e. an excess of avidin was used.

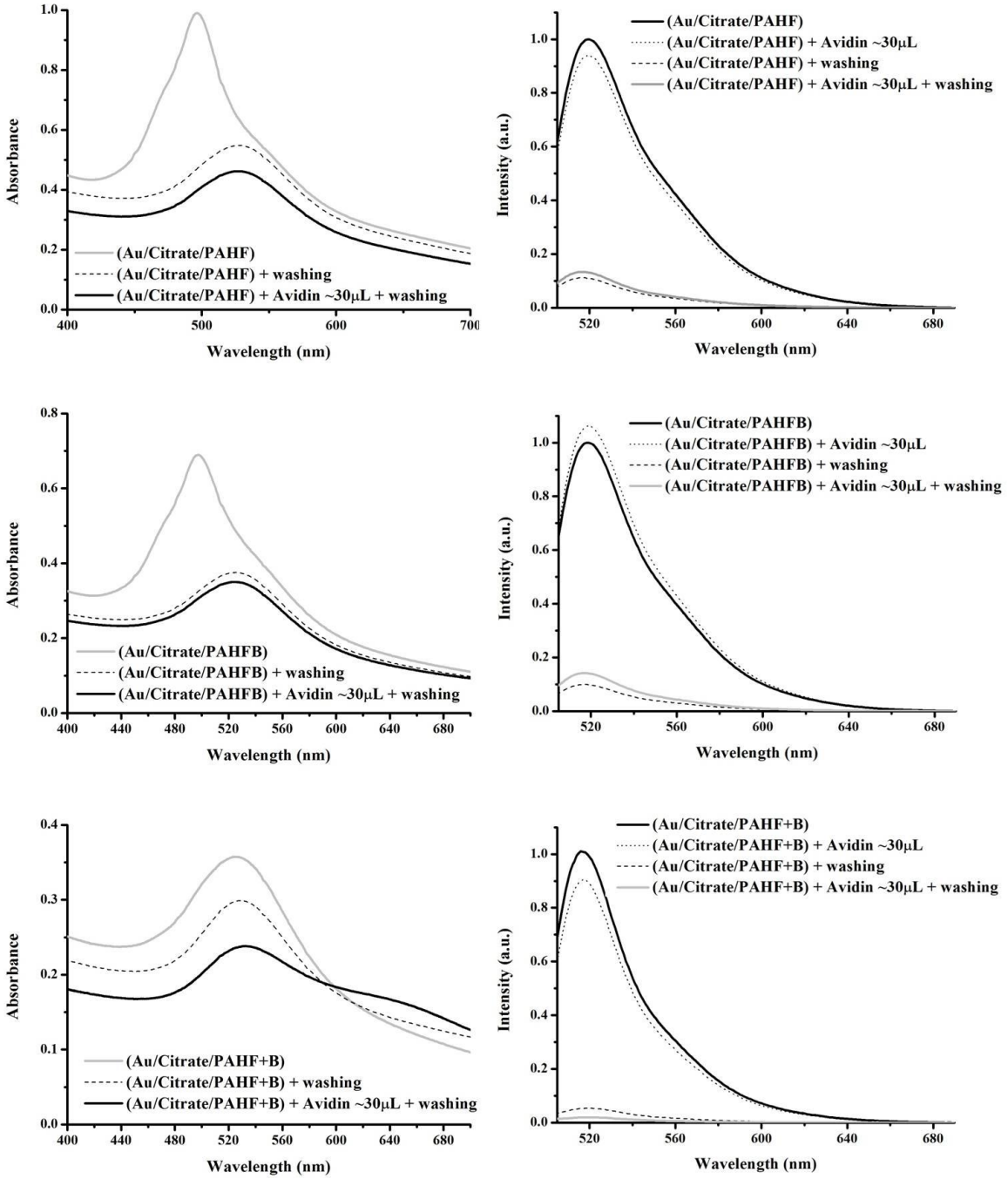

Figure 54 – Visible spectra (left column) and fluorescence spectra – λexc = 494 nm (right column) of the Au/Citrate/PAH assemblies when in the presence of ~30 µL of an avidin solution (0.2 mg/mL).

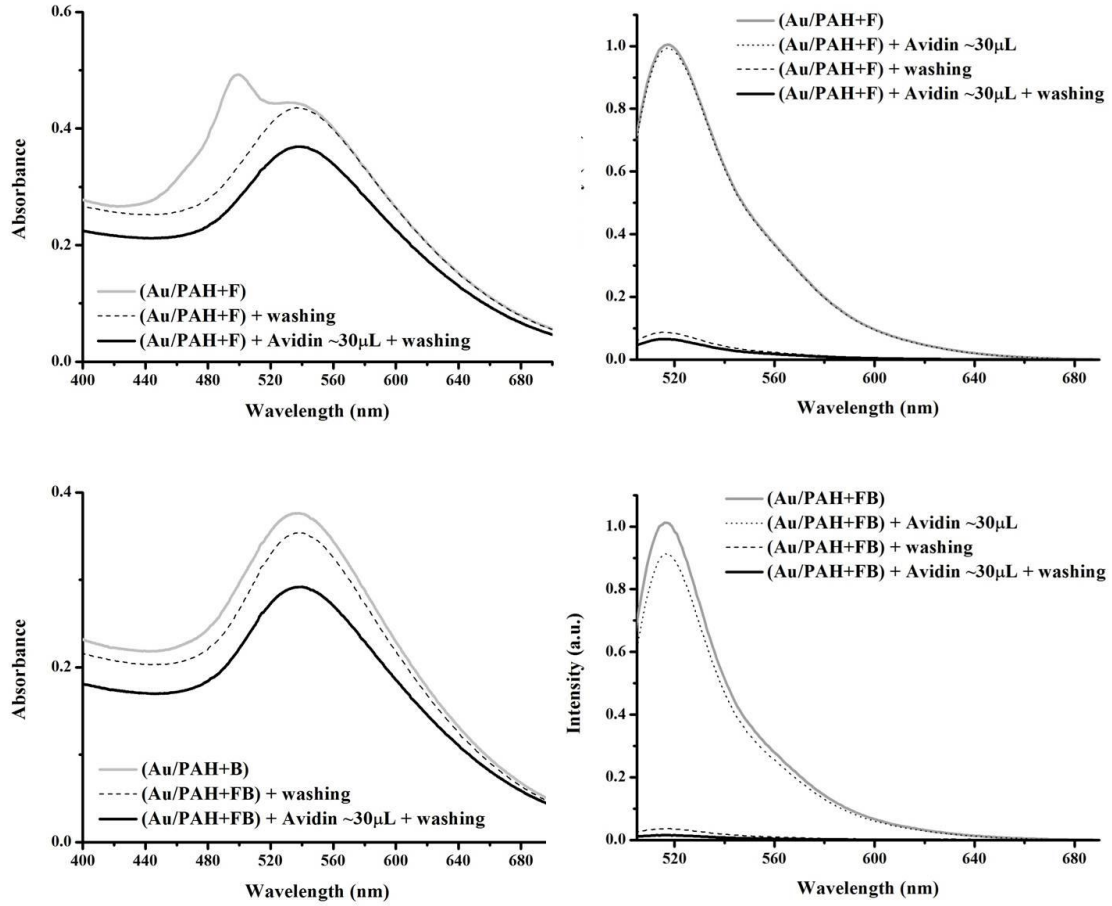

Figure 55 - Visible spectra (left column) and fluorescence spectra – λexc = 494 nm (right column) of the Au/PAH assemblies when in the presence of ~30 µL of an avidin solution (0.2 mg/mL).

Avidin (100 µL) was added to each nanocomposite and the response was monitored by visible and fluorescence spectra. The measurements were carried out after the addition of the avidin, after an hour of contact biotin-avidin and after washing. The visible spectra of the blanks (Figure 56) are similar to those observed when 30 µL of avidin were used. There are however differences in the visible spectra due to the recovery of the nanocomposites. The spectra of Au/Citrate/PAH+B, in the presence of avidin and washed, showed the appearance of a band around 650 nm, like when 30 µL of avidin were added. In this case, the absorbance of the band is more intense, indicating that more aggregation occurred due to the presence of a greater amount of avidin. This result seems to confirm the specific interaction between avidin and biotin. At least for this nanocomposite where

biotin was only added to the hybrid nanostructure in the last stage suggesting that the biotin moieties might be more available on the surface.

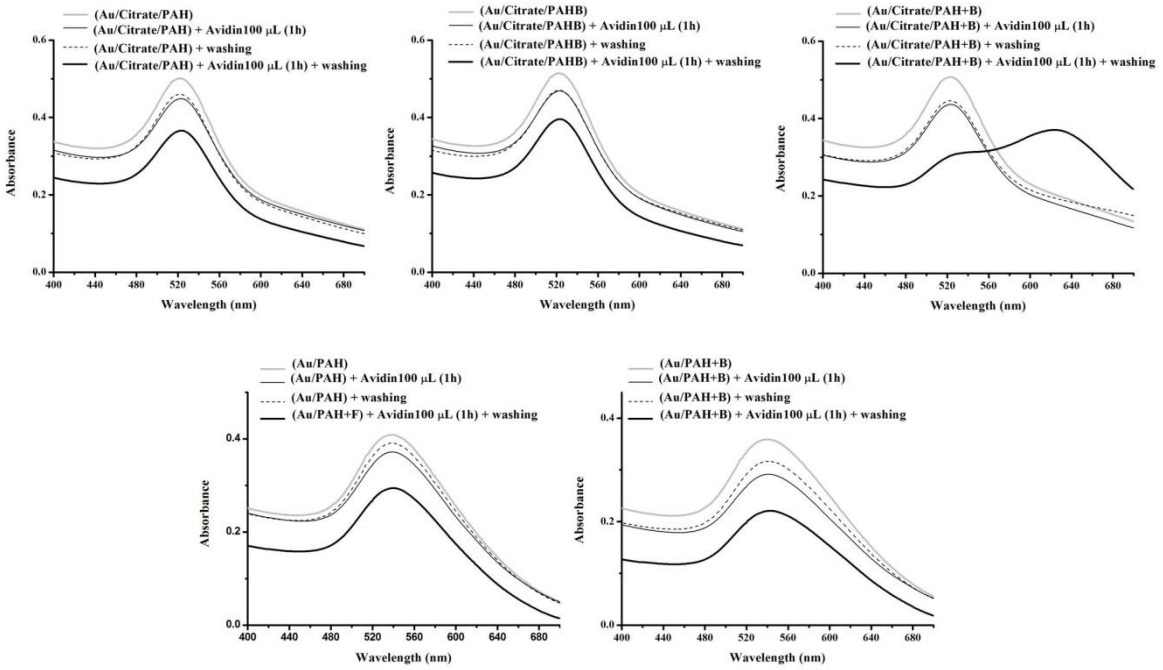

Figure 56 - Visible spectra of Au assemblies when in the presence of 100 µL of an avidin solution (0.2 mg/mL). Top – Au/Citrate/PAH nanocomposites, bottom – Au/PAH nanocomposites.

Regarding the visible spectra of the citrate nanocomposites that contain FITC, shown in Figure 57, the reference (Au/Citrate/PAHF) does not show any change in the absorbance band when in the presence of avidin. However, both samples containing biotin present a band around 650 nm, indicating that aggregation occurred as a result of a specific response. This result also confirmed that the amount of avidin used before was too small to yield an optical response. Note that as expected Au/Citrate/PAHF+B presents more aggregates (band ~650 nm is bigger) than Au/Citrate/PAHFB. Since, in this case the synthesis procedure of Au NPs is the same these different results are due to the methodology of functionalization. Which could indicate that Au/Citrate/PAHF+B has a great amount of linked biotin that Au/Citrate/PAHFB and so the nanostructure is more sensitive to the presence of avidin, or as was said before this nanostructure (Au/Citrate/PAH+B) is destabilize in the presence of avidin due to the functionalization method, since in this case

the amount of avidin added is bigger and the destabilization (aggregation) of the nanostructure increased.

In the fluorescence spectra (Figure 57) the fluorescence intensity of the nanostructures that contain biotin decreased in the presence of avidin in comparison to the reference (Au/Citrate/PAHF). For the Au/Citrate/PAHFB this decrease of the fluorescence intensity is too small, to be considered significant. However the visible spectra showed that aggregation occurred. This optical behavior of the nanocomposites was also observed for the Au/Citrate/PAHF+B with 30 µL of avidin and washed, indicating one more time that this nanostructure could have less biotin than Au/Citrate/PAHF+B so the aggregation is not optically detectable. Concerning the Au/Citrate/PAHF+B with 100 µL of avidin, the decrease of the fluorescence intensity is bigger, indicating more aggregation and is in aggremen with the visible spectra. Regarding the nanostructures prepared *in situ* (Figure 58*)*, the Au/PAH+FB in the presence of avidin showed a decrease of the fluorescence intensity when compared with the reference. However no change was registered in the visible spectra.

The decrease of fluorescence observed, seems to be related with the aggregation state of the Au nanocomposites since in some cases this is confirmed by absorption spectroscopy by the appearance of the band around 650 nm. It is known that quenching occurs when Au NPs are in the presence of a fluorophore occurs quenching. This effect is more extreme when the fluorophore is closer to the Au NPs[47], so, it was thought that when the aggregation occurs the quenching effect is stronger.

The results discussed along this section show that the nanocomposites prepared *in situ* do not respond well to the presence of avidin as only a slight decrease of the fluorescence was observed. Therefore it can be concluded that the synthetic method influences the sensitivity of the nanostructures to the presence of avidin. As regards the functionalization procedure since the functionalization with biotin was carried out following exactly the same procedure this can not be the cause. Indeed Au/PAH NPs do not have a spherical morphology and their SPR band shifted to higher wavelength as a result of the influence of the surrounding environment. The same was observed for the functionalized nanostructures with FITC and/or biotin. This distinct environment around the Au NPs may actually

protect them from aggregation. As a result, their response towards analytes is also affected. This is clearly shows that the *in situ* method still needs to be optimized.

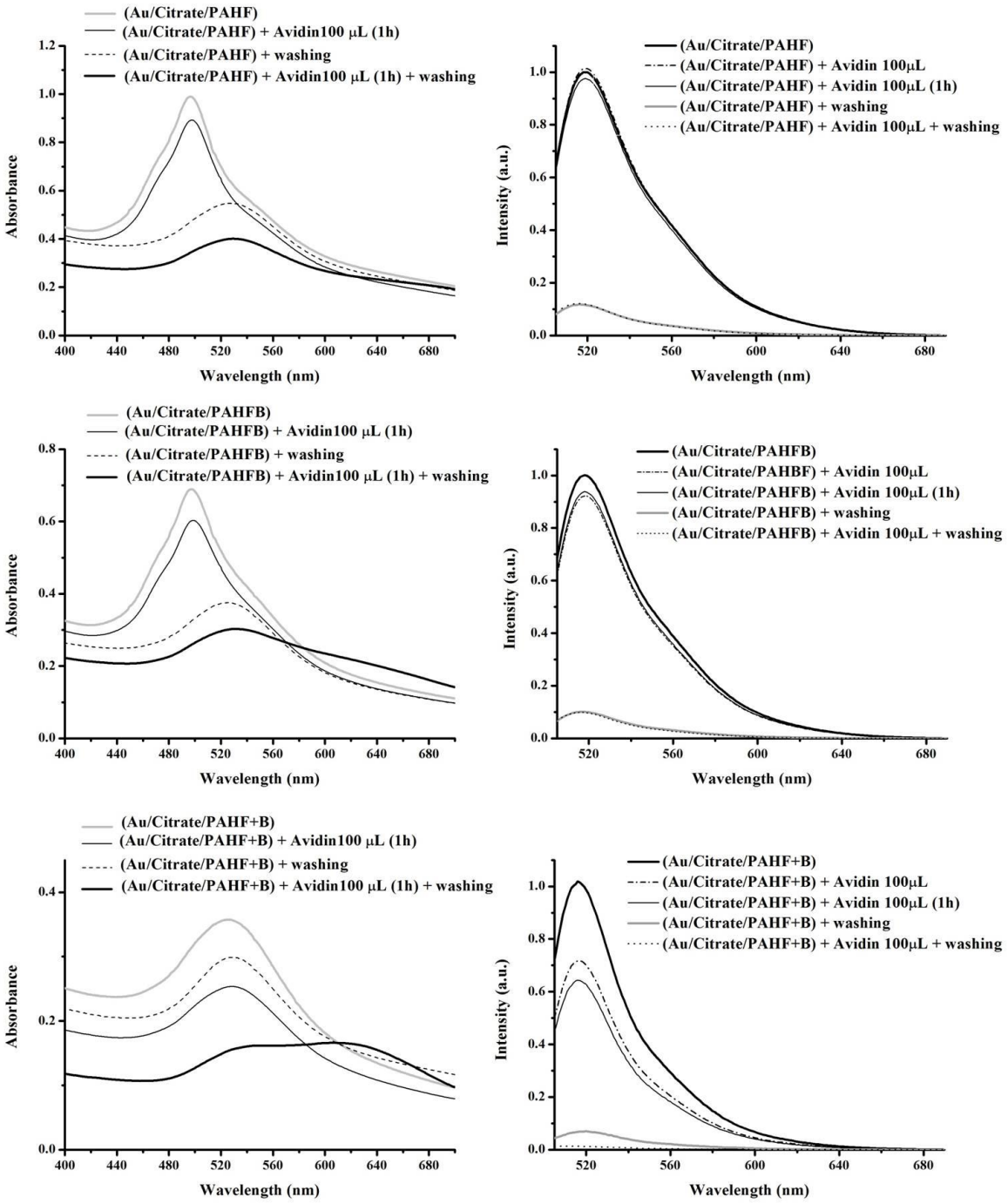

Figure 57 - Visible spectra (left column) and fluorescence spectra – λexc = 494 nm (right column) of the Au/Citrate/PAH assemblies when in the presence of 100 μL of an avidin solution (0.2 mg/mL).

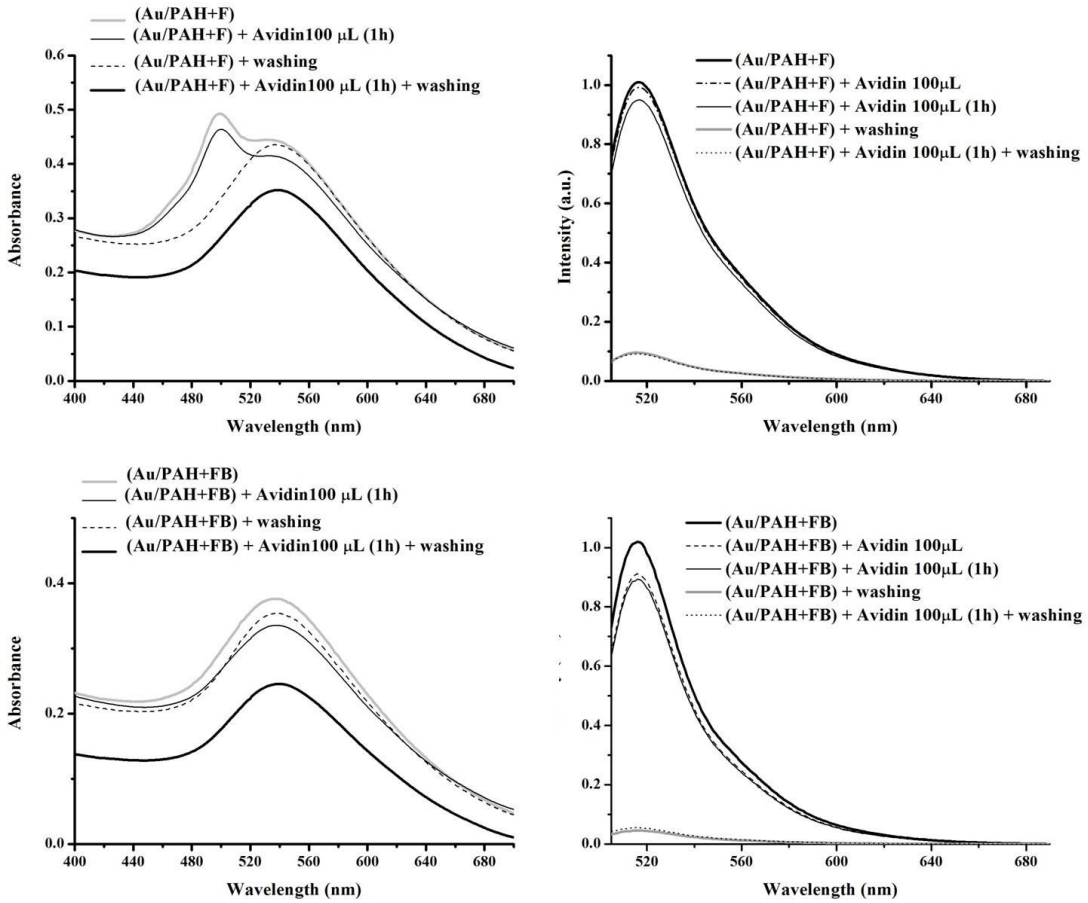

Figure 58 - Visible spectra (left column) and fluorescence spectra – λexc = 494 nm (right column) of the Au/PAH assemblies when in the presence of 100 μL of an avidin solution (0.2 mg/mL).

As a remark, it was observed that the decrease of the intensity of the fluorescence is related with the aggregation state of the nanostructures in the presence of avidin. Moreover, fluorescence spectroscopy seems to be more sensitive to the aggregation state than visible spectroscopy since the decrease of fluorescence was detected prior to the washing cycle, whilst by visible spectroscopy aggregation was only detected after the nanostructures had been washed.

In addition, these preliminary tests regarding the use of the nanostructures prepared seem very promising since the analyte does not have to be labeled with a fluorophore, as reported by others[49]. Moreover, fluorescence spectroscopy proved to be more sensitive to aggregation than visible spectroscopy. Hence it would be an interesting tool to study aggregation and its dependence on the structure of Au assemblies. Nevertheless, different quantities of avidin should be tested and the amount of biotin should be quantified as well as its availability at the surface assessed to confirm these results.

PART IV

CONCLUSIONS AND FUTURE WORK

PART IV – CONCLUSIONS AND FUTURE WORK

The main goal of this work was to prepare Au NPs functionalized with a fluorophore and a biomolecule and apply the resulting hybrid nanostructures towards an optical biosensor.

Two strategies were employed to synthesize Au NPs: i) Au NPs were prepared via the citrate method (- 34.03 mV) and then modified with PAH using the LbL method. The ensuing NPs have positive charge. ii) Au NPs were generated via the *in situ* method, the deprotonated amine groups of PAH act as reducing agente and the PAH stabilizes the Au NPs (+59.77 mV), so the synthesis and the surface modification occur simultaneously. In the second approach a variety of difficulties were encountered when the scale up was performed (10 mL to 50 mL), the major problem was the mass transfer which was solved using a jacket reactor equipped with a mechanical stirred and a thermostatic bath. The huge difference in these scales was the morphology of Au NPs. The Au NPs obtained in the laboratory scale were non spherical, contrary to the ones produced at micro scale. The reaction conditions of scale up in the *in situ* method should be optimized in order to obtained spherical and isolated Au/PAH NPs.

Summarizing the properties of Au NPs obtained in the different strategies: Au/Citrate/PAH NPs have 14.9 ± 2.8 nm diameter and a surface Plasmon resonance (SPR) band at 522 nm; Au/PAH NPs obtained at micro scale have 13.4 ± 2.4 nm of diameter and a SPR at 542 nm; Au/PAH NPs prepared at the so called laboratory scale have 22.0 ± 3.3 nm of diameter and a SPR at 538 nm.

The functionalization process depends of the synthesis method. i) For the NPs prepared via citrate method the PAH was functionalized with the FITC and/or biotin and the Au/Citrate NPs were then coated with functionalized PAH. ii) In the case of Au/PAH NPs, strategies have to be adopted, the modification of the Au/PAH wih the FITC was only achieved when FITC was added to the solution of Au/PAH, i.e. after the synthesis and submitting the product to any washing procedure. pH of this solution is kept around 9 which is the pH value needed to link the isothiocyanate group of FITC to the amine group of PAH. The functionalization with biotin was performed onto the Au/PAH NPs. The covalent linkage between the FITC and biotin to PAH was confirmed by FTIR spectroscopy and the

presence of the FITC in each nanostructure was confirmed by fluorescence spectroscopy (λ_{em} = 519 nm).

In the preparation of the structures it was concluded that the centrifugation/re-dispersion cycles that were preformed during the functionalization play a very important role in the stability of the nanostructures because some PAH adsorbed can be removed and after several cycles losses of the PAH coating seem to take place which lead to flocculation of Au NPs.

The optical response of the prepared nanostructures in the presence of avidin was followed by visible and fluorescence spectroscopy. It was concluded that adding 30 µL of avidin (0.2 mg/mL) to each colloidal solution the optical response was not detectable because the amount of avidin was too small to detect any specific response. Only the Au/Citrate/PAHF+B aggregated in the presence of this amount of avidin with the solution turning blue and precipitated. Addition of 100 µL of avidin (0.2 mg/mL) to all the colloids functionalized with biotin and prepared via the citrate method showed changes in the absorbance and/or fluorescence comparing to the colloids which do not have biotin. These results confirm a specific response. For the NPs prepared *in situ* a possible specific response was only observed by fluorescence spectroscopy associated with the decrease of the fluorescence intensity when avidin was added. The different responses of the nanostructures to the presence of avidin are mainly due to the methodology of Au NPs synthesis. Yet the functionalization strategy used can also affect the response. The nanocomposites prepared via the citrate method showed to be more sensitive to the presence of the avidin.

In conclusion, these preliminary tests showed the potential use of these optical active Au NPs assemblies as biosensor, since a specific response was observed.

In a near future, the synthesis of Au/PAH *in situ* NPs should be optimized. Parameters such as the temperature, the agitation speed, the concentration of the solutions and even the pH can be studied to better understand the parameters that influence the morphology of the ensuing Au NPs and their aggregation. An aspect that should be a major concern in future works is to get stable nanostructures in biological media, i.e. obtain stable Au NPs in

buffer solutions. Another aspect that should be taken into account is the labelling degree of biotin in the PAH, that should be quantified to optimize the functionalization process of PAH. This is an important aspect because of the stabilization of the Au NPs in solution and because of the minimum amount of avidin that the system can to respond. Moreover, it would be interesting to explore the use of others biomolecules such as the antigen/antibody systems in these colloids towards novel biosensors.

Finally, an interesting work that could be developed is to use these Au nanostructures in thin-films and evaluate the optical response when the film is in contact to a solution containing avidin. Furthermore, studies at molecular level, using the Langmuir-Blodgett technique would be interesting to assess the specificity of the interaction between these hybrid nanostructures and biological materials both at the air-water interface as well as upon transference to a solid substrate.

REFERENCES

1. Trindade, T.; da Silva, A. L. D., *Nanocomposite Particles for Bio-Applications*. Pan Stanford Publishing Pte. Ltd.: **2011**.
2. Vidotti, M.; Carvalhal, R. F.; Mendes, R. K.; Ferreira, D. C. M.; Kubota, L. T., Biosensors Based on Gold Nanostructures. *Journal of the Brazilian Chemical Society* **2011,** *22* (1), 3-20.
3. Zeng, S.; Yong, K.-T.; Roy, I.; Dinh, X.-Q.; Yu, X.; Luan, F., A Review on Functionalized Gold Nanoparticles for Biosensing Applications. *Plasmonics* **2011,** *6* (3), 491-506.
4. Buerk, D. G., *Biosensors: Theory and Application*. Technomic Publishing Company, Inc: Lancaster, Pennsylvania U.S.A, **1993**.
5. Cabral, J. M. S.; Aires-Barros, M. R.; Gama, M., *Engenharia Enzimática*. Lidel: Lisboa, **2003**.
6. Siqueira, J. R.; Caseli, L.; Crespilho, F. N.; Zucolotto, V.; Oliveira, O. N., Immobilization of biomolecules on nanostructured films for biosensing. *Biosensors & Bioelectronics* **2010,** *25* (6), 1254-1263.
7. Liu, Y.; Kim, E.; Ghodssi, R.; Rubloff, G. W.; Culver, J. N.; Bentley, W. E.; Payne, G. F., Biofabrication to build the biology-device interface. *Biofabrication* **2010,** *2* (2).
8. Klemic, J. F.; Stern, E.; Reed, M. A., Hotwiring biosensors. *Nature Biotechnology* **2001,** *19* (10), 924-925.
9. Liz-Marzán, L. M., Nanometals: Formation and color. *Materials Today* **2004,** *7* (2), 26-31.
10. Sato, K.; Hosokawa, K.; Maeda, M., Rapid aggregation of gold nanoparticles induced by non-cross-linking DNA hybridization. *Journal of the American Chemical Society* **2003,** *125* (27), 8102-8103.
11. Storhoff, J. J.; Lazarides, A. A.; Mucic, R. C.; Mirkin, C. A.; Letsinger, R. L.; Schatz, G. C., What controls the optical properties of DNA-linked gold nanoparticle assemblies? *Journal of the American Chemical Society* **2000,** *122* (19), 4640-4650.
12. Rosano, C.; Arosio, P.; Bolognesi, M., The X-ray three-dimensional structure of avidin. *Biomolecular Engineering* **1999,** *16* (1-4), 5-12.
13. Diamandis, E. P.; Christopoulos, T. K., The biotin (strept)avidin system - Principles and Applications in biotechnology. *Clinical Chemistry* **1991,** *37* (5), 625-636.
14. Hermanson, G. T., *Bioconjugate Techniques*. 2nd ed.; Elsevier: Rockford, Illinois, USA, **2008**.
15. Kohut, A.; Voronov, A.; Peukert, W., Organization of Functionalized Gold Nanoparticles by Controlled Protein Interactions. *Particle & Particle Systems Characterization* **2005,** *22* (5), 329-335.
16. Aslan, K.; Luhrs, C. C.; Perez-Luna, V. H., Controlled and reversible aggregation of biotinylated gold nanoparticles with streptavidin. *Journal of Physical Chemistry B* **2004,** *108* (40), 15631-15639.
17. Turkevich, J.; Stevenson, P. C.; Hillier, J., A study of the nucleation and growth processes in the synthesis of colloidal gold. *Discussions of the Faraday Society* **1951,** *11*, 55-75.

18. Newman, J.; Blanchard, G., Formation and encapsulation of gold nanoparticles using a polymeric amine reducing agent. *Journal of Nanoparticle Research* **2007,** *9* (5), 861-868.
19. Kumar, S.; Gandhi, K. S.; Kumar, R. In *Modeling of formation of gold nanoparticles by citrate method*, CHEMCON Meeting 2005, Mumbia, India, Dec; American Chemical Society: Mumbia, India, **2004**; pp 3128-3136.
20. Gittins, D. I.; Caruso, F., Tailoring the Polyelectrolyte Coating of Metal Nanoparticles. *The Journal of Physical Chemistry B* **2001,** *105* (29), 6846-6852.
21. Gittins, D. I.; Caruso, F., Multilayered Polymer Nanocapsules Derived from Gold Nanoparticle Templates. *Advanced Materials* **2000,** *12* (24), 1947-1949.
22. Higashi, N.; Takagi, T.; Koga, T., Layer-by-layer fabrication of well-packed gold nanoparticle assemblies guided by a [beta]-sheet peptide network. *Polymer Journal* **2010,** *42* (1), 95-99.
23. Cho, J. H.; Caruso, F., Investigation of the interactions between ligand-stabilized gold nanoparticles and polyelectrolyte multilayer films. *Chemistry of Materials* **2005,** *17* (17), 4547-4553.
24. Caruso, F.; Caruso, R. A.; Mohwald, H., Nanoengineering of inorganic and hybrid hollow spheres by colloidal templating. *Science* **1998,** *282* (5391), 1111-1114.
25. Schneider, G. g. F.; Subr, V.; Ulbrich, K.; Decher, G., Multifunctional Cytotoxic Stealth Nanoparticles. A Model Approach with Potential for Cancer Therapy. *Nano Letters* **2009,** *9* (2), 636-642.
26. Labouta, H. I.; Schneider, M., Tailor-made biofunctionalized nanoparticles using layer-by-layer technology. *International Journal of Pharmaceutics* **2010,** *395* (1-2), 236-242.
27. Schonhoff, M., Self-assembled polyelectrolyte multilayers. *Current Opinion in Colloid & Interface Science* **2003,** *8* (1), 86-95.
28. Schneider, G.; Decher, G., From Functional Core/Shell Nanoparticles Prepared via Layer-by-Layer Deposition to Empty Nanospheres. *Nano Letters* **2004,** *4* (10), 1833-1839.
29. Mayya, K. S.; Schoeler, B.; Caruso, F., Preparation and Organization of Nanoscale Polyelectrolyte-Coated Gold Nanoparticles. *Advanced Functional Materials* **2003,** *13* (3), 183-188.
30. Dorris, A.; Rucareanu, S.; Reven, L.; Barrett, C. J.; Lennox, R. B., Preparation and Characterization of Polyelectrolyte-Coated Gold Nanoparticles. *Langmuir* **2008,** *24* (6), 2532-2538.
31. Schneider, G.; Decher, G., Functional Core/Shell Nanoparticles via Layer-by-Layer Assembly. Investigation of the Experimental Parameters for Controlling Particle Aggregation and for Enhancing Dispersion Stability. *Langmuir* **2008,** *24* (5), 1778-1789.
32. Dumur, F.; Guerlin, A.; Dumas, E.; Bertin, D.; Gigmes, D.; Mayer, C. R., Controlled spontaneous generation of gold nanoparticles assisted by dual reducing and capping agents. *Gold Bulletin* **2011,** *44* (2), 119-137.
33. Selvakannan, P. R.; Mandal, S.; Phadtare, S.; Gole, A.; Pasricha, R.; Adyanthaya, S. D.; Sastry, M., Water-dispersible tryptophan-protected gold nanoparticles prepared by the spontaneous reduction of aqueous chloroaurate ions by the amino acid. *Journal of Colloid and Interface Science* **2004,** *269* (1), 97-102.
34. Newman, J. D. S.; Blanchard, G. J., Formation of gold nanoparticles using amine reducing agents. *Langmuir* **2006,** *22* (13), 5882-5887.

35. Aslam, M.; Fu, L.; Su, M.; Vijayamohanan, K.; Dravid, V. P., Novel one-step synthesis of amine-stabilized aqueous colloidal gold nanoparticles. *Journal of Materials Chemistry* **2004,** *14* (12), 1795-1797.
36. Iwamoto, M.; Kuroda, K.; Zaporojtchenko, V.; Hayashi, S.; Faupel, F., Production of gold nanoparticles-polymer composite by quite simple method. *The European Physical Journal D* **2003,** *24* (1-3), 365-367.
37. Morrow, B. J.; Matijević, E.; Goia, D. V., Preparation and stabilization of monodisperse colloidal gold by reduction with aminodextran. *Journal of Colloid and Interface Science* **2009,** *335* (1), 62-69.
38. Valeur, B., *Molecular fluorescence: Principles and Applications*. Wiley-VCH: Weinheim, Germany, **2002**.
39. Lakowicz, J., *Principles of Fluorescence Spectroscopy*. 2 ed.; Kluwer Academic/Plenum Publishers: New York, **1999**.
40. Richter, B.; Kirstein, S., Excitation energy transfer between molecular thin layers of poly(phenylene vinylene) and dye labeled poly(allylamine) in layer-by-layer self-assembled films. *Journal of Chemical Physics* **1999,** *111* (11), 5191-5200.
41. Peralta, S.; Habib-Jiwan, J.-L.; Jonas, A. M., Ordered Polyelectrolyte Multilayers: Unidirectional FRET Cascade in Nanocompartmentalized Polyelectrolyte Multilayers. *ChemPhysChem* **2009,** *10* (1), 137-143.
42. Wang, L.; Roitberg, A.; Meuse, C.; Gaigalas, A. K., Raman and FTIR spectroscopies of fluorescein in solutions. *Spectrochimica Acta Part A: Molecular and Biomolecular Spectroscopy* **2001,** *57* (9), 1781-1791.
43. Maeda, T.; Nagahara, T.; Aida, M.; Ishibashi, T., Identification of chemical species of fluorescein isothiocyanate isomer-I (FITC) monolayers on platinum by doubly resonant sum-frequency generation spectroscopy. *Journal of Raman Spectroscopy* **2008,** *39* (11), 1694-1702.
44. Zhang, T. K.; Zhu, J. H.; Yao, H. B.; Yu, S. H., Novel fluorescein hierarchical structures fabricated by recrystallization under control of polyelectrolytes. *Crystal Growth & Design* **2007,** *7* (12), 2419-2428.
45. Johnson, I.; Spence, M. T. Z., *The Molecular Probes® Handbook*. 11th ed.; Invitrogen: 2010.
46. Kato, N.; Caruso, F., Homogeneous, competitive fluorescence quenching immunoassay based on gold nanoparticle/polyelectrolyte coated latex particles. *Journal of Physical Chemistry B* **2005,** *109* (42), 19604-19612.
47. Schneider, G.; Decher, G.; Nerambourg, N.; Praho, R.; Werts, M. H. V.; Blanchard-Desce, M., Distance-dependent fluorescence quenching on gold nanoparticles ensheathed with layer-by-layer assembled polyelectrolytes. *Nano Letters* **2006,** *6* (3), 530-536.
48. Aslan, K.; Perez-Luna, V. H., Quenched emission of fluorescence by ligand functionalized gold nanoparticles. *Journal of Fluorescence* **2004,** *14* (4), 401-405.
49. Aslan, K.; Perez-Luna, V. H., Nonradiative interactions between biotin-functionalized gold nanoparticles and fluorophore-labeled antibiotin. *Plasmonics* **2006,** *1* (2-4), 111-119.
50. Rivas, B. L.; Seguel, G. V., Synthesis, characterization of poly(allylamine)chelates with Cu(II), Co(II) and Ni(II). *Polymer Bulletin* **1996,** *37* (4), 463-468.
51. Zucolotto, V.; Ferreira, M.; Cordeiro, M. R.; Constantino, C. J. L.; Balogh, D. T.; Zanatta, A. R.; Moreira, W. C.; Oliveira, O. N., Unusual Interactions Binding Iron Tetrasulfonated Phthalocyanine and Poly(allylamine hydrochloride) in Layer-by-Layer Films. *The Journal of Physical Chemistry B* **2003,** *107* (16), 3733-3737.

52. Tristán, F.; Palestino, G.; Menchaca, J. L.; Pérez, E. a.; Atmani, H.; Cuisinier, F. d. r.; Ladam, G., Tunable Protein-Resistance of Polycation-Terminated Polyelectrolyte Multilayers. *Biomacromolecules* **2009,** *10* (8), 2275-2283.
53. Stuart, B. H., *Infrared spectroscopy: fundamentals and applications*. Wiley: Chichester, **2004**.
54. Lex, A.; Pacher, P.; Werzer, O.; Track, A.; Shen, Q.; Schennach, R.; Koller, G.; Hlawacek, G.; Zojer, E.; Resel, R.; Ramsey, M.; Teichert, C.; Kern, W.; Trimmel, G., Synthesis of a Photosensitive Thiocyanate-Functionalized Trialkoxysilane and Its Application in Patterned Surface Modifications. *Chemistry of Materials* **2008,** *20* (5), 2009-2015.
55. Ojea-Jiménez, I.; Bastús, N. G.; Puntes, V., Influence of the Sequence of the Reagents Addition in the Citrate-Mediated Synthesis of Gold Nanoparticles. *The Journal of Physical Chemistry C* **2011,** *115* (32), 15752-15757.
56. Morag, E.; Bayer, E. A.; Wilchek, M., Reversibility of biotin-binding by selective modification of tyrosine in avidin. *The Biochemical journal* **1996,** *316 (Pt 1)*, 193-9.

ANNEXES

ANNEXE A

DLS measurements of Au/Citrate NPs – Average = 38.81 nm

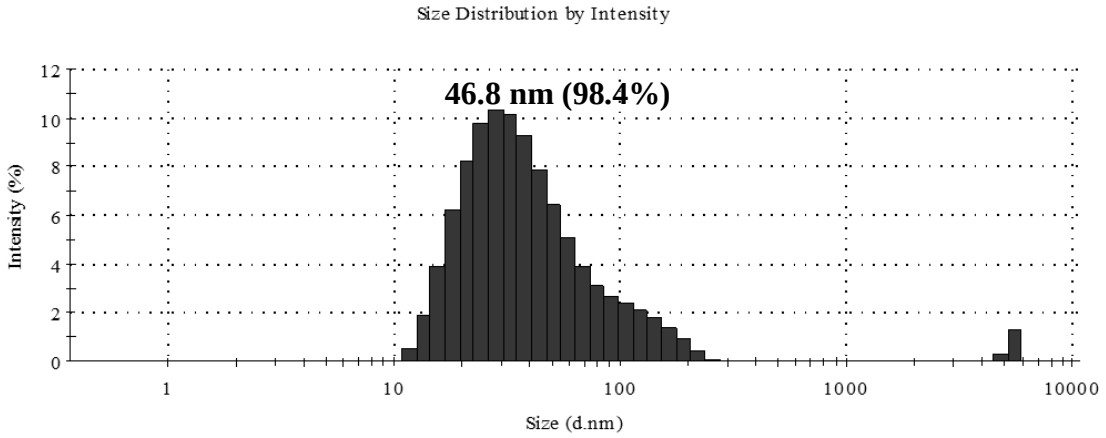

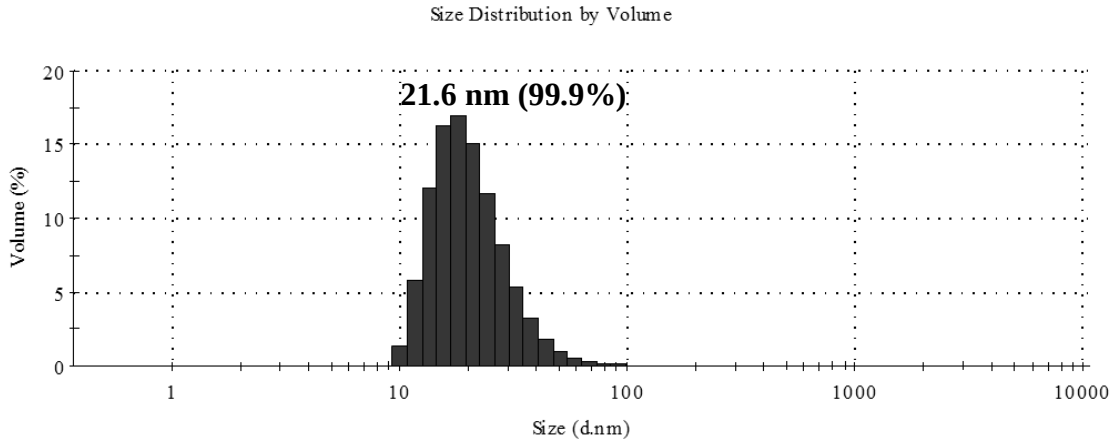

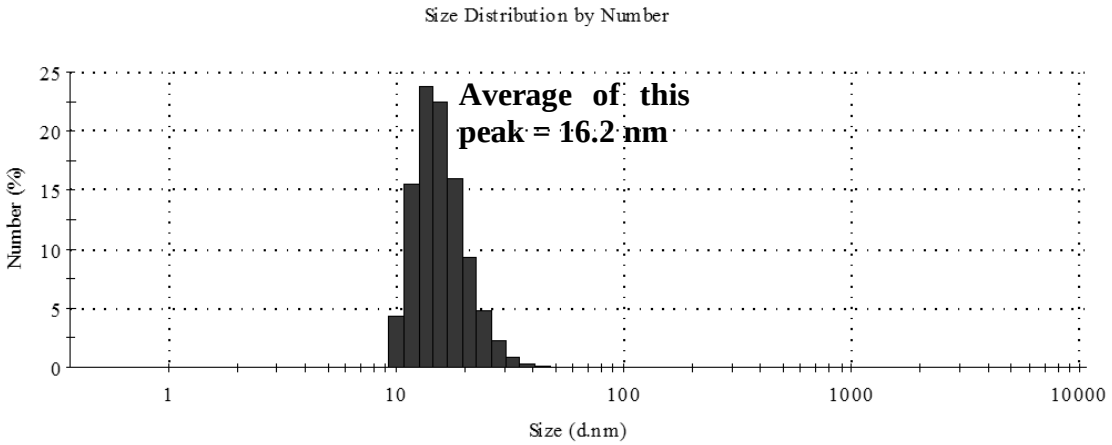

DLS measurements of Au/Citrate/PAH – Average = 42.07 nm

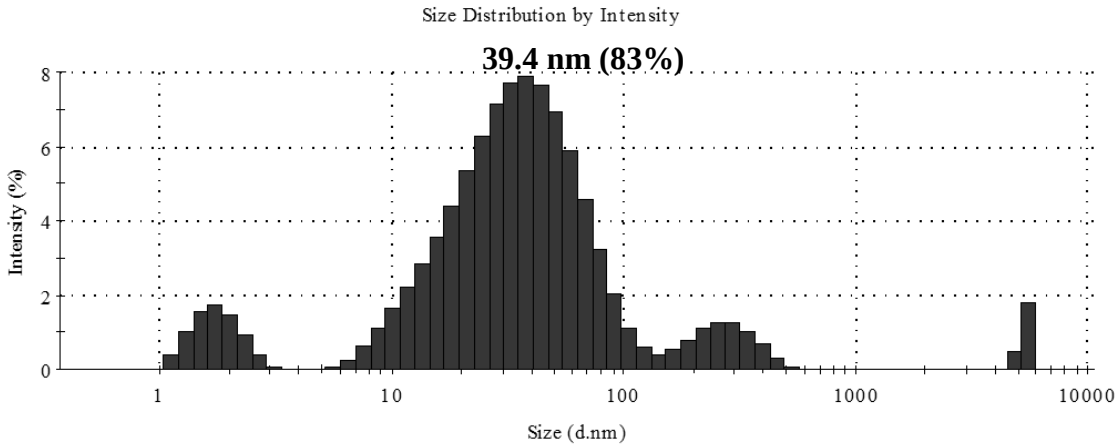

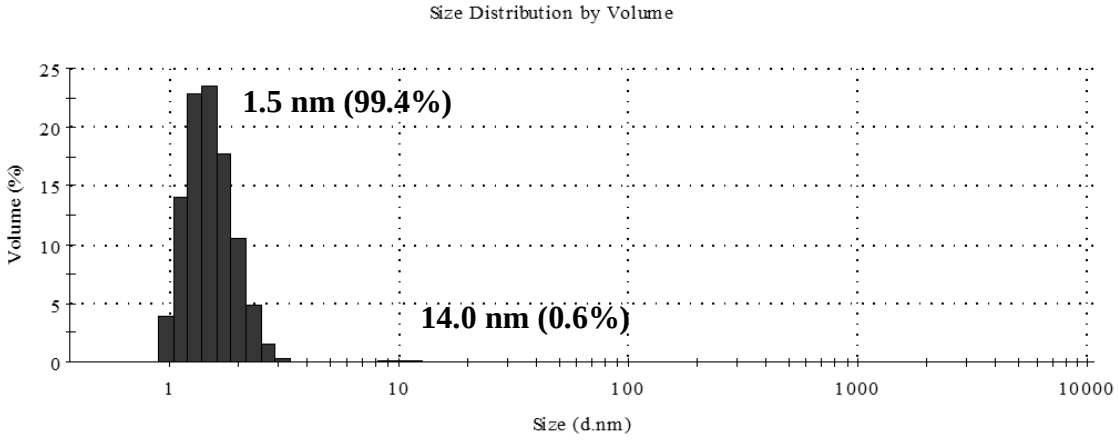

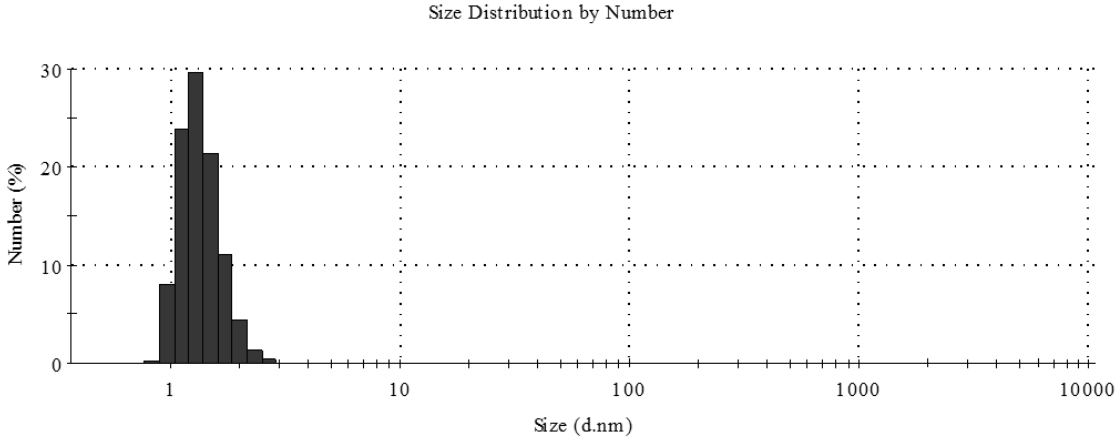

ANNEXE B

Zeta Potential measurements of Au/Citrate/PAH

			Mean (mV)	Area (%)	Width (mV)
Zeta Potential (mV):	55.9	**Peak 1:**	78.6	46.0	8.61
Zeta Deviation (mV):	24.7	**Peak 2:**	24.4	28.3	7.24
Conductivity (mS/cm):	0.115	**Peak 3:**	48.7	25.6	7.44

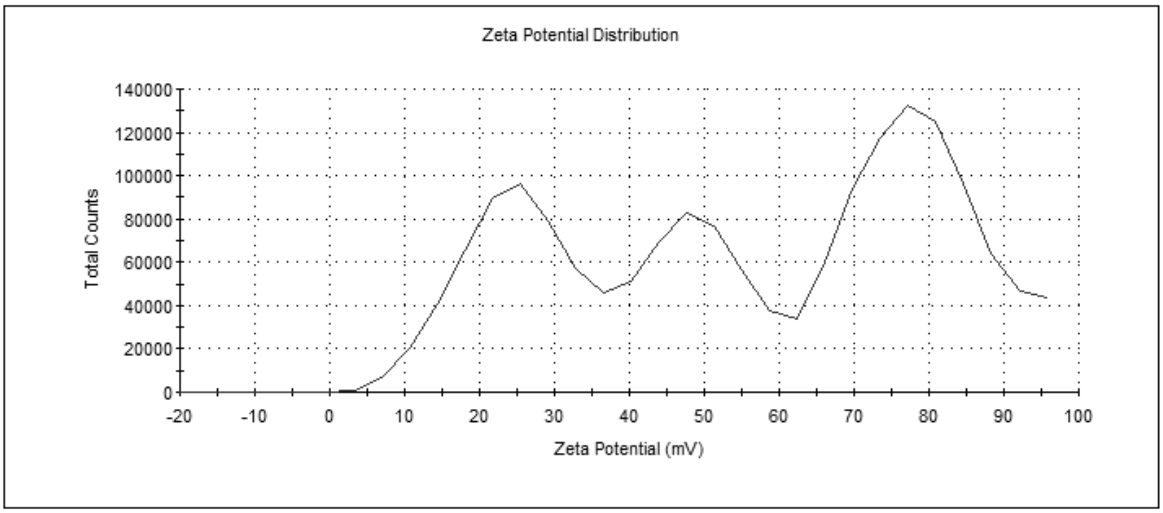

Zeta Potential measurements of Au/Citrate/PAH + washing

			Mean (mV)	Area (%)	Width (mV)
Zeta Potential (mV):	33.2	**Peak 1:**	30.5	90.4	6.35
Zeta Deviation (mV):	10.3	**Peak 2:**	58.8	9.6	3.37
Conductivity (mS/cm):	0.0758	**Peak 3:**	0.00	0.0	0.00

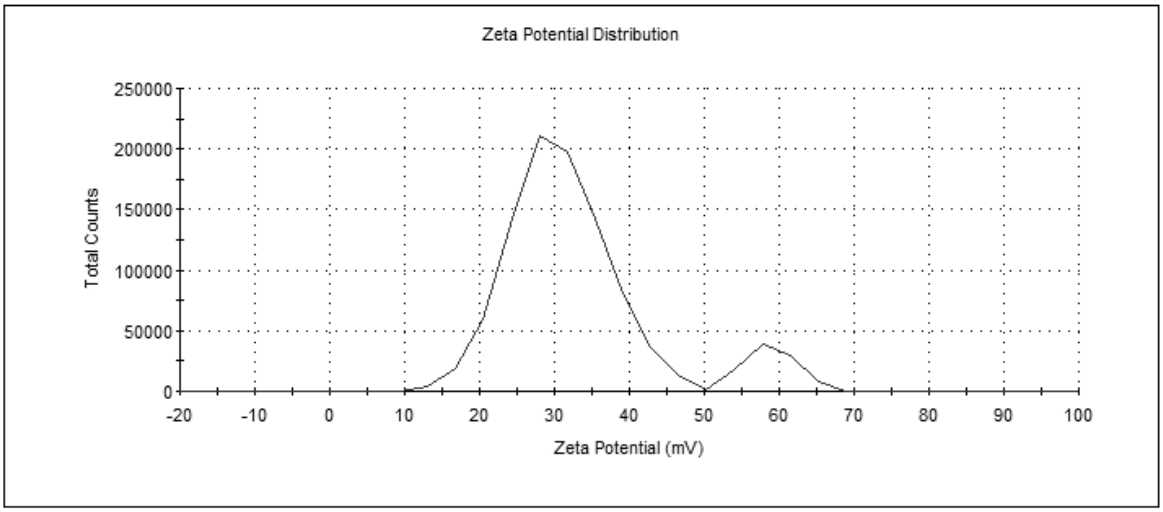

ANNEXE C1

DLS measurements of Au/PAH micro scale

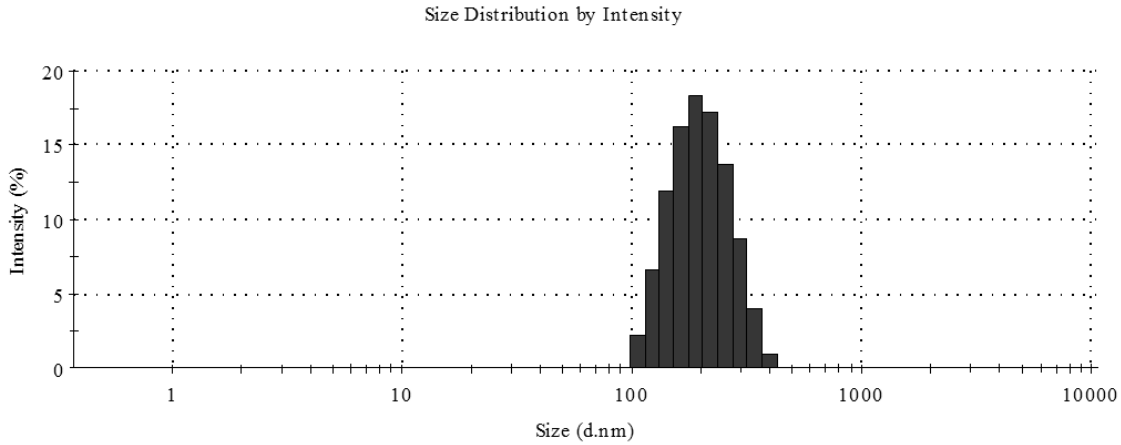

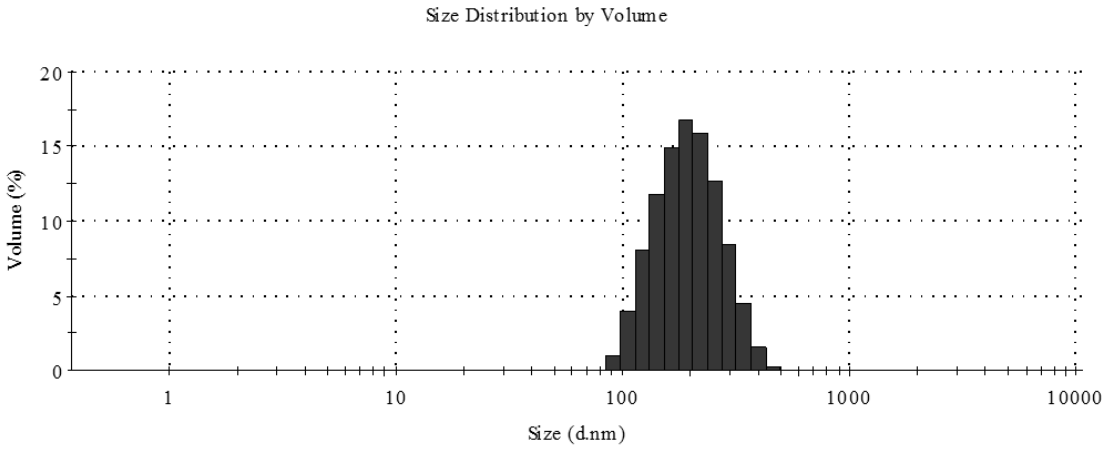

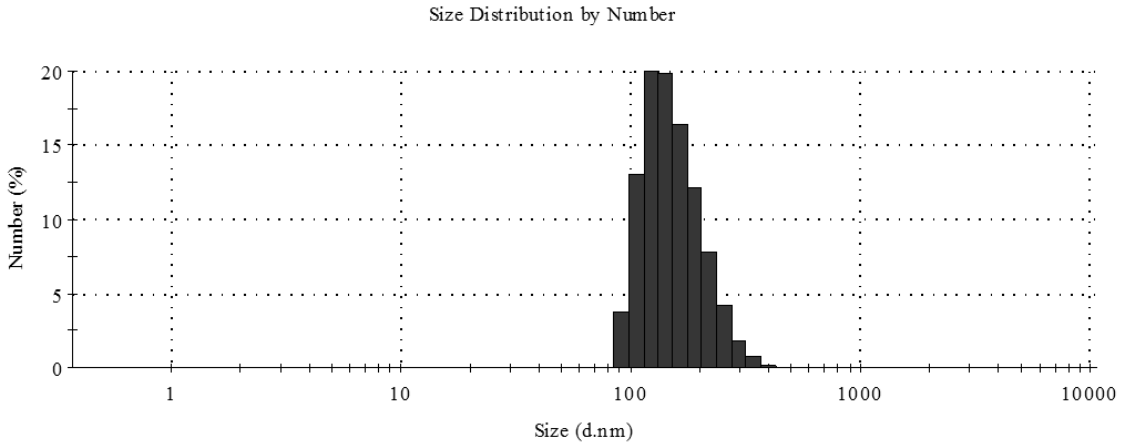

ANNEXE C2

DLS measurements of Au/PAH laboratory scale – Average = 54.13 nm

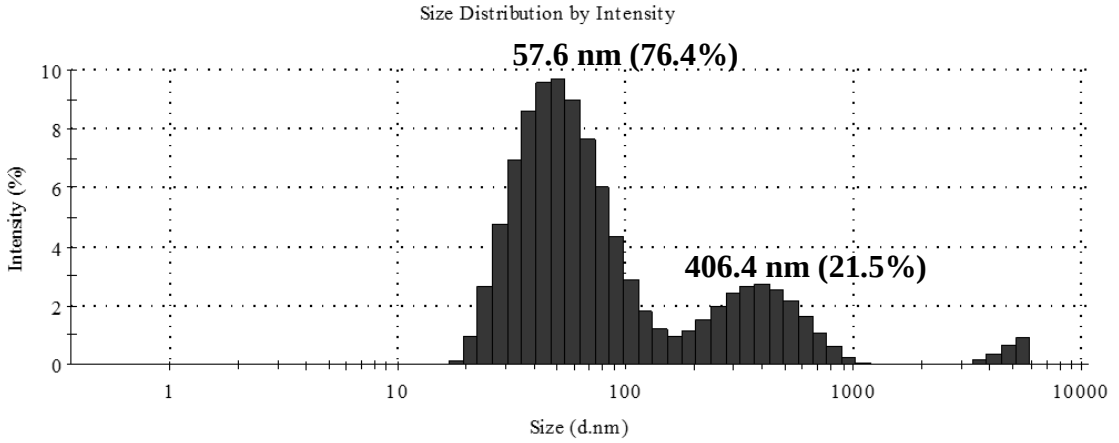

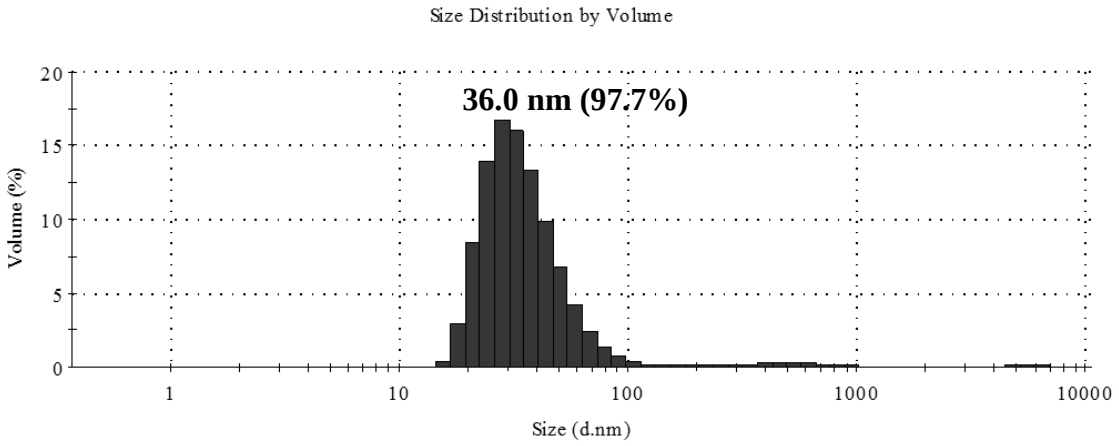

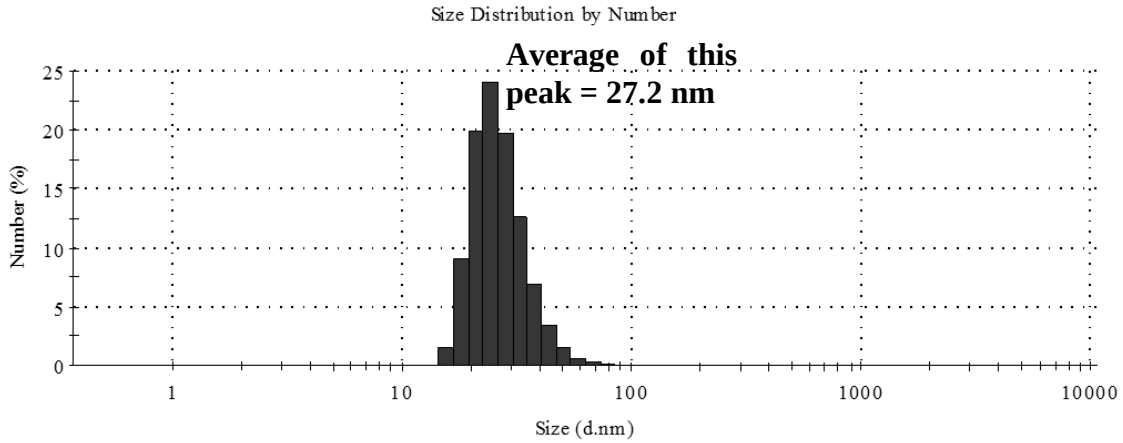

ANNEXE D

Zeta Potential measurements of Au/PAH

			Mean (mV)	Area (%)	Width (mV)
Zeta Potential (mV):	63.1	**Peak 1:**	62.9	98.4	10.6
Zeta Deviation (mV):	11.8	**Peak 2:**	110	0.9	3.32
Conductivity (mS/cm):	0.215	**Peak 3:**	23.9	0.8	3.42

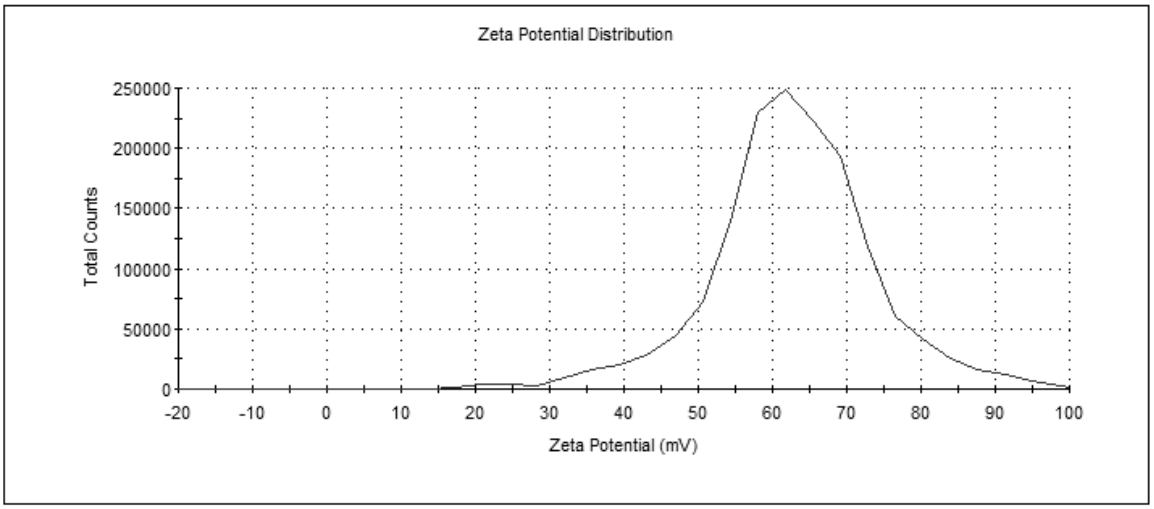

Zeta Potential measurements of Au/PAH + washing

			Mean (mV)	Area (%)	Width (mV)
Zeta Potential (mV):	56.7	**Peak 1:**	71.5	54.5	11.1
Zeta Deviation (mV):	21.8	**Peak 2:**	48.4	25.1	6.35
Conductivity (mS/cm):	0.0923	**Peak 3:**	23.9	19.8	5.73